Transactions of the I·R·E

Professional Group on Antennas and Propagation

VOLUME AP-3 NUMBER 1 JANUARY 1955

Published Quarterly

The Institute of Radio Engineers

TRANSACTIONS OF THE I•R•E® PGAP IS A QUARTERLY PUBLICATION DEVOTED TO EXPERIMENTAL AND THEORETICAL PAPERS ON ANTENNAS AND WIRELESS PROPAGATION OF ELECTROMAGNETIC WAVES

MANUSCRIPTS should be submitted to John B. Smyth, Editor, U. S. Navy Electronics Laboratory, San Diego, California. Manuscripts should be original typewritten copy, double spaced, plus one carbon copy. References should appear as footnotes and include author's name, title, journal, volume, initial and final page numbers, and date. Each paper must have an abstract of not more than 200 words. News items concerning PGAP members and group activities should be sent to the News Editor, Mr. H. A. Finke, Polytechnic Research and Development Company, 55 Johnson Street, Brooklyn, New York.

ILLUSTRATIONS should be submitted as follows: All line drawings (graphs, charts, block diagrams, cutaways, etc.) should be inked uniformly and ready for reproduction. If commercially printed grids are used in graph drawings, author should be sure printer's ink is of a color that will reproduce. All halftone illustrations (photographs, wash, airbrush, or pencil renderings, etc.) should be clean and ready to reproduce. Photographs should be glossy prints. Call-outs or labels should be marked on a registered tissue overlay, not on the illustration itself. No illustration should be larger than 8 x 10 inches.

Copies can be purchased from
THE INSTITUTE OF RADIO ENGINEERS
1 East 79 St., New York 21, N.Y.

PRICE PER COPY: members of the Professional Group on Antennas and Propagation, $1.60; members of the IRE, $2.40; nonmembers, $4.80.

ANNUAL SUBSCRIPTION PRICE: IRE members, $8.50; Colleges and public libraries, $12.75; nonmembers, $17.00.

Entered as second-class matter, at the post office at Menasha, Wisconsin, under the act of August 24, 1912. Acceptance for mailing at a special rate of postage is provided for in the act of February 28, 1925, embodied in Paragraph 4, Section 412, P. L. & R., authorized October 26, 1927.

news and views

Combining of Professional Groups

THE Professional Group Task Force recently appointed to survey the desirability and feasibility of combining Professional Groups have, after a study, come to the following findings:

1. There is no significant general trend among Professional Groups to combine. It appears that the scopes of most of the Professional Groups are sufficiently distinct. It is felt that it is highly desirable that all Professional Groups consider carefully the possibility of joint meetings wherever and whenever feasible.

2. There is no significant general trend among Professional Groups to combine TRANSACTIONS. Several groups have discussed combining certain issues because of possible interest to the joint membership.

3. In order to assist and also perhaps to guide individual Professional Groups in planning joint activities, it is recommended that Headquarters prepare a tabulation listing both horizontally and vertically all individual Professional Groups and placing at the intersection the numbers of IRE members belonging to both groups. This should convey quickly information about split of interest between two Professional Groups and might point in the direction of joint efforts on a quantitative basis.

4. It is recommended that each Professional Group include in its own TRANSACTIONS those abstracts and papers appearing in other TRANSACTIONS which may be of interest to its membership.

Liaison with PROCEEDINGS

As stated in the last issue of the TRANSACTIONS, Roy Spencer is serving as liaison between our quarterly and the PROCEEDINGS. When a technical paper in our field is submitted to the PROCEEDINGS, he is one of the three expert readers appointed. In this fashion, PGAP is represented, we are able to keep informed of papers submitted, and we have a voice in deciding where they should be published. This arrangement has thus far been set up only for PGAP.

The Administrative Committee has been concerned for some time with the subscription rate for the TRANSACTIONS for other than PGAP members. Any arrangement that is made requires complete approval of IRE headquarters. It appears as if a very considerable number of subscriptions can be obtained, and the rate established can determine a substantial amount of income. It is hoped that more information will be available by the time of the next issue.

More local chapters are desirable. San Francisco, New York, Long Island, New Jersey, New England, and other areas have been remiss in getting some activity started. The Administrative Committee would welcome petitions for local chapters but each area seems to require some special spark to get under way. J. S. Brown of Andrew Corporation is responsible for local chapters; enterprising organizers are invited to write him for further information.

More Institutional Listings for the TRANSACTIONS are desirable. These are the company names and their spheres of interest as listed on the back cover. This is the only approved advertising we can employ, but at the present rate of $25.00 a listing per issue and $75.00 for the year, the possible return from this kind of advertising is well worth going after. Our circulation certainly justifies the small expense on the part of the advertising company, particularly in the light of the well-defined audience exposed to the listings. Robert Helliwell of Stanford University is in charge of these listings and he should be contacted for information or arrangements.

WESCON-1954 has made $800.00 available to PGAP for publication of papers presented at the Los Angeles convention this past summer. Papers will be subjected to our standard screening procedures and if accepted a WESCON acknowledgement will be given in a footnote. If we are too meticulous and publish too few WESCON papers the unspent balance of the $800.00 allotment must be returned. Even when the cause is just, it is always sad to contemplate returning money.

National Meetings

The Professional Group on Antennas and Propagation will sponsor four sessions at the 1955 Spring National IRE Convention in New York. Two of the sessions will consist of five papers each on Antennas and a third session will consist of five Propagation papers. The fourth session will be a panel discussion of "Extended Range VHF and UHF Propagation," chaired by Jerome Weisner. It is hoped that panel members will be recruited from Stanford, Bell Labs., the National Bureau of Standards, Cornell, and M.I.T. The availability to PGAP of four sessions at the National Convention should be very gratifying to our membership as a tribute to the high activity of our Professional Group.

Dr. Bolljahn of the PGAP Administrative Committee is in charge of all meetings, symposia, etc. We have been advised that he has prepared a list of about ten national annual meetings that PGAP might conceivably sponsor either individually or jointly. It is hoped that his list will be available shortly.

After the Spring IRE, the next important PGAP meeting will be the Spring URSI in Washington which we have recently been invited to once again co-sponsor.

Group Chapters and Chapter News

The number of PGAP Chapters will soon be increased by 100 per cent with the addition of Chapters at Philadelphia and Washington, D. C., and Los Angeles Orange Belt sub-section.

The Philadelphia Chapter has received the approval of the PGAP Executive Committee and will start its program of activities in the near future. Those members in the Philadelphia area desiring more information on the Chapter activities should contact the organizer Mr. Charles Polk of the Moore School of Engineering of the University of Pennsylvania.

The Washington, D. C., Chapter has been approved by the Executive Committee of the Washington, D. C., Section of the IRE and should get under way before the first of the year. Members in this area should contact Mr. Clarence Stewart of Jansky & Bailey, Inc. for further information.

The Los Angeles Orange Belt sub-section has been initiated by A. W. Walters of Naval Ordnance Laboratory at Corona, California. Members of this area should contact Mr. Walters for further information.

The first regularly scheduled meeting of the Philadelphia Chapter of the IRE Professional Group on Antennas and Propagation was held November 17, 1954 at the Towne Building, University of Pennsylvania. This meeting was held jointly with the Philadelphia Chapter of the IRE Professional Group on Microwave Theory and Techniques. Attendance totaled twenty-two members and guests.

The following officers for the Philadelphia Chapter were unanimously elected: *Chairman:* Mr. Charles Polk, Moore School of Electrical Engineering, University of Pennsylvania; *Vice-Chairman:* Mr. R. A. Dibos, Philco Corporation; and *Secretary:* Mr. S. M. King, I-T-E Circuit Breaker Company.

During the technical portion of the meeting two papers were presented:

"Shielding with Coated Glass or Thin Conductive Surfaces," by Dr. E. I. Hawthorne, University of Pennsylvania. A mathematical analysis of the transmission of electro-magnetic fields through thin conducting planes, infinite in extent, was presented. In particular, two sources were considered: a magnetic and an electric current element assumed normal to the sheet. The field along the axis of the source on the opposite side of the sheet was determined and compared with the field which would exist if the sheet were not present.

"Theoretical Gain of Microwave Reflectors," by D. R. Crosby, R.C.A. The physical behavior of reflectors from the field point of view was described. Various methods of numerical analysis were indicated, and the results of a particular computation were shown.

Both papers proved to be highly informative to the assembled group, and were followed by lively discussions. After the technical papers, the chair announced that the next regularly scheduled meeting would again be a joint meeting of the PGAP and the PGMT&T to be held at 8 P.M. on Wednesday, February 16, 1955, at the University of Pennsylvania. The highlight of this meeting is to be a paper by Dr. S. A. Schelkunoff entitled, "The Early History of the Theory of Dipole Antennas."

Antennas and Propagation People

Mr. Kenneth A. Norton has been appointed chief of the Radio Propagation Engineering Division of the Boulder Laboratories of the National Bureau of Standards in Colorado. He was formerly chief of the Systems Research Laboratory of the NBS Central Radio Propagation Laboratory. When the CRPL moved from Washington, D. C. to Boulder, Mr. Norton's laboratory became a division. The primary responsibilities of this division are tropospheric propagation research and the related studies of frequency utilization. Mr. Norton has been a member of the NBS staff since 1946. He also served previously at the Bureau, in 1929 and 1930. He was a consultant in the Radio Propagation Section of the Office of the Chief Signal Officer from 1944 to 1946, radio and tactical countermeasures analyst in the Operational Research Section of the Eighth Air Force in England from 1943 to 1944, and Assistant Director of the Operational Research Group in the Office of the Chief Signal Officer from 1942 to 1943. Prior to World War II, he was for a number of years on the staff of the Technical Information Section of the Federal Communications Commission. Mr. Norton is a native of Rockwell City, Iowa, and received the B.S. degree in physics from the University of Chicago in 1928.

Dr. Ralph J. Slutz has been appointed Chief of the Radio Propagation Physics Division of the National

Bureau of Standards Boulder Laboratories in Colorado. This division is a part of the Bureau's Central Radio Propagation Laboratory. Dr. Slutz will direct the Bureau's research on the physics of radio propagation with particular reference to the ionosphere. Prior to joining the Central Radio Propagation Laboratory early in 1954, Dr. Slutz was well known for his role in the design and construction of SEAC, one of the Bureau's electronic digital computers, and for his research on the application of electronic computers to the solution of problems in theoretical physics. From 1949 to 1953 Dr. Slutz was Assistant Chief of the NBS Electronic Computer Laboratory. From 1946 to 1948, he was a design engineer at the Institute for Advanced Study at Princeton, New Jersey, doing research on electronic computer design; from 1942 to 1945 he was a member of Division 2 of the Office of Scientific Research and Development, investigating the effects of bomb and projectile explosion and impact; and in 1937 and 1938 he was with Bell Telephone Laboratories.

Professor Samuel Silver of the University of California has recently returned from a sabbatical year during which time he engaged in research in two European universities. Traveling with his family on a Guggenheim Fellowship for Research in Diffraction, he divided his time between the Royal Technical Institute in Copenhagen, Denmark and Cambridge University in England. Before returning to Berkeley he attended the eleventh General Assembly of URSI in the Hague, Netherlands. In addition to his activities in the technical programs of the Assembly, Professor Silver was honored by re-election as President of the International Commission on Radio Waves and Circuits (Commission VI of URSI) for the coming three-year period.

Dr. E. C. Jordan, formerly professor of Electrical Engineering at the University of Illinois, has been named Chairman of the Electrical Engineering Department of that University.

Dr. V. H. Rumsey, previously head of the Antenna Laboratory at Ohio State University, has been appointed professor of Electrical Engineering at the University of Illinois.

Dr. Chen To Tai has recently been appointed Associate Professor in the Department of Electrical Engineering at Ohio State University, where he will teach antenna courses and do research in the Antenna Laboratory. Dr. Tai is well known for his many papers on antenna theory. Born in 1915 in Soochow, China, he came to the United States in 1943, and received his D.Sc. degree from Harvard University in 1947. From 1943 to 1949 he was a teaching fellow and a research associate specializing in antennas at Harvard University. In 1949 he joined the Stanford Research Institute where he was Senior Research Physicist. Dr. Tai is a member of Sigma Xi and the American Physical Society.

Dr. A. H. Waynick and *Dr. H. G. Booker* are on a year's leave of absence on a special teaching assignment to Cavendish Laboratory in Cambridge, England.

Correspondence

In the October, 1954 issue of the PGAP Transactions, the Editor asked for opinions on several topics. W. Sichak of the Federal Telecommunications Laboratories has sent us his.

"First, the Editor and the reviewers are to be commended for the decreasing time lag between receipt of a paper and its publication. One valid criticism of the Proceedings of the I.R.E. in previous years was that papers took over a year (on the average) to be published. With good teamwork, it should be possible to publish papers in less than six months, as is done by the American Physical Society.

"Papers on microwave components should not be published by the PGAP, but rather by the Group on Microwave Theory and Techniques. Papers on Radio Astronomy should by all means be published by PGAP, because the subject is closer to the interest of this Group than to that of any other IRE Group; the antennas and techniques used can be of use in other fields; and the data collected by radio astronomers is useful even now, since in the design of a modern radio relay link consideration must be given to cosmic noise sources that might come within the beam of the receiving antenna.

"Good papers from our friends abroad should be encouraged, since we have no monopoly on good ideas. Further, it might encourage more of us to read foreign journals and thus decrease our technical insularity.

"The reference to special handling of student papers is not understood. If it means lowering the standards for student authors, I vote against it."

Acknowledgment

We wish to thank the following people for their assistance in the preparation of this section: C. H. Stewart of Jansky & Bailey, Washington, D. C.; George Sinclair of the University of Toronto, Toronto, Canada; Allen R. Ellis of the Stanford Research Institute, Stanford, California; and R. L. Mattingly of Bell Laboratories, Whippany, N. J.

contributions

Double Parabolic Cylinder Pencil-Beam Antenna*

R. C. SPENCER†, F. S. HOLT†, H. M. JOHANSON†, AND J. SAMPSON‡

Summary—**Radiation from a point source placed on the focal line of a parabolic cylinder is reflected in succession from this cylinder and from a second parabolic cylinder crossed so that its focal line coincides with the directrix of the first cylinder. The two reflections result in a parallel beam. The theory is applicable to both microwaves and light. The advantages of shipping the cylinders in the form of flat sheets and the possibilities of independent control of horizontal and vertical beamwidths and shapes are pointed out. Experimental models have been built and tested.**

Introduction

IN CONTRAST to the usual microwave pencil-beam antenna formed by allowing energy from a point source to reflect once from a paraboloid of revolution, the device to be discussed makes use of successive reflections from *two parabolic cylinders* with elements at *right angles*, each cylinder collimating the beam in one plane. Functionally, the point source and first parabolic cylinder could be replaced by a parabolic pillbox[1] or any other equiphase line source.

The idea of using crossed cylindrical lenses has long been known in optics[2], but the application to pencil beams appears to be new. More recently, the use of crossed cylindrical reflectors has been introduced in connection with X-ray microscopes[3,4], where the phenomenon of total reflection of X-rays at grazing incidence lends itself to the use of curved metal reflectors.

Kirkpatrick and Baez[3] discuss the use of two *crossed elliptic cylinder mirrors* to form a real image of a point and the use of two *parallel* parabolic reflectors to form a real line image of a point. In references 3 and 4, the reflectors are approximated by sections of circular cylinders. In 4, the elliptic cylinder is approximated by a bent optical flat.

Geometry

Fig. 1 (opposite) shows a perspective drawing of the two parabolic cylinders. The first cylindrical surface S_1 is given by the equation

$$y^2 = 4fx = 2lx, \tag{1}$$

where f is the focal length and $l=2f$ is the semilatus rectum. The point F with co-ordinates $(f, 0, 0)$ lies on the focal line of S_1. The line DD' is the image of point F in S_1; i.e., any ray emitted from F and incident on S_1 at P_1 is reflected as though it originated on DD'.

The formula for the second cylindrical surface S_2 is given by the equation

$$(x+f)^2 = 4f(z+f). \tag{2}$$

This surface has been so oriented that it meets the following conditions: (a) its focal line coincides with DD', (b) it contains the point F, and (c) any ray emitted radially from DD' is reflected parallel to the positive z axis. Under these conditions, S_2 has the same focal length f as S_1, and the point V with co-ordinates $(-f, 0, -f)$ lies on the vertex line of S_2.

It is evident, therefore, that any ray FP_1P_2 emitted from a point source located at F will, after successive reflections from S_1 and S_2, be directed parallel to the positive z axis. If either (b) or (c) on S_2 were relaxed, then other combinations of relative focal lengths and orientations would be possible.

* Original manuscript received by the PGAP, June 21, 1954; revised manuscript received, October 11, 1954. The geometric design was discussed under the same title, by R. C. Spencer, in Air Force Cambridge Research Center Rep. No. E5084; April, 1952.

† Air Force Cambridge Research Center, Cambridge, Mass.

‡ Now in the U. S. Navy.

[1] S. Silver, "Microwave antenna theory and design," *M.I.T. Rad. Lab. Ser.*, vol. 12, pp. 151, 494; 1949.

[2] J. P. C. Southall, "Mirrors, Prisms and Lenses," The Macmillan Company, New York, N. Y., ch. IX; 1933.

[3] P. Kirkpatrick and A. V. Baez, "Formation of optical images by X-rays," *Jour. Opt. Soc. Amer.*, vol. 38, pp. 766–774; 1948.

[4] W. Ehrenberg, "The Production of converging beams by total reflection," *Jour. Opt. Soc. Amer.*, vol. 39, pp. 741–746; 1949.

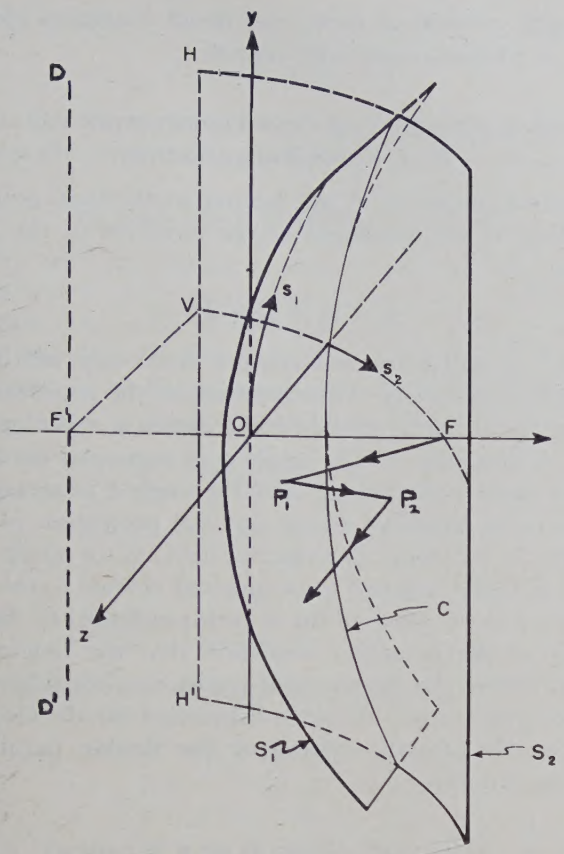

Fig. 1—Orthogonal curvilinear co-ordinate systems on surfaces S_1 and S_2.

Calculation of the Co-ordinates of Common Intersection

The x, y, and z co-ordinates of the intersection of the two parabolic cylinders with $2f=l=1$ were calculated using (1) and (2). The curve of intersection may be written in the following parametric form:

$$\left.\begin{aligned} x &= t^2/2 \\ y &= t \\ z &= \frac{(t^2+1)^2}{8} - \frac{1}{2} \end{aligned}\right\}. \qquad (3)$$

Table I contains numerical values of x, y, and z as computed from (3). The range on t (that is, y) is from 0 to 2 in increments of 0.1.

Method of Developing Cylinders onto Flat Sheets

The curve of intersection of the two surfaces S_1 and S_2 is a three-dimensional space curve that we shall denote as C (see Fig. 1). If the surfaces S_1 and S_2 are separately developed into planes, the intersection curve in each case becomes a plane curve; however, these two plane curves are not identical. In the construction of the double cylindrical reflector, it is desirable to know the co-ordinates of these plane curves in order that they may be laid out on flat sheets before the sheets are bent into parabolic cylinder shape.

Curves of $z=$constant in the surface S_1 are all identical parabolas and S_1 is defined to be the arc length along any of these parabolas as measured from the z axis (see Fig. 1). Similarly, the curves of $y=$constant in the surface S_2 are all identical parabolas and s_2 is defined to be the arc length along any of these parabolas as measured from the vertex line HH'. In Table I we already have the x, y, and z co-ordinates of the intersection curve C. In order to obtain the s_1, z co-ordinates of C as measured in the surface S_1, it is necessary to determine s_1 as a function of either z or y; that is, the arc length of a parabola as a function of its co-ordinates. Similarly, in order to obtain the s_2, y co-ordinates of C as measured in the surface S_2, it is necessary to determine s_2 as a function of either x or z. Tables of parabolic arc length vs co-ordinates were computed by the Center of Analysis, Massachusetts Institute of Technology.[5] The last two columns of Table I were obtained from these parabolic arc length tables.

TABLE I

Coordinates of the Curve of Intersection of the Two Parabolic Cylinders

Point No.	t	x	y	z	s_1	s_2
0	0.0	0.000	0.0	−0.3750	0.0000	0.5201
1	.1	.005	.1	− .3725	.1002	.5257
2	.2	.020	.2	− .3648	.2013	.5426
3	.3	.045	.3	− .3515	.3044	.5709
4	.4	.080	.4	− .3318	.4104	.6110
5	0.5	0.125	0.5	−0.3047	0.5201	0.6636
6	.6	.180	.6	− .2688	.6343	.7293
7	.7	.245	.7	− .2225	.7536	.8091
8	.8	.320	.8	− .1638	.8786	.9043
9	.9	.405	.9	− .0905	1.0098	1.0166
10	1.0	0.500	1.0	0.0000	1.1478	1.1478
11	1.1	.605	1.1	.1105	1.2928	1.3003
12	1.2	.720	1.2	.2442	1.4452	1.4766
13	1.3	.845	1.3	.4045	1.6053	1.6799
14	1.4	.980	1.4	.5952	1.7733	1.9136
15	1.5	1.125	1.5	0.8203	1.9495	2.1814
16	1.6	1.280	1.6	1.0842	2.1339	2.4874
17	1.7	1.445	1.7	1.3915	2.3269	2.8363
18	1.8	1.620	1.8	1.7472	2.5284	3.2327
19	1.9	1.805	1.9	2.1565	2.7387	3.6819
20	2.0	2.000	2.0	2.6250	2.9579	4.1893

The straight-line elements of the cylinder S_1 along which the z co-ordinate is measured, together with the parabolas along which s_1 is measured, form an orthogonal curvilinear co-ordinate system on the surface S_1. When the cylinder is developed into a plane, this co-ordinate system becomes a rectangular system in the plane. The s_1, z co-ordinates of the intersection curve C are given in Table I. Fig. 2(a), next page, shows a plot of this curve on the developed surface S_1. Similarly, the

[5] R. C. Spencer and G. E. Reynolds, "A Table of Normalized Parabolic Coordinates and Arc Lengths," Air Force Cambridge Research Center Report No. E4083; July, 1951.

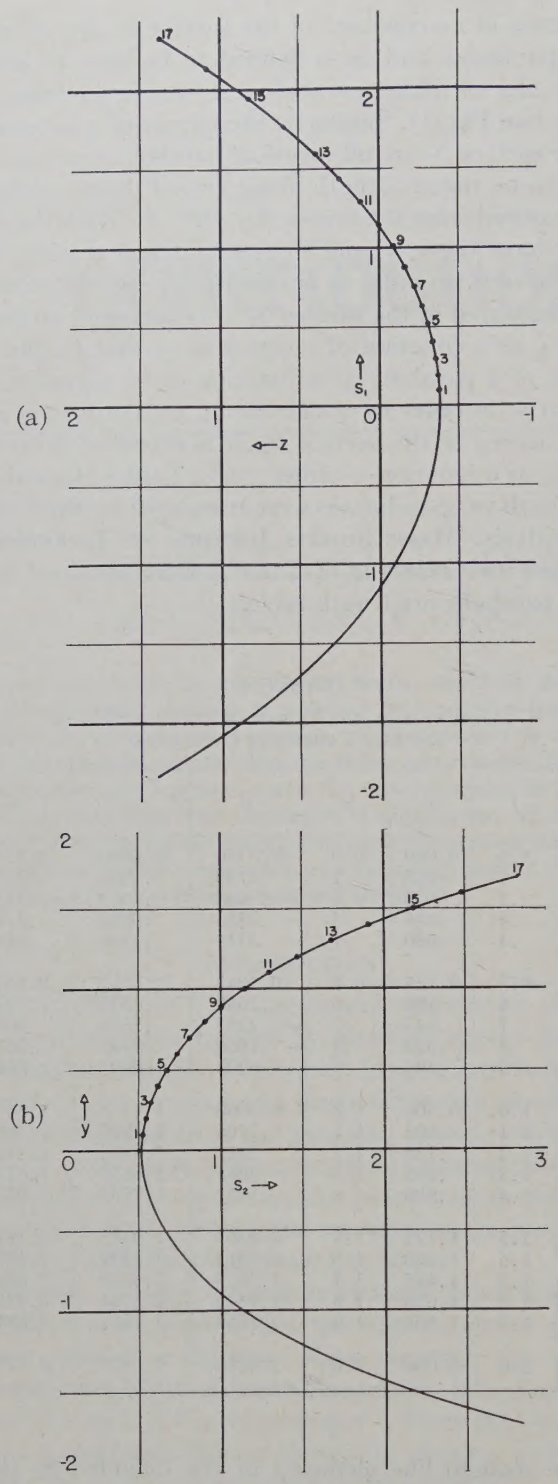

Fig. 2—(a) Curve of intersection developed on surface S_1. (b) Curve of intersection developed on surface S_2.

cylinder S_2 contains an s_2, y orthogonal curvilinear co-ordinate system that becomes a rectangular system when S_2 is developed into a plane. The s_2, y co-ordinates of the curve of intersection are given in Table I, and a plot of this curve on the developed surface S_2 is shown in Fig. 2 (b). Note that certain points along the intersection curves, as shown in Figs. 2 (a) and (b), are numbered according to the first column of Table I. When the developed surfaces S_1 and S_2 are returned to their parabolic cylindrical form and fitted together, identically numbered points will coincide.

Investigation of Feed Orientation for Zero Cross-Polarization

Assume an electric dipole located at the focal point F (see Fig. 3) and polarized in the direction of the unit vector

$$\hat{u} = \hat{i}a + \hat{j}b + \hat{k}c, \tag{4}$$

where $\hat{i}$, $\hat{j}$, and $\hat{k}$ are unit vectors in the x, y, and z directions respectively. The directions of the rays leaving the source are determined by the angles ϕ and θ, measured at the point F. The angle ϕ is measured between the xy plane and the ray, and the angle θ is measured between the negative x axis and the projection of the ray on the xy plane. The electric field vector along any ray is initially assumed to be directed normal to the ray and to lie in the plane of the $\hat{u}$ vector and the ray. Satisfaction of the boundary condition that the tangential component of the electric field vanish on each reflecting surface leads to the following expression for the electric field on the aperture plane of the double parabolic cylinder antenna:

$$\overline{E} = \frac{1}{\sin \gamma} \{\hat{i}[(a \cos \theta - b \sin \theta) \sin \phi + c \cos \phi] + \hat{j}[a \sin \theta + b \cos \theta]\}. \tag{5}$$

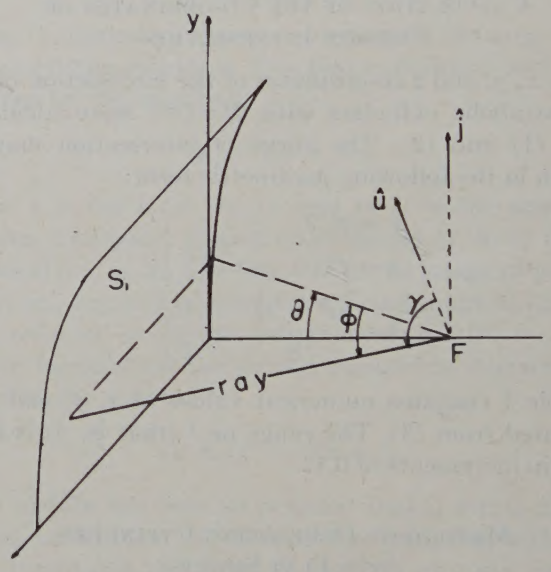

Fig. 3—Feed orientation and polarization.

If there is to be no cross-polarization, that is, if $\overline{E}$ is to have a constant direction, the components of $\overline{E}$ must be proportional, as follows:

$$K[(a \cos \theta - b \sin \theta) \sin \phi + c \cos \phi] = a \sin \theta + b \cos \theta.$$

The independence of the variables θ and ϕ and the linear independence of the functions $\sin \theta$ and $\cos \theta$ lead to the

following result:

$$a = b = K = 0.$$

Since $|_u| = 1$, we have $c = 1$; and (4) shows that this requires the source to be polarized parallel to the z-axis.

Illumination Over the Aperture

An exact ray-tracing analysis of the antenna leads to a geometric optics approximation of the aperture illumination. Assuming an isotropic source at the feed position, the illumination over the aperture is found to be proportional to a function separable in the normalized co-ordinates x/f and y/f as follows:

$$P = kF(x/f)G(y/f), \tag{6}$$

$$F(x/f) = 24.63 \frac{1 + x/f}{[4 + (1 + x/f)^2]^2}, \tag{7}$$

$$G(y/f) = \frac{4}{4 + (y/f)^2}. \tag{8}$$

Fig. 4 shows plots of these normalized functions.

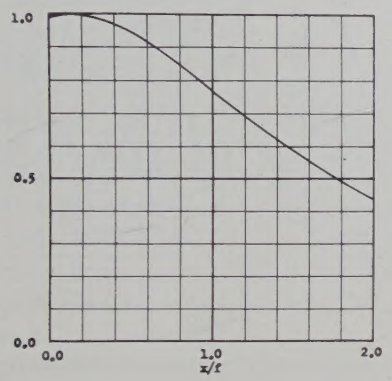

(a)

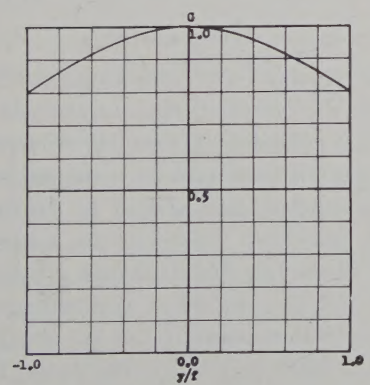

(b)

Fig. 4—Aperture illumination. (a) x direction. (b) y direction.

Experimental Model Design

An experimental model of the double parabolic cylinder antenna with aperture 1 foot by 1 foot, $f = 6$ inches was designed and built. Full use was made of the table computed by Spencer and Reynolds[5] in calculating the shapes of the flat sheets that were later bent to form the parabolic cylinder surfaces. In Fig. 5 (a) the reflector surfaces and the component parts of the supporting framework are shown laid out prior to assembly.

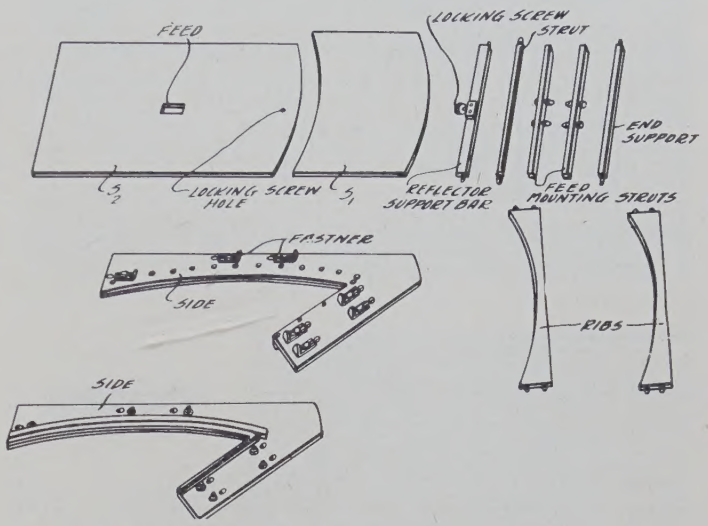

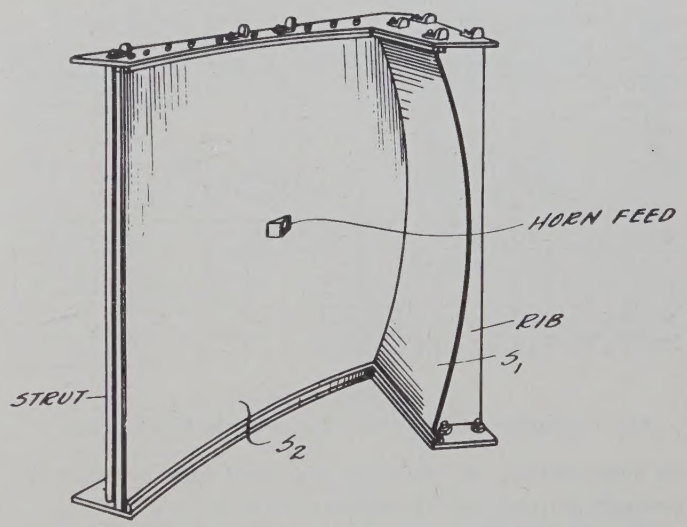

Fig. 5—Experimental model. (a) Disassembled. (b) Assembled.

The assembled antenna is shown in Fig. 5 (b). The mechanical design in this particular model features compact packaging in the disassembled state as well as simple rapid assembly and take-down procedures through use of dowels and slide snap fasteners.

The amplitude-tapering effects of the system as shown in Figs. 4 (a) and (b) were taken into account in the design of a K-band ($\lambda = 1.25$ cm) horn feed that theoretically produced at least a 10 db illumination taper over the final aperture in both the x and y directions. It is evident from Fig. 4 (a) that if the primary pattern of the feed were symmetric in ϕ (see Fig. 3), then the final aperture illumination would be asymmetrical in the x direction. This asymmetry in illumination introduced purely by the geometry of the system was counteracted

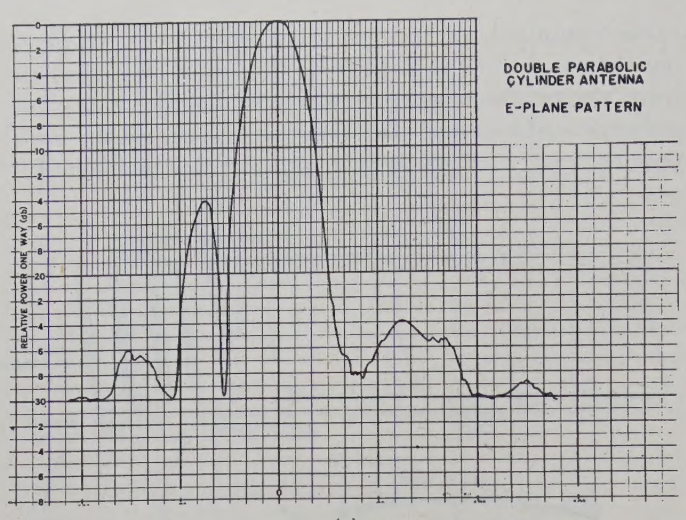

(a)

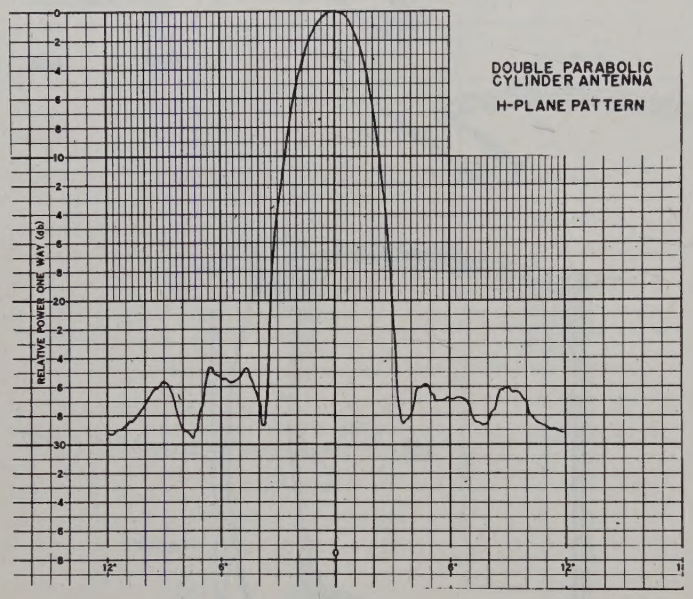

(b)

Fig. 6—Experimental patterns taken with the K-band model.

to some extent by orienting the feed horn so that its primary pattern was asymmetrical in ϕ.

Experimental patterns taken with the K-band model are shown in Fig. 6 (a) and (b). It is felt that the asymmetry of the side lobes in the E-plane pattern is the result of interference by the reflector S_1 with the final columnated radiation from reflector S_2 (see Fig. 5 (b)).

Shaped Beam Design (Cosecant Squared)

After reflection from the first parabolic cylinder S_1, all radiation striking the second parabolic cylinder S_2 appears to originate from a line source located along the line DD' (see Fig. 1, page 5). Hence it is necessary to redesign only the cylinder S_2 in order to produce a shaped fan beam.

Using the method suggested by L. J. Chu,[6] the design of the second cylindrical surface S_2 of the experimental model was modified to produce a $\csc^2 \theta$ fan beam over the range 2 to 20 degrees. Experimental elevation and azimuth patterns are shown in Fig. 7 (a) and 7 (b).

[6] R. C. Spencer, "Synthesis of Microwave Diffraction Patterns with Application to $csc^2\ \theta$ Patterns," Mass. Inst. Tech. Rad. Lab. Report No. 272(54-24), pp. 5–7; June 23, 1943.

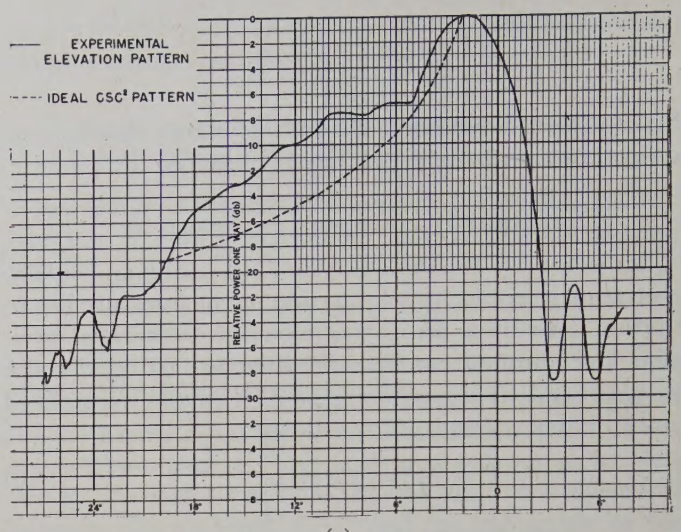

(a)

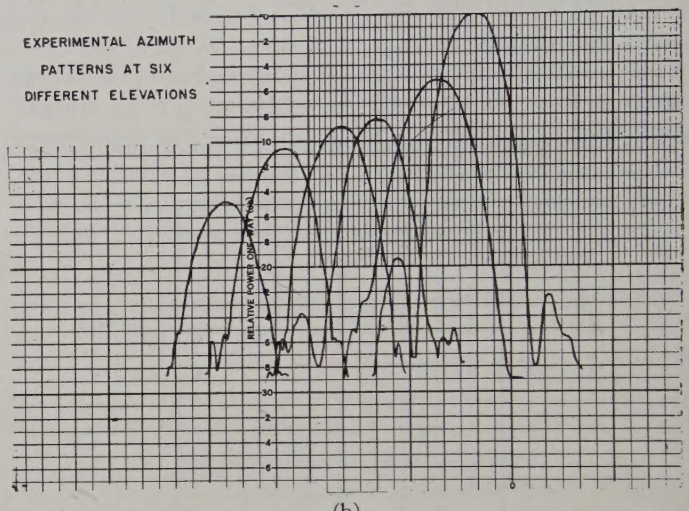

(b)

Fig. 7—Experimental elevation and azimuth patterns.

Conclusion

The double parabolic cylinder antenna has several advantages over the conventional paraboloid. Each of its surfaces, being cylindrical, can be stamped from flat sheets. The system itself can be designed so that it can be easily dismantled and stored or transported in a compact flat package. There is an absence of cross-polarization. Since the first reflector effectively focuses in one plane and the second in the orthogonal plane, a degree of independent control can be obtained over the beam shapes in both planes by modifying the appropriate reflecting surfaces. In particular, the second surface S_2 can be modified to obtain $csc^2\ \theta$ patterns.

Acknowledgement

The authors wish to acknowledge the aid of Norris Hansen and the Antenna Lab. Shop in the design and fabrication of experimental models, and of the Ipswich Antenna Pattern Test Unit in obtaining patterns.

An Atmospherics Analyzer*

PERRIN F. SMITH†

Summary—**The enormously powerful radiation from lightning discharges has been used as a tool for the study of the ionosphere at very low frequencies. Previous workers have calculated the height of the ionosphere and the distance to the radiation source by application of the ray theory of multiple ionospheric reflections. Time measurements for use in the height and distance formulas were obtained by direct measurement of recorded oscillograms. Time resolution was limited and the calculations were extremely tedious.**

This paper describes a complete system which records the received atmospheric wave form and simultaneously derives a plot of the time intervals between peaks of the wave form vs time. The time-interval plot greatly facilitates data reduction by means of a simple curve-fitting technique. Accuracy of measurement of height and distance is limited chiefly by the validity of the multiple reflection theory and the assumption of a simple layer structure in the ionosphere. The time differences are measured more accurately than is ordinarily possible with direct measurement on the waveform. The system automatically derives frequency-time plots for whistling atmospherics and relates the whistler to preceding impulsive atmospherics. Consumption of photographic film is low. The system can be used to visually monitor tape-recorded atmospherics.

Introduction

THE ENORMOUSLY powerful radiation from lightning discharges is potentially a powerful tool for the study of the ionosphere at very low frequencies. Analysis of certain types of recorded waveforms will indicate the average height of the ionosphere over the transmission path and the distance to the discharge.

This paper describes a recording system for atmospherics which presents data from the received waveforms in a partially reduced form, greatly facilitating the determination of the height of the ionosphere and the distance to the discharge. The time resolution of the system is increased several times over the resolution obtainable with a single-sweep display. The ease of data reduction with the analyzer described should make practical a statistical study of a large number of waveforms.

Ionospheric Propagation of Atmospherics

For the commonly occurring case of fairly small losses in the ionosphere, simple ray theory is sufficient to explain the important features of the observed waveforms.[1] The single pulse of radiation from the lightning discharge is received at a distant point a number of times, each time corresponding to a particular number of hops between earth and ionosphere. The ionosphere is assumed to be a smooth perfectly reflecting layer. Budden[1,2] has proposed a general theory to explain the propagation of atmospherics initiated by lightning discharges.

The transmission time of the nth-order pulse may be shown from the geometry to be

$$t_n = \frac{2n}{c}\sqrt{2R(R+h)\left(1-\cos\frac{D}{2Rn}\right)+h^2}, \quad (1)$$

where n = number of reflections at the ionosphere, t_n = time of arrival of the nth impulse, c = velocity of light, h = virtual height of reflection at the ionosphere, R = radius of earth, and D = great-circle distance to radiation source.

If $\cos D/2Rn$ is approximated by the first two terms of the series, we have very closely

$$t_n = \frac{1}{c}\sqrt{D^2\left(1+\frac{h}{R}\right)+4n^2h^2}. \quad (2)$$

When the order of reflection is known, the following expressions for the height of the ionosphere and the distance to the source can be derived from (2):

$$h = \frac{c}{2}\sqrt{\frac{T_1T_2(T_1+T_2)}{(r^2-q^2)T_1-(q^2-p^2)T_2}} \quad (3)$$

$$D^2 = \frac{\left(\dfrac{4h^2(q^2-p^2)-c^2T_1^2}{2cT_1}\right)^2-4p^2h^2}{1+\dfrac{h}{R}}, \quad (4)$$

where p, q, and r are pulse orders and

$$T_1 = t_q - t_p$$
$$T_2 = t_r - t_q.$$

The first two or three pulses arriving at a receiver from a long distance tend to merge, so that the first clearly defined pulses received are usually of the second or third order.[3]

Others[4,5] have made use of (3) and (4) in determining h and D by directly measuring the recorded waveform. Accuracy of measurement is very important, as is evident from (3), because the height measurement depends on a difference of differences. Order must be determined

* Original manuscript received by the PGAP, February 19, 1954; revised manuscript received July 20, 1954.

This paper was presented at the joint meeting of the International Scientific Radio Union, USA Natl. Com. and Can. Natl. Com., and the IRE PGAP in Ottawa, Can.; October 6, 1953.

† Associate Engineer, International Business Machines Corp., Engineering Laboratory, San Jose, Calif.

[1] K. G. Budden, "The propagation of a radio-atmospheric," *The Philosophical Magazine*, vol. 42, pp. 1–19; 1951.

[2] K. G. Budden, "The propagation of a radio-atmospheric II," *The Philosophical Magazine*, vol. 43, pp. 1179–1200; 1952.

[3] For the adverse but typical case of $D = 2000$ km and $h = 90$ km, the exact result for t_1 differs from the approximation found from (2) by about 1.5 per cent. The approximation improves rapidly with increasing n. The chief limitations on accuracy are the validity of the simple ray theory and experimental error.

[4] P. G. F. Caton and E. T. Pierce, "The waveforms of atmospherics," *The Philosophical Magazine*, vol. 43, pp. 393–409; 1952.

[5] W. J. Kessler and S. E. Smith, "An atmospheric waveform receiver," Proc. I.R.E., vol. 39, p. 676; June, 1951.

by a trial-and-error procedure and h and D should be found for several groups of pulses to obtain average results. If many waveforms are to be analyzed, the data reduction problem becomes difficult.

Curves of the time separation between pulses of the received waveform vs time may be prepared from (2) for a range of values of h and D. Each curve will have a characteristic shape. The atmospherics analyzer generates a dot pattern on an oscilloscope from each received wave form which is essentially the Δt vs t plot from (2). By curve-fitting on a photographic record of the generated dot pattern it is possible to select very rapidly the "best" height and distance curve from a family based on (2).

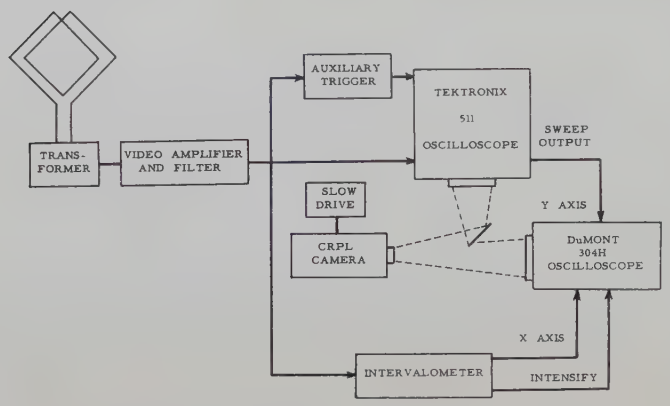

Fig. 1—Block diagram of recording system.

A block diagram of the recording system is shown in Fig. 1. The loop antenna is mounted in a manner to permit rotation to null out power line hum or interfering stations. The wide-band amplifier is of conventional design and has a pass band from approximately 1 kc to 20 kc. The limited pass band was necessitated by interference from nearby low-frequency transmitters. The resolution of the system was not significantly increased by including frequency components above 20 kc; in fact, an upper frequency limit of 10 kc was found adequate.

The auxiliary trigger device is provided to assure that the sweep will be initiated at the beginning of a received waveform regardless of the sign of the first half-wave.

The sweep output of the synchroscope is direct-coupled to the y-axis input of the direct-coupled oscilloscope (a DuMont 304H). The two oscilloscopes then sweep together.

The intervalometer is essentially a linear-sweep generator which re-initiates its sweep upon the occurrence of each input pulse. The time separation between pulses is thus measured by the excursion of the corresponding sweep. The reference point for time measurement on each pulse is taken as the positive peak of the pulse, identified as the point of zero first derivative.

The operation of the intervalometer can be understood by reference to Fig. 2, which shows the separate waveform operations in detail.

The input pulse is amplified to a convenient level, then base-clipped at a positive voltage sufficiently high to eliminate low amplitude components of the pulse and interference. The positive portion of the clipped waveform is differentiated, peak-clipped, and differentiated again to obtain a narrow pulse at the point of zero derivative of the input pulse. This derived pulse triggers a delay multivibrator, which triggers a second multivibrator which delivers a large positive pulse to a sweep circuit. The sweep circuit is simply a power triode, biased to cutoff, which has a condenser between plate and ground. An input pulse to the sweep tube causes it to conduct heavily and discharge the sweep condenser to zero, assisted by stray inductance in the circuit. The circuit must operate on irregularly occurring inputs, hence must be capable of discharging the sweep condenser and its output-coupling condenser from the power supply voltage to zero in a time less than the minimum expected interval (about 30 μsec) between input pulses.

The positive pulse from the delay multivibrator is used as a z-axis intensifying signal to the direct-coupled oscilloscope. A short bar of light then appears on the oscilloscope screen at the time of the peak of each input pulse. At the end of the short intensification period, the sweep circuit discharges to zero.

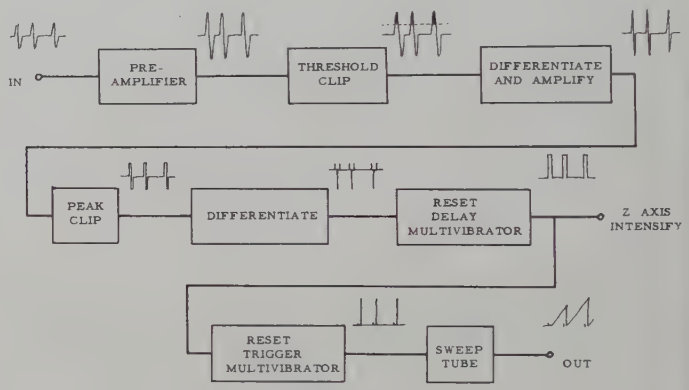

Fig. 2—Waveform operations of intervalometer.

The presentations of both oscilloscopes are recorded on a single 35-mm film strip by means of the camera and mirror system shown in Fig. 1. The shutterless camera is driven at approximately $\frac{3}{4}$ inch per second. Fig. 3 (opposite) illustrates the nature of the presentation. The received waveforms are recorded in the lower half of the picture, time running downward the output of the intervalometer, in the upper half of the picture, increasing time difference running from the center upward. The long-time sweep runs right to left and is approximately 9 msec in duration. Film motion is opposite to the sweep motion. Note that the origin of the atmospheric waveform and the origin of the locus of points derived from the waveform are displaced from each other on the record. A rear-surfaced mirror was used in making these pictures, hence the faint "ghost" in the waveform record which must be disregarded.

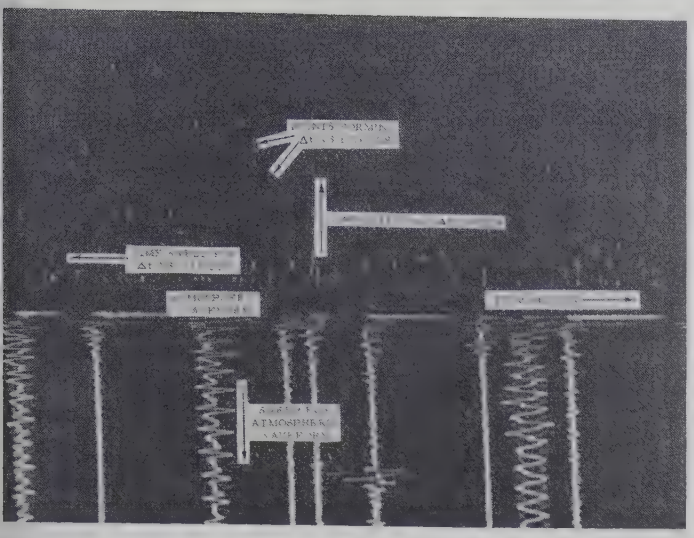

Fig. 3—Typical good atmospheric waveform and derived locus.

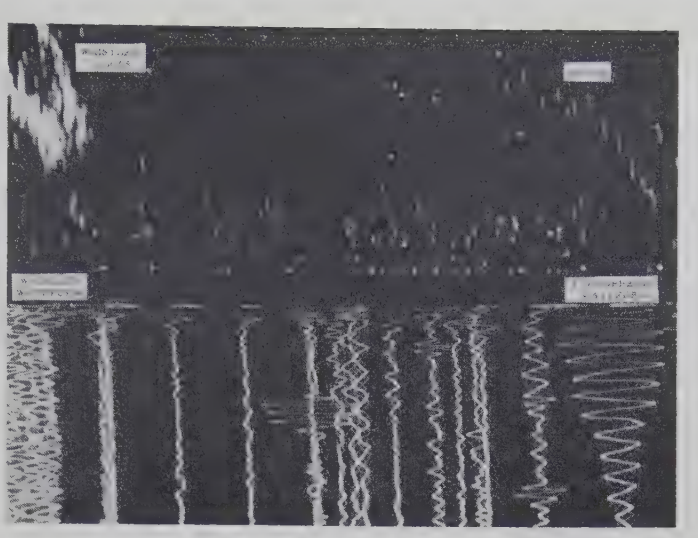

Fig. 4—Atmospheric waveforms followed by whistler.

In studying atmospherics, it has been found convenient and economical to record the atmospherics on magnetic tape and to operate the system with the tape record. Visual monitoring of the intervalometer presentation is used to decide what portions of the tape record are of sufficient interest to photograph.

Sample Records and Discussion

Fig. 3 is a good example of a locus resulting from an atmospheric waveform which is well explained by the simple theory of (2). One curve of time separation between pulses vs total time may be fitted to the locus of points from a family of curves previously computed from (2). There will be one best fit for a given height and distance.[6] The locus and waveform on the right side of Fig. 4 illustrates the limitations of the assumption of a simple layer structure in the ionosphere.

The atmospheric waveform indicated on the right side of Fig. 4 is of the type classified by Caton and Pierce[4] as "quasi-sinusoidal." Note how a locus is defined in the presence of many waveforms occurring at nearly the same time. Note also that the locus in this case departs from the smooth shape predicted by (1). The reason for the slightly erratic pattern is apparent from the skewed shape of the pulses in the wave form itself. The act of fitting a curve to the locus accomplishes essentially the same result as finding h and D from (3) and (4) for several intervals measured on a waveform and averaging the results. The erratic points at the end of the intervalometer locus correspond to the distorted pulses at the end of the waveform. The best fit to this rather poor locus is $h=90$ km and $D=1{,}500$ km.

[6] Note that h and D are not found by direct application of (3) and (4) but by identifying a particular change of time interval with time. Constant errors in measuring the time intervals will shift the locus slightly, producing errors in curve matching roughly proportional to the shift. Application of (3) and (4) involves the difference of differences between intervals, and small errors in reading individual intervals can produce large errors in h and D.

Curve-fitting by eye has the advantage of much greater speed and also permits one to reject points on a locus which apparently do not belong to the locus or to give them a weighted value. About seven points are necessary to identify a locus with a curve. The accuracy is chiefly limited by the quality of the locus obtained.

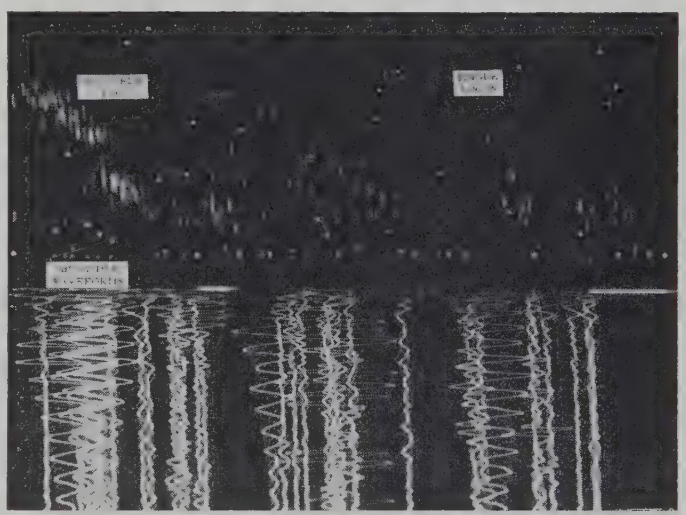

Fig. 5—Multiple atmospherics.

Good loci should give height to ± 3 km and distance to ± 50–200 km, depending upon the distance. Poor loci should give two or three times this error. The group of multiple atmospherics on the left side of Fig. 5 is probably of the same origin as in Fig. 4, observed at the same time. It is difficult to fit curves accurately to loci from rapid multiples at low film speeds.

The atmospheric discussed above was followed approximately one second later by a large whistler[7] (see left side of Fig. 5). This whistler was of sufficient ampli-

[7] A whistler is a relatively rare atmospheric which is usually heard as a musical tone descending from approximately 5 kc to about 1.5 kc in a period between 0.25 second and 1.5 seconds. The musical tone often has a swishing sound.

tude to trigger the synchroscope almost continually. Operation of the intervalometer during the dead time between synchroscope sweeps caused the bright bands to be recorded as in Fig. 4 with the time base provided by film motion. Note that a second weaker band is recorded which diminishes in frequency more rapidly than the brighter band. This effect has been observed by Potter,[8] but not while simultaneously recording the atmospheric preceding the whistler. The author has observed the tendency to form discrete bands which change frequency at different rates in most of the larger whistlers studied. The second band appears to diminish in frequency roughly twice as fast as the main bright band. Many whistlers appear to have maximum amplitude at the asymptotic limiting frequency of the large atmospheric that often precedes the whistler.

An "integrated locus" characteristic of an electrical storm giving rise to atmospherics may be obtained by making exposures of several seconds without film motion. With good conditions, the superposition of the loci from many individual atmospherics will form a single clearly defined locus which is characteristic of the layer height and the distance to the storm.

Conclusion

The recording system described should be a useful tool for the study of the ionosphere at very low frequencies by the use of atmospherics. With the addition of a direction-finding function, sources of lightning activity might be located and tracked. The ease of obtaining height and distance data makes practical the statistical study of large numbers of waveforms. Great economy is obtained by first recording the atmospherics on magnetic tape. Following that the interesting parts of the record are visually selected for transcription to film.

Two improvements of the recording system for atmospherics described in this paper are suggested. The first is to produce points on the locus from both positive and negative half-cycles of the atmospheric waveform. The second improvement is to make the base-clip level for a given pulse depend on the amplitude of the preceding pulse.

[8] R. K. Potter, "Analysis of audio frequency atmospherics," Proc. I.R.E., vol. 39, pp. 1067–1069; September, 1951.

Acknowledgment

The author gratefully acknowledges the suggestions and criticism of R. A. Helliwell of Stanford University. The completion of the work was partially supported by the Air Force Cambridge Research Center under Contract AF19 (604)-795. The initial work was supported in part by the Bureau of Standards under Contract CST-10751. While engaged in the development of this device, the author was attending Stanford University under a scholarship from the Douglas Aircraft Company, Inc. The presentation of the paper in Ottawa, Canada, was sponsored by the International Business Machines Corporation.

A Single-Control Tuning Circuit for Electrically Small Antennas*

R. E. WEBSTER†

Summary—**It is often desirable to tune electrically small antennas at their feed terminals. An "L" matching circuit for this purpose is considered. It is shown that one fixed element and one variable tuning element are adequate for certain small antennas. The manner in which losses affect the circuit effiiciency and the single-control tuning feature is discussed. Application of the technique to a tunable cavity antenna is noted.**

Introduction

ELECTRICALLY small antennas may be considered as nonresonant high-Q two-terminal networks. When such antennas are resonated with an ideal tuning element, the circuit half-power percentage bandwidth is given by

$$HPBW = \frac{1}{Q} = \frac{R_a}{|X_a|} = \frac{G_a}{|B_a|}, \quad [1]$$

where the antenna impedance is

$$Z_a = R_a + jX_a = \frac{1}{Y_a} = \frac{1}{G_a + jB_a}.$$

It is well appreciated that variable tuning is necessary if an impedance match is desired over a frequency bandwidth larger than a few per cent. A minimum of two tuning elements is required to match Z_a to a fixed real impedance, and generally both elements must be variable. The following comments concern a simple "L" matching circuit which, when used with impedances

* Original manuscript received by the PGAP, June 21, 1954. This article is based on work done under a contract between the Ohio State Univ. Res. Foundation and the Signal Corps Eng. Labs., Ft. Monmouth, N. J.

† Research Associate, Antenna Lab., Ohio State Univ., Columbus, Ohio.

[1] C. G. Montgomery, R. H. Dicke, and E. N. Purcell, "Principles of Microwave Circuits," McGraw-Hill Book Co., Inc., New York, N. Y., Sec. 4–13; 1948.

obtained with small antennas, can consist of one fixed and one variable tuning element. The required antenna is one for which $R_a = K_1 f^2$ or $G_a = K_2 f^2$ (the K's are arbitrary constants and f denotes frequency). This frequency dependence is realized in certain small dipoles, loops, and slots.

Definitions

The electrically small antennas considered are (1) dipoles less than 0.20 wavelength long, (2) loops less than 0.10 wavelength in diameter, and (3) slots less than 0.40 wavelength long. The frequency dependence of R_a or G_a mentioned above is satisfied approximately for these dipoles and loops, and for some slot configurations of these dimensions.[2,3]

The term "percentage bandwidth" will be used throughout to indicate

$$\frac{1}{Q} = \frac{R_a}{|X_a|} = \frac{G_a}{|B_a|}$$

when the antenna is resonated, the tuning elements being fixed. This is the fixed tuned bandwidth of the antenna and is not to be confused with the "tunable band."

The term "tunable band" is defined as the frequency range over which the antenna reflection coefficient is reduced to a specified value by proper adjustment of one tuning element.

The "tuning efficiency" is defined as follows:

$$\text{percent tuning efficiency} = \frac{\text{power delivered to antenna}}{\text{power input to tuning circuit}} \times 100.$$

The tuning efficiency is maximum when the tuning circuit losses are minimized. Since the losses in lumped circuit elements are proportional to the energy storage, the most efficient circuit will have the least stored energy. Thus a highly capacitive antenna will be tuned most efficiently by the minimum inductive reactance required for resonance. The circuits discussed here will achieve this maximum tuning efficiency when they are composed of lumped elements.

Single-Control Tuning Circuits

Basic Circuits

The approach will be to combine the Kf^2 frequency dependence of R_a or G_a with the reactance of one variable tuning element in such a manner that the second required tuning reactance will have the form $X_2 = K_3 f$ or $X_2 = -K_4/f$ (a lumped inductance or capacitance, respectively). Thus the second tuning element may remain fixed.

The circuit of Fig. 1 is an equivalent circuit proposed for the Tunable Cavity Antenna developed at this laboratory and described at the 1953 I.R.E. National Conference on Airborne Electronics.[4] Constructional and

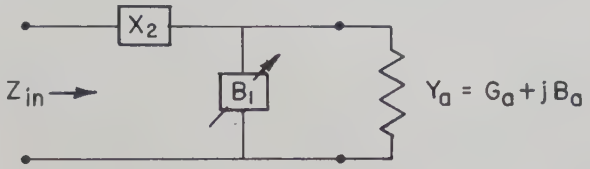

Fig. 1

operational details of this antenna are given in a technical report.[5] The assumptions for the circuit are that $G_a = K_2 f^2$ and $G_a \ll |B_a|$. The expression for Z_{in} is

$$Z_{in} = jX_2 + \frac{1}{G_a + j(B_1 + B_a)} = \frac{G_a}{G_a^2 + (B_1 + B_a)^2} + j\left[X_2 - \frac{(B_1 + B_a)}{G_a^2 + (B_1 + B_a)^2}\right]. \quad (1)$$

Let

$$\frac{G_a}{G_a^2 + (B_1 + B_a)^2} = R_{in} \quad (2)$$

and

$$X_2 - \frac{(B_1 + B_a)}{G_a^2 + (B_1 + B_a)^2} = 0, \text{ so that } Z_{in} \text{ is a constant real impedance.} \quad (3)$$

Then, from (2),

$$(B_1 + B_a) = \pm \sqrt{\frac{G_a}{R_{in}} - G_a^2}. \quad (4)$$

Substituting (4) in (3),

$$X_2 = \pm \sqrt{\frac{R_{in}}{G_a} - R_{in}^2}. \quad (5)$$

Eq. (3) is accomplished by properly adjusting B_1, and (5) results. With the additional condition $G_{in} = 1/R_{in} \gg G_a$, (5) becomes

$$X_2 \cong \pm \sqrt{\frac{R_{in}}{G_a}} = \pm \sqrt{\frac{R_{in}}{K_2 f^2}} = \pm \frac{1}{2\pi f C}, \quad (6)$$

[2] H. A. Wheeler, "Fundamental limitations of small antennas," Proc. I.R.E., vol. 35, pp. 1479–1484; December, 1947.

[3] M. H. Cohen, T. H. Crowley, and C. A. Levis, "The aperture admittance of a rectangular waveguide radiating into half space," Project Rep. 339-22, Antenna Lab., The Ohio State Univ. Res. Found., prepared under Contract W33(038)ac21114 with Air Res. and Dev. Command, Wright Air Dev. Center, Wright-Patterson Air Force Base, Ohio; November 14, 1951.

[4] D. R. McCoy, "Small tunable cavity antenna for nominally circular polarization," *Airborne Electronics*; 1953. Abstract of papers delivered at the 1953 I.R.E. Nat. Conf. on Airborne Electronics, Dayton, Ohio; May 11–13, 1953.

[5] R. W. Masters and D. R. McCoy, "A tunable cavity antenna," Tech. Rep. 486-13 (Confidential) Antenna Lab., The Ohio State Univ. Res. Found., prepared under Contract AF 18(600)-85, Air Res. and Dev. Command, Wright Air Dev. Center, Wright-Patterson Air Force Base, Ohio; November 5, 1953.

where

$$C = \sqrt{\frac{K_2}{4\pi^2 R_{in}}}.$$

Thus X_2, when taken to be negative, can be realized as a fixed capacitor. Then, in (3), (B_1+B_a) must also be negative. If $R_{in}>1$ (a typical value may be 50Ω), and since $|B_a| \gg G_a$, it is seen in (2) that B_1 must be of opposite sign from B_a and of somewhat different magnitude. Thus, if B_a is negative, B_1 must be positive and slightly smaller than B_a. The result is a single-control tuning circuit for use with small loops and slots subject to the following conditions:

(a) $G_a = K_2 f^2$

(b) $G_a \ll G_{in}$

(c) $(B_1 + B_a) = -\sqrt{G_a G_{in} - G_a^2}$

(d) $X_2 \cong -\sqrt{\frac{R_{in}}{G_a}}.$

B_1 is a variable capacitor, X_2 is a fixed capacitor.

The same argument can be applied to the dual of this circuit (see Fig. 2). In this case the conditions for a constant real input admittance ($Y_{in}=G_{in}$) are:

(a) $R_a = K_1 f^2$

(b) $R_a \ll R_{in}$

(c) $(X_1 + X_a) = -\sqrt{R_a R_{in} - R_a^2}$

(d) $B_2 \cong -\sqrt{\frac{G_{in}}{R_a}}.$

The antenna impedance is assumed to be capacitive with $|R_a| \ll |X_a|$. The resulting circuit is a fixed inductor B_2 and a variable inductor X_1 suitable for tuning short dipoles.

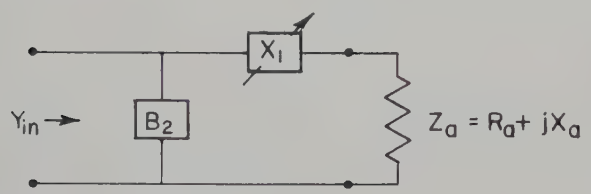

Fig. 2

Lossless tuning elements have been assumed. On this basis the tunable band is limited only by the percentage bandwidth desired at low frequencies and by the degeneration of conditions (a) and (b) at high frequencies (when the antennas become electrically large). In practice, however, circuit losses will considerably affect the tunable band as well as the tuning efficiency of the system.

Effect of Losses

Circuit losses should reduce the tunable band and the tuning efficiency, especially since the antennas of interest present very small radiation resistances. Consider first the tunable band. If loss factors R_2 and G_1 are assigned to the elements of Fig. 1, modified (5) is

$$X_2 = \sqrt{\frac{(R_{in} - R_2)}{(G_a + G_1)} - (R_{in} - R_2)^2}. \quad (7)$$

If $G_1 \ll G_a$ and $R_2 \ll R_{in}$, X_2 will retain the form of a fixed capacitor with the desired l/f variation. As frequency is decreased, however, $G_a \to 0$ as f^2, and may actually become smaller than G_1, thus producing a frequency dependence of X_2 different from l/f. A similar difficulty could be produced by a large R_2. A fixed capacitor may still be used for X_2, although the tunable band will be somewhat reduced. Thus the low-frequency end of the tunable band can be limited by circuit losses while the high-frequency limit is specified by the conditions (b). If the losses are appreciable over the entire theoretical tunable range, of course, the actual tunable band becomes very small. These effects apply equally to the dual circuit of Fig. 2, where modified (5) becomes

$$B_2 = \sqrt{\frac{(G_{in} - G_2)}{(R_a + R_1)} - (G_{in} - G_2)^2}. \quad (8)$$

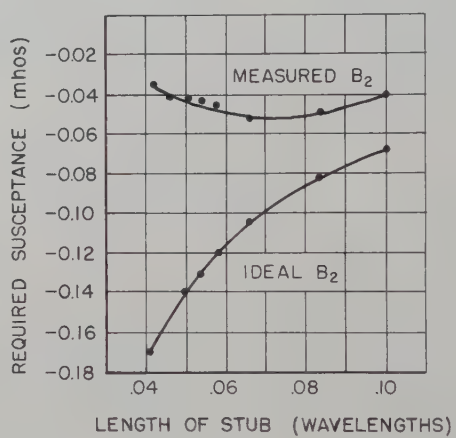

Fig. 3

Measurements made in the 250- to 600-mc range with coaxial-line tuning elements connected to a short vertical stub protruding from a horizontal ground screen demonstrated these effects. The circuit of Fig. 2 was simulated. Elements X_1 and B_2 were adjusted at each frequency to obtain a match to a 50-ohm slotted line. The tuned condition was determined by observing the standing wave on the slotted line. A directional coupler between the signal source and slotted line facilitated the tuning adjustments. Impedances of the tuning elements were then computed from measured positions of their shorting plungers. Fig. 3 shows a plot of the measured B_2 as a function of the electrical length of the stub. R_1 was the major loss resistance. The curve is of the form predicted by (8) when R_1 and R_a dominate at the low and high frequencies, respectively. The ideal variation of B_2, assuming lossless elements, is also shown in

ig. 3; it corresponds in frequency dependence to a xed lumped inductor. The measured B_2 will approach he ideal variation as the circuit losses approach zero. n the presence of losses, however, it is apparent that a xed inductance can be used to simulate the measured B_2 over a reduced tunable band. The resulting reflection oefficient, $|\rho|$, at a particular frequency is

$$|\rho| = \frac{|\Delta B_2|}{|\sqrt{(2Y_0)^2 + (\Delta B_2)^2}|}. \tag{9}$$

here ΔB_2 is the difference between measured B_2 [or B_2 s calculated by (8)], and B_2 of the fixed inductor. The orresponding expression for the circuit of Fig. 1 is

$$|\rho| = \frac{|\Delta X_2|}{|\sqrt{(2Z_0)^2 + (\Delta X_2)^2}|}. \tag{10}$$

f ΔB_2 is made equal to zero at 350 mc (0.058 wave- ength stub) by the use of a suitable fixed inductance, he reflection coefficients of Fig. 4 would result for the tub of measured B_2 given in Fig. 3.

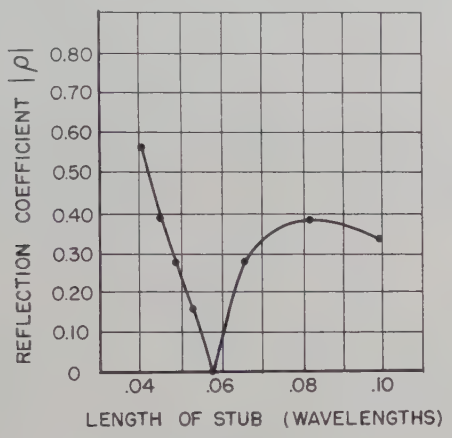

Fig. 4

Similar measurements made with coaxial-line tuning lements and a small loop antenna showed even more ronounced effects of losses on the tunable band be- ause of the correspondingly smaller radiation resist- nces. Such loops have one advantage over dipoles, owever, in that the required capacitive tuning ele- nents are superior in many instances to dipole tuning nductors with regard to losses.

The tuning efficiency for the circuit of Fig. 1 (with oss components added) is obtained by writing the ex- ressions for power input and power delivered to the ntenna in terms of the circuit voltages and currents. he result is

$$\text{per cent } E_{ff} = \frac{100}{1 + \frac{G_1}{G_a} + \frac{R_2}{G_a}[(G_a + G_1)^2 + (B_a + B_1)^2]}, \tag{11}$$

which for high-Q tuning elements ($G_1 \ll B_1$, $G_2 \ll B_2$, and $G_1 < G_a$) and with condition (b) satisfied, reduces simply to

$$\text{per cent } E_{ff} = \frac{100}{1 + \frac{G_1}{G_a} + \frac{G_2}{G_a}}, \tag{12}$$

or, for the dual circuit of Fig. 2,

$$\text{per cent } E_{ff} = \frac{100}{1 + \frac{R_1}{R_a} + \frac{R_2}{R_a}}. \tag{13}$$

Application

The application of these single-control tuning circuits is limited by losses in the tuning elements and in the antenna. Comparison of those losses with the antenna radiation conductance or resistance will indicate the efficiency [according to (11)] and the tunable band [from (7) and (10)] to be expected. The circuit of Fig. 1 where high-Q lumped capacitors can be used would seem to be most promising. The tunable cavity antenna mentioned previously embodies this feature. A tunable band of two to one with a reflection coefficient less than 0.15 has been obtained with this antenna for an aperture between one eighth wavelength and one fourth wavelength square.[5]

The problem of obtaining suitable inductances for use in the dual circuit of Fig. 2 is more formidable. The obvious procedure in this case is (a) obtaining the maximum Q inductance for X_1, (b) use of dipole with as large R_a/X_a ratio as possible, and (c) obtaining an optimum tunable band by adjusting the dipole length to achieve a compromise between condition (b) and the length for a minimum R_1.

The percentage bandwidth as defined above is a property of the antenna alone. It can be maximized by adjustment of the antenna for maximum R_a and minimum X_a.

Analysis of the circuits was based on the characteristics of lumped elements. The desired frequency dependence of the fixed tuned element, however, also results approximately for the case of a short length of coaxial line. Such an element may be useful when a fixed inductor or capacitor at high frequencies is desired. Coaxial lines may also be used to obtain the variable reactances. However, loss resistances and discontinuity susceptances must be taken into consideration with care in the selection of an element for a particular frequency.

Acknowledgment

The author wishes to thank Mr. R. W. Masters for his helpful advice.

Design of Line-Source Antennas for Narrow Beamwidth and Low Side Lobes*

T. T. TAYLOR†

Summary—It is well known that the phenomenon of radiation from line-source antennas is very similar to that of the diffraction of light from narrow apertures. Unlike the optical situation, however, antenna design technique permits the use of other-than-uniform distributions of field across the antenna aperture. Line source synthesis is the science of choosing this distribution function to give a radiation pattern with prescribed properties such as, for example, narrow angular width of the main lobe and low side lobes. In the present article the mathematical relationships involved in the radiation calculation are studied from the point of view of function theory. Some conclusions are drawn which outline the major aspects of synthesis technique very clearly. In particular, the problem of constructing a line source with an optimum compromise between beamwidth and side-lobe level (analogous to the Dolph-Tchebycheff problem[1] in linear array theory) is considered. The ideal pattern is $\cos \pi\sqrt{u^2-A^2}$, where $u=(2a/\lambda)\cos\theta$, a is the half-length of the source, and $\cosh \pi A$ is the side-lobe ratio. Because of theoretical limitations, this pattern cannot be obtained from a physically realizable antenna; nevertheless its ideal characteristics can be approached arbitrarily closely. The procedure for doing this is given in detail.

Introduction

THE term *line source* may be applied to any antenna which embodies a long, narrow, and straight geometry and which depends upon variations in field or current strength with respect to the longitudinal co-ordinate as the basis for its directivity. It is implied that these currents or fields are continuous functions of this longitudinal co-ordinate, hence arrays of discrete elements will not be considered as such. It is well known, however, that arrays of a large number of elements are most conveniently analyzed by regarding them as continuous distributions, therefore the remarks made here will apply—in this sense—to such arrays.

The pattern of a line source contains an element factor and a space factor. The element factor depends upon the type and orientation of fields or currents which make up a typical segment of the source, and usually has little directivity, at least in the direction in which it would augment the directivity of the space factor. The space factor is the highly directive factor; it is dependent for its shape upon the relative variation of field or current strength along the source and is the object of the antenna designer's art. In shaping the space factor, the designer may or may not wish to take cognizance of the element factor. In this article it will be assumed that he does not and that the objective is to design a space factor with the narrowest beamwidth and lowest side lobes consistent with both the available aperture and the necessity for avoiding a super-gain line source.

Let the line source, which has a total length $2a$, have a distribution function $g(x)$. Then the space factor is given by the familiar Fourier-transform relationship

$$S(v) = k\int_{-a}^{a} g(x)e^{ikxv}dx, \tag{1}$$

where $v=\cos\theta$ as illustrated in Fig. 1 and k is the free space wave number, $2\pi/\lambda$. It will be advantageous to introduce new variables as follows:

$$p = \frac{\pi x}{a} \tag{2}$$

$$u = \frac{2av}{\lambda}. \tag{3}$$

The quantity $\lambda/2a$ will be known as a *standard beamwidth*[2] and will prove useful later. With these substitutions, (1) becomes

$$S(u) = \frac{2a}{\lambda}\int_{-\pi}^{\pi} g(p)e^{ipu}dp. \tag{4}$$

The factor $2a/\lambda$ will be dropped and the integral denoted $F(u)$:

$$F(u) = \int_{-\pi}^{\pi} g(p)e^{ipu}dp. \tag{5}$$

Eq. (5) expresses the basic relationship which will be studied here.

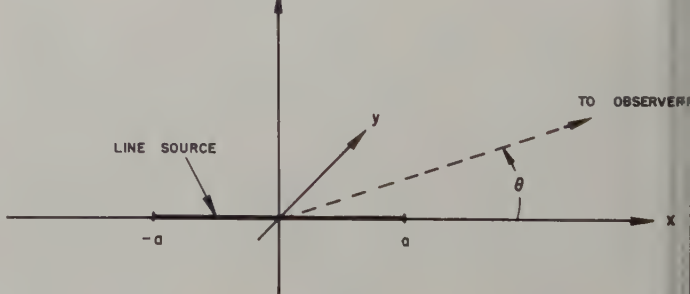

Fig. 1

Properties of the Distribution Function

It now becomes necessary to specify the hypotheses which the function $g(p)$ must satisfy in order that the results of this analysis will be applicable. An exhaustive

* Original manuscript received by the PGAP, April 26, 1954; revised manuscript received October 11, 1954. The work reported in this article was performed at the Hughes Aircraft Company and has been described in Hughes Aircraft Company Tech. Memo. No. 316. The work was sponsored by the Air Force Cambridge Research Center, Cambridge, Mass., under Contract AF 19(604)-262.

† California Institute of Technology, Pasadena, Calif.; formerly Research Physicist, Hughes Aircraft Co., Culver City, Calif.

[1] C. L. Dolph, "A current distribution for broadside arrays which optimizes the relationship between beamwidth and side-lobe level," Proc. I.R.E., vol. 34, pp. 335–348; June, 1946.

[2] The beamwidth between half-power points of a uniformly illuminated line source is 0.8859 of a standard beamwidth.

enerality is not attempted here; nevertheless, it is felt hat a high degree of relevancy to the physical situation achieved.

It is necessary, in antenna work, that $g(p)$ be single-alued, uniformly bounded, and at least piece-wise con-nuous in $-\pi<p<\pi$. However, anyone conversant with uch work will grant that there exists a large class of prac-ically important cases in which not only $g(p)$, but all its erivatives as well, are continuous over the full in-erval $-\pi<p<\pi$. This article is specifically concerned ith functions of the latter type and all general state-ents made henceforth are to be understood as apply-ng only to distributions which obey this hypothesis. he restriction, however, is not as stringent as might be upposed. All analytically expressible functions which re non-singular in the aforementioned interval, such s the uniform function $\cos p/2$, $J_0(p)$ (and an infinitude f others which have no specific names), belong to this lass. In fact, any function which is continuous in the nterval under discussion can be approximated arbi-rarily exactly by a member of this class. This article ill also, incidentally, be concerned only with even dis-ribution functions, since these are sufficient for the urpose at hand, namely the optimization of the com-romise between beamwidth and side-lobe level.

The degree of abruptness with which the source dis-ribution begins and ends at $p=\pm\pi$ will be a matter of onsiderable importance. Let the symbol "$\sim$" be read is asymptotic to." Then suppose that

$$\left.\begin{aligned} g(p) &\sim K(p+\pi)^\alpha \quad \text{as} \quad p\to-\pi \\ g(p) &\sim K(\pi-p)^\alpha \quad \text{as} \quad p\to+\pi \end{aligned}\right\}. \tag{6}$$

he quantity K is a non-zero constant in these equa-ions. The real parameter α, if an integer, is equal to the ultiplicity of the zeros in $g(p)$ at $p=\pm\pi$. Thus if $=0$, $g(p)$ assumes the fixed non-zero value K at these wo points and the distribution is said to have a "pedes-al." If $\alpha=1$, the distribution falls to zero linearly at its nds as in cosine distributions. If $\alpha=2$, it falls to zero uadratically as in cosine-squared distributions. All alues of α greater than -1, both integral and non-ntegral, will be considered. The not-uniformly-bounded istributions corresponding to α in the range $-1<\alpha<0$ re included in order to achieve a degree of completeness ecessary for later arguments, even though such values re not regarded as being physically realizable. If $g(p)$ s known analytically, α may be found by taking the mit as p approaches $-\pi$ of $(p+\pi)\,g'(p)/g(p)$, or the mit as p approaches π of $(p-\pi)\,g'(p)/g(p)$. Evidently, t is possible to write $g(p)$ as the product

$$g(p) = h(p)(\pi^2 - p^2)^\alpha, \tag{7}$$

here $h(p)$ is an even function which does not vanish at $=\pm\pi$ and which fulfills the other requirements apply-ng to $g(p)$.

Let us now reconsider (5) from the point of view of nction theory. Let the variables p and u be imbedded the complex domains ξ and z respectively, such that $\xi=p+iq$ and $z=u+iv$. The functions $g(p)$ and $F(u)$ are then profiles on the axes of reals of the functions $g(\xi)$ and $F(z)$. The visible range of the z-plane[3] is the real segment $-2a/\lambda\leqq u\leqq 2a/\lambda$, and a unit distance in the z-plane corresponds to one standard beamwidth (see Fig. 2). The integral in (5) becomes the limit at

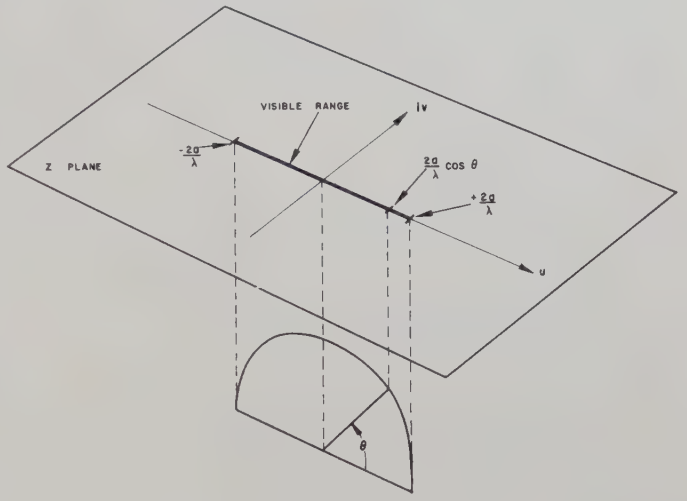

Fig. 2

τ tends to zero of the integral along C of Fig. 3, beginning at $-\pi+\tau$ and following the axis of reals to $\pi-\tau$ in the ξ plane. The limiting process is necessary because of the formal consideration of negative values of α.

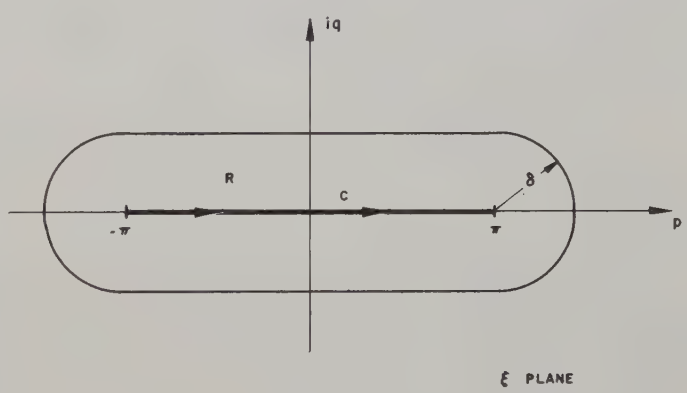

Fig. 3

Eq. (5) becomes

$$F(z) = \lim_{\tau\to 0}\int_C g(\xi)e^{i\xi z}d\xi. \tag{8}$$

This $g(\xi)$ is, of course, equal to the product $h(\xi)\ (\pi^2-\xi^2)^\alpha$. If we cut the ξ plane from $-\infty$ to $-\pi$ and from $+\pi$ to $+\infty$, then $(\pi^2-\xi^2)^\alpha$ is regular in this cut plane and should be regarded as being on its principal branch. Since it is desired that the asymptotic behaviour of

[3] An observer who travels around the line source to examine its radiation pattern will cover all real angles in the range $0\leqq\theta\leqq\pi$. This coverage is translated into the point set $-2a/\lambda\leqq u\leqq 2a/\lambda$, $v=0$, in the z-plane by the relationship $u=(2a\cos\theta)/\lambda$ as shown graphically in Fig. 2. Hence the term *visible range* is applied to this point set. The profile of $F(z)$ on the visible range is the only part of $F(z)$ which ormally enters into the formation of the radiation pattern.

$g(p)$ as p approaches $\pm\pi$ be as indicated in (6), i.e., be embodied entirely in the factor $(\pi^2-\xi^2)^\alpha$, it is essential that $h(\xi)$ be regular at least in neighborhoods of $-\pi$ and $+\pi$ and be different from zero at these points. Moreover, if $g(p)$ and all its derivatives are to be continuous in $-\pi<p<\pi$, $h(\xi)$ must be regular in a domain which contains this interval in its interior. Thus it is sufficient if $h(\xi)$ is different from zero at $\xi=\pm\pi$ and regular in the race-track shaped region R of Fig. 3, where δ is the arbitrarily small but non-vanishing radius of the ends of the region.

The hypotheses of this analysis may therefore be summarized as follows:

1. $g(p)$ is the profile on the real interval $-\pi<p<\pi$ of the principal branch of the function $h(\xi)$ $(\pi^2-\xi^2)^\alpha$.
2. $h(\xi)$ is regular in the region R of Fig. 3.
3. $h(\xi)$ does not vanish at $\xi=\pm\pi$.
4. $h(\xi)$ is even.
5. α is real and must be greater than or equal to zero for physically realizable distributions; however, values of α between -1 and zero will be considered for completeness of analysis.

Pattern Theorems

In this section, some basic theorems concerning the properties of the function $F(z)$ will be proved.

Theorem I: $F(z)$ is an even function of z.

This is a very simple theorem. Because of the evenness of $h(\xi)$ and of the factor $(\pi^2-\xi^2)^\alpha$, the transformation may be written as follows:

$$F(z)=\lim_{\tau\to 0}\int_0^{\pi-\tau} 2h(p)(\pi^2-p^2)^\alpha\cos pz\,dp, \qquad (9)$$

since $\cos p(-z)=\cos pz$, $F(-z)=F(z)$, and $F(z)$ is even.

Theorem II: $F(z)$ is an entire function of z.

Eq. (9) will be adopted as the point of departure in the proof of this theorem. It will be necessary and sufficient to show that:

1. The integrand is itself entire for every p in the interval $0\leqq p\leqq\pi-\tau$.
2. The integrand is continuous with respect to p for every p in the interval $0\leqq p\leqq\pi-\tau$ and for every z in the entire finite plane.
3. The limit of (9) is approached uniformly for z in G, where G is any closed bounded subset of the entire finite plane.

Conditions 1 and 2 are evidently satisfied. To demonstrate the fulfillment of condition 3, it must be shown that the difference, $f(z,\tau)$, between the integral in (9) and its limit is uniformly bounded for z in G and that this bound tends to zero as τ tends to zero. Evidently,

$$f(z,\tau)=\int_{\pi-\tau}^{\pi} 2h(p)(\pi+p)^\alpha(\pi-p)^\alpha\cos pz\,dp. \qquad (10)$$

A function is always uniformly bounded on a closed bounded set within its domain of regularity. Thus, for p in the closed interval $\pi-\tau\leqq p\leqq\pi$ and z in G, $|2h(p)(\pi+p)^\alpha|$ is bounded by some constant A, and since $\cos pz$ is entire with respect to z for every value of p in the stated interval, $|\cos pz|$ is bounded by another constant B. Therefore

$$|f(z,\tau)|\leqq AB\int_{\pi-\tau}^{\pi}(\pi-p)^\alpha dp \qquad (11)$$

$$|f(z,\tau)|\leqq\frac{AB\tau^{(1+\alpha)}}{1+\alpha}. \qquad (12)$$

Since $\alpha>-1$,

$$\lim_{\tau\to 0}|f(z,\tau)|=0 \qquad (13)$$

for every z in G, hence condition 3 is satisfied and $F(z)$ is entire. For further background in connection with this proof the reader should consult Copson.[4]

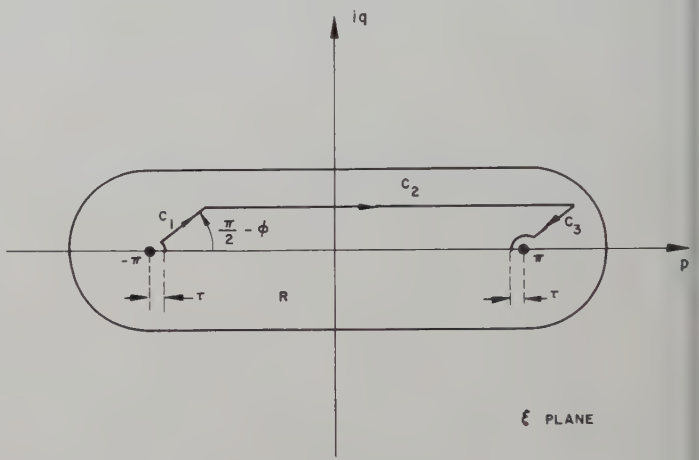

Fig. 4

Theorem III: as z tends to infinity, $F(z)$ has the following asymptotic forms

$$F(z)\sim h(\pi)(2\pi)^{1+\alpha}\Gamma(1+\alpha)\frac{\cos\pi\left(z-\frac{1+\alpha}{2}\right)}{\pi(z)^{1+\alpha}}$$

for $\operatorname{Re} z>0$ (14)

$$F(z)\sim h(\pi)(2\pi)^{1+\alpha}\Gamma(1+\alpha)\frac{\cos\pi\left(-z-\frac{1+\alpha}{2}\right)}{\pi(-z)^{1+\alpha}}$$

for $\operatorname{Re} z<0$ (15)

$$F(z)\sim h(\pi)(2\pi)^{1+\alpha}\Gamma(1+\alpha)\frac{e^{\pi|z|}}{2\pi|z|^{1+\alpha}}\quad\text{for Re } z=0. \qquad (16)$$

Proof of (14) depends upon deforming the contour C into the contour C_1 C_2 C_3 and subsequently allowing the radius of the small arcs to shrink to zero (see Fig. 4).

[4] E. T. Copson, "Theory of Functions of a Complex Variable," Oxford University Press, pp. 107 ff., 116; 1935.

It is easily shown that even for $-1<\alpha<0$ the contributions along the small arcs vanish. We begin by saying:

$$\left.\begin{aligned} & z = re^{i\phi} \\ & -\frac{\pi}{2} < \phi < \frac{\pi}{2}\,; \quad \phi \text{ is constant} \\ & r \to \infty \end{aligned}\right\}. \tag{17}$$

The angle ϕ determines the direction taken by the two parallel legs of the contour. The length of these legs is b, $\tau<b<\delta$. Let I_1 be the integral along C_1. Then

$$\left.\begin{aligned} \xi &= -\pi + \rho e^{i(\pi/2-\phi)} \\ d\xi &= d\rho e^{i(\pi/2-\phi)} \end{aligned}\right\} \tag{18}$$

$$I_1 = \lim_{\tau\to 0} \int_{\tau}^{b} h(\xi)(\pi - \xi)^{\alpha}\rho^{\alpha} e^{i\alpha(\pi/2-\phi)} e^{-i\pi z-\rho r} e^{i(\pi/2-\phi)} d\rho \tag{19}$$

$$I_1 = e^{-i\pi z} e^{i(1+\alpha)(\pi/2-\phi)} \lim_{\tau\to 0} \int_{\tau}^{b} h(\xi)(\pi - \xi)^{\alpha}\rho^{\alpha} e^{-\rho} d\rho. \tag{20}$$

Make a change of variable. Let $\rho = t/r$:

$$I_1 = \frac{e^{-i\pi(z-(1+\alpha)/2)}}{z^{1+\alpha}} \lim_{\tau\to 0} \int_{\tau r}^{br} h\left[-\pi + \frac{te^{i(\pi/2-\phi)}}{r}\right] \left[2\pi - \frac{te^{i(\pi/2-\phi)}}{r}\right]^{\alpha} t^{\alpha} e^{-t} dt. \tag{21}$$

The only significant contribution to this integral takes place at some finite t, specifically at $t=0$ if $\alpha\leqq 0$ or at $t=\alpha$ if $\alpha>0$. Hence two of the factors of the integrand can be removed as r tends to infinity; these become simply $h(-\pi)\ (2\pi)^{\alpha}$. Thus:

$$I_1 = \frac{e^{-i\pi(z-(1+\alpha)/2)} h(-\pi)(2\pi)^{\alpha}}{z^{1+\alpha}} \lim_{\tau\to 0, r\to\infty} \int_{\tau r}^{br} t^{\alpha} e^{-t} dt. \tag{22}$$

Since τ goes to zero independently of r, we may substitute zero for the lower limit. Then as r tends to infinity, the upper limit tends to infinity and the integral tends to $\Gamma(1+\alpha)$. Hence,

$$I_1 = h(-\pi)(2\pi)^{1+\alpha}\Gamma(1+\alpha) \frac{e^{-i\pi(z-(1+\alpha)/2)}}{2\pi(z)^{1+\alpha}}. \tag{23}$$

Similarly,

$$I_3 = h(\pi)(2\pi)^{1+\alpha}\Gamma(1+\alpha) \frac{e^{i\pi(z-(1+\alpha)/2)}}{2\pi(z)^{1+\alpha}}. \tag{24}$$

On C_2 we have

$$\left.\begin{aligned} \xi &= p + be^{i(\pi/2-\phi)} \\ d\xi &= dp \end{aligned}\right\}, \tag{25}$$

$$I_2 = \int_{-\pi}^{\pi} h(\xi)(\pi^2 - \xi^2)^{\alpha} e^{ipz} e^{-br} dp. \tag{26}$$

Here the function $h(\xi)\ (\pi^2-\xi^2)^{\alpha}$ is uniformly bounded on C_2 by some constant B. Then

$$|I_2| \leqq 2\pi B e^{\pi r \sin|\phi|} e^{-br}. \tag{27}$$

But the magnitude of one or the other of the two integrals I_1 or I_3 (depending upon the sign of ϕ) tends to $Kr^{-(1+\alpha)}\ e^{\pi r \sin|\phi|}$ for large r. Therefore $|I_2|$ will, for large r, always be negligible with respect to $|I_1|$ or $|I_3|$ or, if $\phi=0$, to both $|I_1|$ and $|I_3|$. The total integral is thus the sum of (23) and (24). Since $h(-\pi)=h(\pi)$ this sum is simply (14). Exp. (15) may be derived by deforming the contour as in Fig. 5, or by appealing to

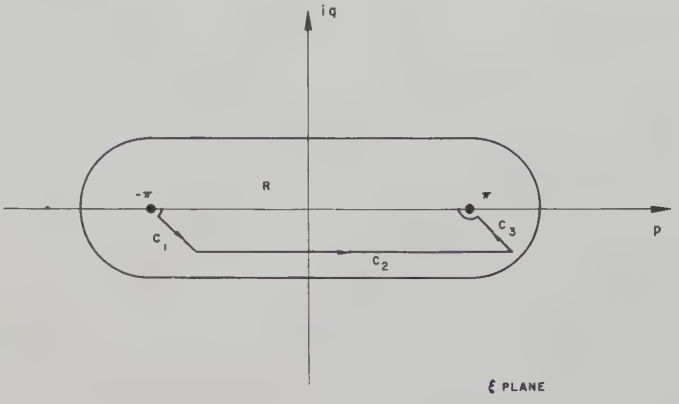

Fig. 5

Theorem I. Exp. (16) is simply the limiting form of both (14) and (15), and can also be derived by the methods used in obtaining (14) and working on the undeformed contour C. It is interesting to notice that when α is a non-negative integer there are no singularities at $\xi=\pm\pi$.

TABLE I

α	asymptotic form of $F(z)$
0	$h(\pi)(2\pi)\dfrac{\sin \pi z}{\pi z}$
1	$h(\pi)(2\pi)^2\dfrac{\cos \pi z}{\pi z^2}$
2	$h(\pi)(2\pi)^3(2)\dfrac{\sin \pi z}{\pi z^3}$
3	$h(\pi)(2\pi)^4(6)\dfrac{\cos \pi z}{\pi z^4}$

The contour of Fig. 4 can be swung around until it conforms to that of Fig. 5 without making a separate analysis. The net result, that one asymptotic expression suffices for all z, $|z|$ sufficiently large, is shown in Table I above. As a further consequence of Theorem III, it is seen that *the asymptotic behaviour of $F(z)$ depends only upon the manner in which $g(p)$ acts at the ends of the line source.* If there is a pedestal, the asymptotic form must be $\sin \pi z/\pi z$. If $g(p)$ falls to zero linearly at the ends of the line source the asymptotic form must be $\cos \pi z/\pi z^2$; if quadratically, it must be $\sin \pi z/\pi z^3$, etc. The decay rate of the remote side lobes in $F(z)$ is thus irrevocably fixed by conditions at the ends of the line source.

Theorem IV: Let the zeros of $F(z)$ be grouped in pairs: $\pm z_1$, $\pm z_2$, etc., and numbered in such a way that the moduli of the members of successive pairs do not decrease. Then the members of the nth zero pair tend to the positions $\pm (n+\alpha/2)$ as n tends to infinity.

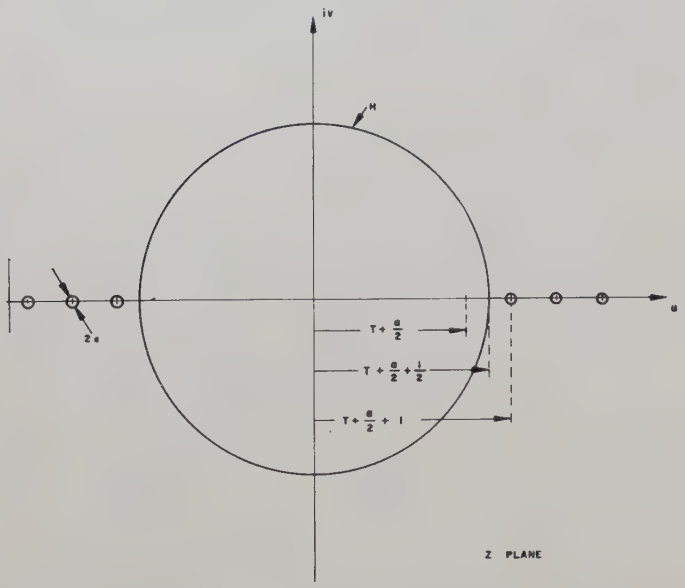

Fig. 6

In Fig. 6, circles of very small fixed radius ϵ have been drawn around the points $\pm[T+(\alpha/2)+k]$ where T and k are integers and $k=1, 2, 3, \cdots$. The large circle H has a radius of $T+(\alpha/2)+(1/2)$. Now if T is made large enough but finite, this system of circles will cover all the zeros of $F(z)$, for if the circle H is sufficiently large, $F(z)$ will approach its asymptotic form arbitrarily exactly in the region outside of H and the zeros of the asymptotic form of $F(z)$ do lie at the points $\pm[T+(\alpha/2)+k]$. The question which must be settled is that of the number of zeros within H. These zeros constitute a bounded set and their number cannot be infinite, for if it were they would have a limit point and $F(z)$ would have an essential singularity within H, a condition which contradicts the entirety of $F(z)$. Let the number of these zeros be $2M$, M an integer. Then $F(z)$ can be approximated arbitrarily exactly by the product of a polynomial of degree $2M$ and a canonical product on zeros outside of H located at the points $\pm[T+(\alpha/2)+k]$ where k runs from one to infinity.[5]

The only defect in this approximation is embodied in the small distances between the actual zeros of $F(z)$ and the points $\pm[T+(\alpha/2)+k]$ but these distances can be made smaller than any fixed ϵ by taking T large enough. The approximation, then, is

$$F(z) \doteq P_{2M}(z)\prod_{k=1}^{\infty}\left[1-\frac{z^2}{\left(T+\frac{\alpha}{2}+k\right)^2}\right]. \tag{28}$$

This canonical product is expressible in Γ functions, for

$$\frac{\left[\Gamma\left(T+\frac{\alpha}{2}+1\right)\right]^2}{\Gamma\left(T+\frac{\alpha}{2}+1+z\right)\Gamma\left(T+\frac{\alpha}{2}+1-z\right)} = \prod_{k=1}^{\infty}\left[1-\frac{z^2}{\left(T+\frac{\alpha}{2}+k\right)^2}\right]. \tag{29}$$

Hence from (28) the asymptotic form of $F(z)$, as $|z|$ becomes much greater than the radius of the circle H, is

$$F(z)\sim\frac{Kz^{2M}}{\Gamma\left(T+\frac{\alpha}{2}+1+z\right)\Gamma\left(T+\frac{\alpha}{2}+1-z\right)}, \tag{30}$$

where K is a constant including both the coefficient of z^{2M} in the polynomial and $[\Gamma(T+\alpha/2+1)]^2$. Now

$$\frac{1}{\Gamma(A)\Gamma(1-A)}=\frac{\sin \pi A}{\pi}. \tag{31}$$

Let $A=[z-T-(\alpha/2)]$. Then

$$F(z)\sim(-1)^T Kz^{2M}\frac{\sin\pi\left(z-\frac{\alpha}{2}\right)}{\pi}\cdot\frac{\Gamma\left(z-T-\frac{\alpha}{2}\right)}{\Gamma\left(z+T+\frac{\alpha}{2}+1\right)}. \tag{32}$$

By appealing to the Stirling approximation for $\Gamma(\mu)$, valid where $|\mu|$ is large and where a wedge-shaped region covering the negative axis of reals is excluded, it can be shown that

$$\frac{\Gamma\left(z-T-\frac{\alpha}{2}\right)}{\Gamma\left(z+T+\frac{\alpha}{2}+1\right)}\sim\frac{1}{z^{2T+1+\alpha}} \tag{33}$$

in a region which is even more extensive than that defined by $Re\ z>0$. Then certainly for $Re\ z>0$

$$F(z)\sim\frac{(-1)^T Kz^{2M}\cos\pi\left(z-\frac{1+\alpha}{2}\right)}{z^{2T}\pi z^{1+\alpha}}. \tag{34}$$

But by Theorem III, $F(z)$ is asymptotic to a constant $\times\cos\pi[z-(1+\alpha)/2]/\pi z^{1+\alpha}$ in the region defined by

[5] The technique of synthesizing the space factor of a line source by setting up the product of a polynomial and an entire transcendental function where the latter has the same zero arrangement as that just discussed here has been mentioned earlier by the author in less general terms in an unpublished paper, "An antenna pattern synthesis method with discussion of energy storage considerations," presented at the U.R.S.I. Washington Meeting; April 1951. Here, the quantity $T+(\alpha/2)$ is equal to the $N/2$ in that paper; only cases corresponding to non-negative integer values of α were treated.

Re $z>0$. *Hence we must conclude that* $M=T$ *and that there are* $2T$ *zeros within the circle* H. Therefore the zero within the ϵ neighborhood of $T+(\alpha/2)+1$ must have been a member of the $T+1$st pair of zeros, that within an ϵ neighborhood of $T+(\alpha/2)+2$ must have been a member of the $T+2$nd pair, etc. Therefore z_n tends to $n+(\alpha/2)$ as n tends to infinity, and the theorem is true.

Basic Design Considerations

We are now in a position to state some definite conclusions regarding the design of line sources for highly directive patterns. We have seen that the pattern of a finite line source, the even distribution function of which decays with the exponent α at the ends of the source, must have the following essential characteristics:

1. $F(z)$ must be an even entire function of z, $z=u+iv$.
2. The remote side lobes of $F(z)$ must decay as $|u|^{-(1+\alpha)}$.
3. The remote zeros of $F(z)$ must lie on the axis of reals and the members of the nth zero pair must approach the positions $\pm[n+(\alpha/2)]$ as n tends to infinity. The remote zeros are separated by unit intervals on the real axis.

Since, from the function-theoretic point of view, two entire functions with the same asymptotic behavior are but trivially different, we may expect any entire function possessing the characteristics noted to be the space factor of some hypothetical line source. Space factors will differ from one another, then, only in two aspects:

1. The value of α.
2. The placement of the central zeros; i.e., the zeros near the origin in the z-plane.

As with the space factors of arrays of discrete elements, zeros are precious items. In highly directive patterns they are used to "hold down" the average level of $F(z)$ in the side-lobe region and their absence over even a relatively short range permits a large lobe to appear. As an aid in visualizing this, the harmonic function $\log|F(z)|=U(u,v)$ may be regarded as describing an elastic surface which is supported at infinity and weighted down by small heavy weights at each of the zeros.

Since we are primarily concerned with the profile of $F(z)$ along the axis of reals, it is important to realize that the average value of this profile in the side-lobe region can best be minimized if all the zeros are on the axis of reals. A zero just off this axis produces a dip but not a null in the profile. Furthermore, it is a matter of experience[6] that if, in a given portion of the side-lobe region, a fixed number of zeros are available, the average side-lobe level will be lower if these zeros are spread out approximately uniformly rather than grouped in twos or threes or some other multiplicity. Therefore the first design conclusion is that for highly directive patterns, the central zeros of $F(z)$ should be simple zeros on the axis of reals. The remote zeros must follow this law anyway, hence, *for highly directive patterns all the zeros of* $F(z)$ *should be simple zeros on the axis of reals.*

Let us next consider the selection of a value of α. First of all, to insure that $g(p)$ will be uniformly bounded α must be greater than or equal to zero. But as α is increased the zeros of $F(z)$ abdicate from the central region of the z-plane, since the nth zero pair tends to the position $\pm[n+(\alpha/2)]$. Increasing α by one unit is tantamount to throwing away one zero. It is true that high values of α mean rapid decay rates of the remote side lobes, but since any side-lobe structure within the central region can be obtained anyway, and since the central region can be extended to cover the visible range, $-(2a/\lambda)\leqq u\leqq(2a/\lambda)$, a rapid decay rate of the remote side lobes will not be a normal desideratum in line-source design. *It follows, then, that* α *should have the smallest possible value, zero, and that the best distribution function for generating a highly directive pattern will have a pedestal.*

If α is to be zero, the remote zeros must be asymptotic to the integers; the whole design technique becomes a question of positioning the central zeros along the axis of reals in such a way that the best beamwidth is obtained compatible with the level of the central side lobes and in such a way that the members of the nth zero pair smoothly approach the positions $\pm n$.

An Entire Function with Uniform Side Lobes

Before proceeding with the technique of practical line-source design, it will be essential to formulate the ideal space factor, i.e., an entire function with uniform side lobes. Later it will become apparent that a practical line source can have a space factor whose characteristics approach the characteristics of this ideal space factor arbitrarily closely and that the ideal cannot be imitated exactly without resorting to super-gain.

G. J. van der Maas[7] has shown that as the number of elements of a Dolph-Tchebycheff array is indefinitely increased, the space factor approaches a function which (expressed in the present notation) is

$$F_0(u, A) = \cos \pi\sqrt{u^2 - A^2}. \tag{35}$$

Here A is an adjustable real parameter having the property that $\cosh \pi A$ is the side-lobe ratio. This function (35) is evidently the profile on the axis of reals of the entire function

$$F_0(z, A) = \cos \pi\sqrt{z^2 - A^2}, \tag{36}$$

[6] As an example, consider the entire function $f_1(z)=\cos \pi z$, which has equally spaced zeros and uniform lobes. Move the two zeros which straddle the origin together to form a double zero at the origin. The function becomes

$$f_2(z) = \frac{z^2 \cos \pi z}{z^2 - (\frac{1}{2})^2}.$$

The remote behavior is unchanged but the two central lobes of $f_2(z)$ have risen to 1.38 compared with 1.00 for $f_1(z)$.

[7] G. J. van der Maas, "A simplified calculation for Dolph-Tchebycheff arrays," *Jour. Appl. Phys.*, vol. 25, pp. 121–124; January, 1954.

which can be shown to have the zeros

$$z_n = \pm \sqrt{A^2 + (n - \tfrac{1}{2})^2}; \quad n = 1, 2, 3 \cdots \infty. \tag{37}$$

This entire function is clearly the ideal space factor. Its side-lobe region ($u^2 > A^2$) is populated by an infinite number of equal lobes of unit amplitude; its main lobe appears in the region $u^2 < A^2$ and has adjustable amplitude, as was pointed out. Nevertheless this space factor is unrealizable beecause the remote side lobes do not decay and the members of the nth zero pair are asymptotic to $\pm[n-(1/2)]$, both of which conditions correspond to an α value of -1, a value which contradicts the uniform boundedness of $g(p)$. However, any good practical space factor must have characteristics resembling those of $F_0(z, A)$ in the central region of the z-plane, but in the remote regions its side lobes must decay as $1/z$ and its zeros must tend to the integers, not the integers minus one-half. The problem is becoming clearer: in the central region the zero positions must be related to those of $F_0(z, A)$ but in the remote regions, the nth zero must tend to $\pm n$. A solution to this problem is proposed below.

Synthesis of a Practical Line Source Approaching Arbitrarily Closely to the Ideal

Let the practical space factor resemble the following function in the central region:

$$F_1(z, A) = \cos \pi \sqrt{\left(\frac{z}{\sigma}\right)^2 - A^2}, \tag{38}$$

the zeros of which are

$$z_n = \pm \sigma \sqrt{A_2 + (n - \tfrac{1}{2})^2}. \tag{39}$$

The constant σ is a number somewhat greater than unity. One can visualize (38) as an ideal space factor slightly dilated horizontally. Now let us choose σ such that eventually one of the zeros of $F_1(z, A)$ becomes equal to the corresponding integer, designated $\bar{n}$. Then

$$z_{\bar{n}} = \pm \bar{n} = \pm \sigma \sqrt{A^2 + (\bar{n} - \tfrac{1}{2})^2}, \tag{40}$$

whereupon σ is defined by

$$\sigma = \frac{\bar{n}}{\sqrt{A^2 + (\bar{n} - \tfrac{1}{2})^2}}. \tag{41}$$

We now propose to construct an entire function with the following zeros:

$$\begin{aligned} z_n &= \pm \sigma \sqrt{A^2 + (n - \tfrac{1}{2})^2} && \text{for } 1 \leqq n < \bar{n} \\ z_n &= \pm n && \text{for } \bar{n} \leqq n < \infty. \end{aligned} \tag{42}$$

The canonical product is

$$F(z, A, \bar{n}) = C \prod_{n=1}^{\bar{n}-1} \left\{1 - \frac{z^2}{\sigma^2[A^2 + (n - \tfrac{1}{2})^2]}\right\} \prod_{n=\bar{n}}^{\infty} \left(1 - \frac{z^2}{n^2}\right). \tag{43}$$

Let the second product be denoted $Q_{2(\bar{n}-1)}(z)$ to agree with the notation of the unpublished paper referred to earlier. This product has some convenient equivalent expressions:

$$Q_{2(\bar{n}-1)}(z) = \prod_{n=\bar{n}}^{\infty} \left(1 - \frac{z^2}{n^2}\right) \tag{44}$$

$$= \frac{[\Gamma(\bar{n})]^2}{\Gamma(\bar{n} + z)\Gamma(\bar{n} - z)} \tag{45}$$

$$= \frac{[(\bar{n} - 1)!]^2}{(\bar{n} - 1 + z)!(\bar{n} - 1 - z)!} \tag{46}$$

$$= \frac{\sin \pi z}{\pi z \prod_{n=1}^{\bar{n}-1} \left(1 - \frac{z^2}{n^2}\right)}. \tag{47}$$

The entire function with the zeros of (42) is

$$F(z, A, \bar{n}) = CQ_{2(\bar{n}-1)}(z) \prod_{n=1}^{\bar{n}-1} \left\{1 - \frac{z^2}{\sigma^2[A^2 + (n - \tfrac{1}{2})^2]}\right\}. \tag{48}$$

Here C is an arbitrary constant; if it is taken equal to $\cosh \pi A$ then $F_0(o, A) = F(o, A, \bar{n})$. Let us suppose that this has been done, then

$$\lim_{\bar{n} \to \infty} F(z, A, \bar{n}) = F_0(z, A); \tag{49}$$

for as $\bar{n}$ increases, more and more of the zeros of $F(z, A, \bar{n})$ follow the pattern of (39) and simultaneously $\sigma \to 1$, hence (49) is as stated. *Thus $F(z, A, \bar{n})$ defines a two-parameter family of entire functions whose members approach the ideal space factor arbitrarily closely as $\bar{n}$ is increased.* The value of $\bar{n}$, which is finite in any practical case, is of considerable significance. In relationship to the pattern, the points $\pm \bar{n}$ divide the region of uniform side lobes ($|u| < \bar{n}$) from the region of decaying side lobes ($|u| > \bar{n}$) where here, as before, $z = u + iv$. As $\bar{n}$ is increased, the region of uniform side lobes extends farther out from the main beam. In the region of uniform side lobes the lobes actually decrease slightly as $|u|$ increases and their initial level is very slightly lower (that is, better) than the design level, η. (Note that $\pi A = \text{arc cosh } \eta$.) The chief disparity between the practical pattern and the ideal is in the beamwidth, which is greater than the ideal by a factor almost exactly equal to σ. However, $\bar{n}$ does not have to be very large to make σ only a few per cent greater than unity.[8]

To summarize, the members of the pattern family $F(z, A, \bar{n})$ have two independent characteristics:

1. The design side-lobe ratio, η.
2. The boundary of the region of uniform side lobes, $\bar{n}$, an integer.

[8] For example, if the design side-lobe level is to be 25 db, $\eta = 17.78$; $A = 1.137$. Then if $n = 5$, $\sigma = 1.077$ and the beamwidth of the practical pattern will be only 7.7 per cent greater than that of $F_0(z, 1.137)$, the ideal pattern.

TABLE II

(1) Design side-lobe ratio (in db)	(2) η (Side-lobe voltage ratio)	(3) $\frac{180\beta_0}{\pi}$ (in deg.)	(4) A^2	(5) Values of the parameter σ						
				$\bar{n}=2$	$\bar{n}=3$	$\bar{n}=4$	$\bar{n}=5$	$\bar{n}=6$	$\bar{n}=7$	$\bar{n}=8$
0	1.00000	28.65	0.00000	1.33333	1.20000	1.14286	1.11111	1.09091	1.07692	1.06667
5	1.77828	34.49	0.14067	1.29351	1.18672	1.13635	1.10727	1.08838	1.07514	1.06534
10	3.16228	40.33	0.33504	1.24393	1.16908	1.12754	1.10203	1.08492	1.07268	1.06350
15	5.62341	45.93	0.58950	1.18689	1.14712	1.11631	1.09528	1.08043	1.06949	1.06112
20	10.0000	51.17	0.90777	1.12549	1.12133	1.10273	1.08701	1.07490	1.06554	1.05816
25	17.7828	56.04	1.29177	—	1.09241	1.08698	1.07728	1.06834	1.06083	1.05463
30	31.6228	60.55	1.74229	—	—	1.06934	1.06619	1.06079	1.05538	1.05052
35	56.2341	64.78	2.25976	—	—	—	1.05386	1.05231	1.04923	1.04587
40	100.0000	68.76	2.84428	—	—	—	—	1.04298	1.04241	1.04068

Once these two parameters have been chosen, the pattern, the distribution function, and all other relevant data may be calculated. In selecting $\bar{n}$, it is essential to avoid values that are too small; the change from $F_1(z, A)$ to $F(z, A, \bar{n})$, in which the trans-$\bar{n}$ zeros migrate to the integers, must be such as never to increase the spacing between any of these zeros. In order that this condition be fulfilled, $\bar{n}$ must be chosen such that a unit increase in $\bar{n}$ does not increase σ. Practically, this means that for a space factor with a design side-lobe ratio of 25 db, $\bar{n}$ must be at least 3, and that for a design side-lobe ratio of 40 db, it must be at least 6. Apart from this limitation one has considerable liberty in the choice of $\bar{n}$; large values make σ more nearly equal to unity, thereby sharpening the beam; however, the additional benefit obtained in this way soon becomes negligible. If $\bar{n}$ is increased sufficiently beyond the endpoint of the visible range, $2a/\lambda$, all the visible side lobes tend to become uniform. Such large values of $\bar{n}$ have the effect of supergaining the line source, a phenomenon which will be considered in detail in the next section. The choice of $\bar{n}$ may also be influenced by considerations of gain.

The beamwidth of the ideal space factor (in standard beamwidths) is a function of the side-lobe ratio only. It may be derived[9] from (35) and is given rigorously as follows:

$$\beta_0 = \frac{2}{\pi}\sqrt{(\operatorname{arc\,cosh}\eta)^2 - \left(\operatorname{arc\,cosh}\frac{\eta}{\sqrt{2}}\right)^2}. \qquad (50)$$

A curve showing the relationship (51) is presented in Fig. 7. The beamwidth of an $F(z, A, \bar{n})$ space factor is given by the following extremely good approximation:

$$\beta \doteq \sigma\beta_0 = \frac{\bar{n}\beta_0}{\sqrt{A^2 + (\bar{n} - \frac{1}{2})^2}}. \qquad (51)$$

Table II (above) shows relationships among various quantities discussed here. Column (1) of the table contains the design side-lobe ratio in decibels—a quantity which is usually chosen first in any synthesis procedure. Column (2) is self-explanatory. Column (3) gives β_0 expressed in degrees. This must be multiplied by $\lambda/2a$ to get the ideal beamwidth for a given line source. Column (4) gives the parameter A^2. Column (5) gives the parameter σ for several possible choices of $\bar{n}$. As an example, suppose a line source with a 30-db side-lobe level is required and that the aperture-to-wavelength ratio is 50, that is $(2a/\lambda)=50$. Then the ideal beamwidth is 60.55/50 or 1.211 deg. If it is decided to use an $\bar{n}$ of eight, $\sigma=1.05052$, and the practical beamwidth, that is, the beamwidth of the function $F(z, A, \bar{n})$, is 1.272 deg. The zeros of the pattern and the pattern itself may be readily calculated using σ and A^2. The places in the table where there is no entry for σ correspond to choices of $\bar{n}$ which are too small, as has been explained earlier.

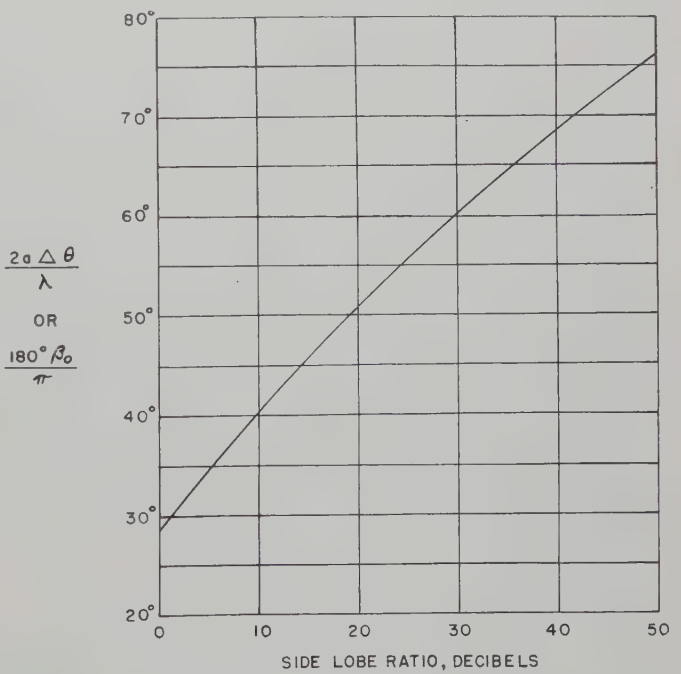

Fig. 7—Beam width vs. side-lobe ratio for ideal space factor.

[9] R. J. Stegen, "Excitation coefficients and beamwidths of Tchebycheff arrays," PROC. I.R.E., vol. 41, pp. 1671–74; November, 1953.
Stegen has derived essentially the same formula by considering Dolph-Tchebycheff arrays of large numbers of elements.

Gain and Super-Gain in Line Source Antennas

In this article the term *gain of a line source* means the ratio of power flux radiated in the direction of maximum intensity to the value of this flux averaged over all directions. If θ, ϕ are spherical co-ordinates in terms of which the radiation field is described and if $P(\phi, \theta)$ is the element factor (with dimensions of power-per-unit solid angle), the total power flux pattern is simply $P(\theta, \phi) \mid S(\cos\theta) \mid^2$. With θ_1, ϕ_1 representing the direction of maximum intensity, the gain is given by

$$G = \frac{P(\theta_1, \phi_1) \mid S(\cos\theta_1) \mid^2}{\frac{1}{4\pi}\int_0^{2\pi}\int_0^{\pi} P(\theta, \phi) \mid S(\cos\theta) \mid^2 \sin\theta d\theta d\phi}. \quad (52)$$

It has been mentioned that $P(\theta, \phi)$ usually has little directivity, especially in the θ co-ordinate. If $S(\cos\theta)$ is strongly directive and not endfire (θ_1 not near 0 or π), then a very good approximation for the gain is obtained by assuming that S has the properties of an impulse function and that $P(\theta_1, \phi)$ can therefore be factored out of the θ integral

$$G \doteq \frac{P(\theta_1, \phi_1)}{\frac{1}{2\pi}\int_0^{2\pi} P(\theta_1, \phi) d\phi} \cdot \frac{\mid S(\cos\theta_1) \mid^2}{\frac{1}{2}\int_0^{\pi} \mid S(\cos\theta) \mid^2 \sin\theta d\theta}. \quad (53)$$

The second factor in the above will be called G_0 and is the gain which the entire antenna would have if the element factor were isotropic; from the point of view of line-source design, G_0 is the quantity which one would naturally discuss when comparing various line sources on the basis of gain. In the present case the beam is presumed to be broadside and $\cos\theta_1 = 0$. Replacing $\cos\theta$ by ν, G_0 becomes

$$G_0 = \frac{\mid S(0) \mid^2}{\frac{1}{2}\int_{-1}^{1} \mid S(\nu) \mid^2 d\nu} = \frac{4a}{\lambda} \frac{\mid F(0) \mid^2}{\int_{-2a/\lambda}^{2a/\lambda} \mid F(u) \mid^2 du}. \quad (54)$$

The quantity $\lambda G_0/4a$, which will be called the specific gain, is of considerable importance in what is to follow. It is, of course, given by

$$\lambda G_0/4a = \frac{\mid F(0) \mid^2}{\int_{-2a/\lambda}^{2a/\lambda} \mid F(u) \mid^2 du}. \quad (55)$$

Now consider a line source with a distribution $g(p)$ of fixed functional form and let the ratio of physical length to wavelength be increased. This produces no change in $F(u)$, which is related to $g(p)$ through (5), however, it obviously changes the specific gain via the limits of the integral in (55). For very small values of $2a/\lambda$, the specific gain changes rapidly with respect to this quantity; when, however, $2a/\lambda$ passes into the region where the side lobes of $F(u)$ have become low and are getting lower by virtue of their asymptotic decay properties, the specific gain becomes practically constant and undergoes but little further change if $2a/\lambda$ increases all the way to infinity. As an example, the specific gain of a uniform distribution is plotted with respect to $2a/\lambda$ in Fig. 8. Evidently, the limiting value of the specific gain is an important line-source parameter, especially since it depends only upon the functional form of $g(p)$. This is shown by the following expression, in which the Parseval formula[10] for Fourier integrals has been employed:

$$(\lambda G_0/4a)_\infty = \frac{\mid F(0) \mid^2}{\int_{-\infty}^{\infty} \mid F(u) \mid^2 du} = \frac{\left| \int_{-\pi}^{\pi} g(p) dp \right|^2}{2\pi \int_{-\pi}^{\pi} \mid g(p) \mid^2 dp}. \quad (56)$$

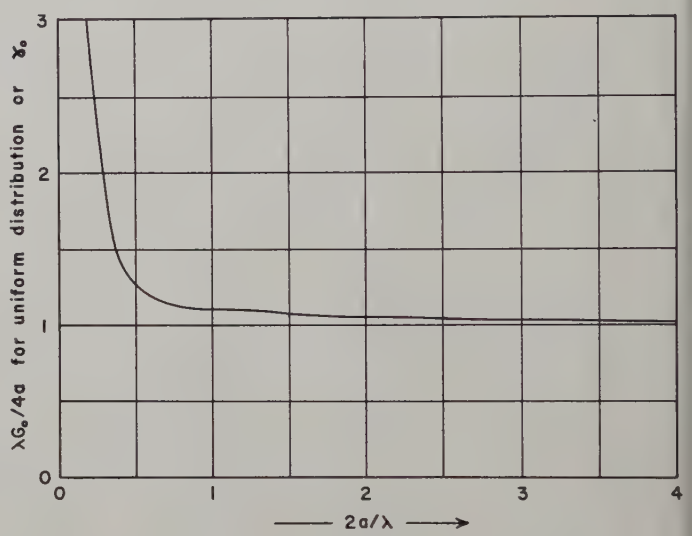

Fig. 8

If $g(p)$ is now varied, it is easy to prove that $(\lambda G_0/4a)_\infty$ takes on its greatest possible value, namely unity, when $g(p)$ is uniform. It is in this sense, and only in this sense, that a uniform distribution has a specific gain greater than that of any other type of line-source distribution.

When $2a/\lambda$ is finite, distributions with arbitrarily high specific gains can be synthesized—at least on paper. Starting with the space factor of the uniform distribution, $\sin\pi u/\pi u$, one can form the space factors for such super-gain distributions merely by rearranging the existing zeros to give an increased concentration of zeros in the visible range. This larger supply of zeros can be used to reduce the width of the main lobe while holding the relative level of the visible side lobes constant, thus enhancing the specific gain. At the same time, however, $(\lambda G_0/4a)_\infty$ must decrease because it had its

[10] E. C. Titschmarsh, "Theory of Fourier Integrals," Oxford University Press, pp. 50–51; 1948.

reatest possible value before the rearrangement of the eros took place. *It follows that super-gaining must increase the value of the ratio of* $\lambda G_0/4a$ *to* $(\lambda G_0/4a)_\infty$ *with espect to the value it would have if the distribution were niform.* This ratio, which has been called the super-ain ratio,[5] is given by

$$\gamma = \frac{\lambda G_0/4a}{(\lambda G_0/4a)_\infty} = \frac{\int_{-\infty}^{\infty} |F(u)|^2 du}{\int_{-2a/\lambda}^{2a/\lambda} |F(u)|^2 du}. \quad (57)$$

When this ratio is evaluated for a uniform distribution, t will be designated γ_0; the expression for this is

$$\gamma_0 = \frac{\pi/2}{Si(4\pi a/\lambda) - \dfrac{\sin^2(2\pi a/\lambda)}{(2\pi a/\lambda)}}. \quad (58)$$

Since $(\lambda G_0/4a)_\infty = 1$ for a uniform distribution, γ_0 is umerically equal to the specific gain in that case and s therefore also illustrated by Fig. 8.

It is seen from (57) that γ is the ratio of the total area o the visible area under $|F(u)|^2$; evidently, then, super-aining must increase the relative level of the invisible obes. Large values of γ also imply large ratio between nean square value of $g(p)$ and visible area under $|F(u)|^2$,

$$\gamma = \frac{\dfrac{1}{2\pi}\int_{-\pi}^{\pi} |g(p)|^2 dp}{\left(\dfrac{1}{2\pi}\right)^2 \int_{-2a/\lambda}^{2a/\lambda} |F(u)|^2 du}. \quad (59)$$

This means that, given two line sources with radiating lements which are identical and with respect to which he approximation of (53) applies, then the mean square alues of $g(p)$ in the two cases will be to each other as he two values of γ, when both sources are radiating the ame total power. This is but one of many ways of eaching the conclusion that line sources with an ap-reciable amount of super-gaining are impractical.

Up to this point, the term super-gain has been used o refer to line-source distributions whose specific gains re higher than that of a uniform distribution with the ame ratio of physical length to wavelength. It has been roved that such sources must have associated with hem values of γ which are greater than γ_0. The con-erse is not necessarily true, for high values of γ may esult from the movement of zeros into the visible range or the purpose of giving more character to the pattern, s in beam shaping, in ways which would not increase he specific gain. The debilities of super-gain sources esult, not from the increased gain, but from the in-reased value of γ. For this reason, it would be prefer-ble to extend the definition of a super-gain source to nclude all sources for which γ is greater than γ_0, whether the specific gain is greater than that of the cor-esponding uniform distribution or not. Super-gain is sed in this wider sense hereafter.

The answer to the question of how large a value of γ/γ_0 can be tolerated in a particular situation will depend upon many factors, most of which cannot be considered here. It seems reasonable, however, to look upon source distributions for which γ exceeds γ_0 by a factor of ten or more with extreme caution. The quantity $(\lambda G_0/4a)_\infty$ is especially sensitive to any shifting of the zeros into or toward the visible range and it can undergo a ten-fold change with very little provocation.

Several articles[5,11–20] dealing directly or indirectly with the subject of super-gain have appeared. Woodward and Lawson[17] base their article upon a two-dimensional formulation of the aperture problem but it contains concepts closely related to those developed here.

It remains to discuss $F(z, A, \bar{n})$ line sources from the point of view of super-gain. If $\bar{n}$ is less than $2a/\lambda$, the change from the space factor of a uniform distribution to an $F(z, A, \bar{n})$ space factor involves no migration of zeros into or toward the visible range, but only a rearrangement of the zeros already there, and the increase in γ/γ_0 will be inconsequential if it occurs at all. Even if $\bar{n}$ is somewhat larger than $2a/\lambda$, the relative area under the invisible lobes may still be small, especially if the design side-lobe level is low. Of course, if $\bar{n}$ is increased indefinitely, a point will be reached where further increase of $\bar{n}$ will have little effect upon the visible pattern but will continue to raise the level of the invisible lobes, making them approach the design level; the source can thus acquire an arbitrarily high degree of super-gaining. There is, of course, no need to resort to large values of $\bar{n}$ in order to realize most of the beam-sharpening potentialities of $F(z, A, \bar{n})$ sources, and hence there will rarely be any occasion to use such sources under conditions which would make γ/γ_0 large, even though this is theoretically possible.

By letting $\bar{n}$ tend to infinity, one approaches the ideal space factor, $F_0(z, A)$; the latter, therefore, has an infinite super-gain ratio associated with it. For this reason, it is inconceivable that a non-super-gain source could out-perform the ideal space factor with regard to the

[11] W. W. Hansen, "Notes on Microwaves," published in limited edition by engineers of Sperry Gyroscope Co., Inc., vol. 3, pp. 88–100; 1941–1944.

[12] S. A. Schelkunoff, "A mathematical theory of linear arrays," *Bell Sys. Tech. Jour.*, vol. 22, pp. 80–107; January, 1943.

[13] C. J. Bouwkamp and N. G. de Bruijn, "The problem of optimum antenna current distribution," *Phillips Res. Reports*, vol. 1, pp. 135–158; 1945–1946.

[14] A. Laemmel, "Source distribution functions for small high gain antennas," Microwave Res. Inst., Polytech. Inst. of Brooklyn, Report R-137-47, PIB-88; April 4, 1947.

[15] H. J. Riblet, "Note on the maximum directivity of an antenna," Proc. I.R.E., vol. 36, pp. 620–623; May, 1948.

[16] R. M. Wilmotte, "Note on practical limitations in the directivity of antennas," Proc. I.R.E., vol. 36, pp. 878; July, 1948.

[17] P. M. Woodward and J. D. Lawson, "The theoretical precision with which an arbitrary radiation pattern may be obtained from a source of finite size," *Jour. IEE*, vol. 95, pp. 363–370; 1948.

[18] T. T. Taylor, "A discussion of the maximum directivity of an antenna," Proc. I.R.E., vol. 36, p. 1135; September, 1948.

[19] L. J. Chu, "Physical limitations of omni-directional antennas," *J. Appl. Phys.*, vol. 19, pp. 1163–1175; December, 1948.

[20] N. Yaru, "A note on super-gain antenna arrays," Proc. I.R.E., vol. 39, pp. 1081–1085; September, 1951.

compromise between beamwidth and side-lobe level, especially if the visible range is extensive enough to include at least one complete pair of side lobes. The beamwidth-side-lobe relationship given in (51) and illustrated in Fig. 7 may therefore be regarded as the practical optimum compromise for the space factor of a line source. The words, " . . . for the space factor of . . . " are used advisedly, because it is possible to exploit the element factor (when there are collinear current elements, for example) and use a space factor with an increasing side-lobe characteristic to give a flat side-lobe characteristic in the total pattern. A small reduction of beamwidth can be achieved thus, as Sinclair and Cairns[21] have shown for arrays of discrete elements, but such techniques are beyond this article's scope.

The Inverse Transform and the Limiting Specific Gain

In calculating the distribution function $g(p)$ to give the space factor $F(z, A, \bar{n})$, the synthesis method of Woodward[22] will be used. Let $g(p)$ be analyzed into its Fourier components:

$$g(p) = \begin{cases} \sum_{m=-\infty}^{\infty} D_m e^{-imp} & p^2 \leqq \pi^2 \\ 0 & p^2 < \pi^2 \end{cases}. \tag{60}$$

By applying the Fourier transform (5) to this expression, term by term, the following result is obtained:

$$F(z) = 2\pi \sum_{m=-\infty}^{\infty} D_m \frac{\sin \pi(z - m)}{\pi(z - m)}. \tag{61}$$

The terms $\sin \pi(z-m)/\pi(z-m)$ are displaced from one another by integral steps along the axis of reals in the z-plane, hence the principal maximum of any coincides with a zero of all others. It follows that $F(m) = 2\pi D_m$, or

$$D_m = \frac{F(m)}{2\pi}. \tag{62}$$

Thus the Fourier coefficients of $g(p)$ are simply the pattern values at the integers. Since the space factors which have been considered are even functions, $D_{-m} = D_m$, and $g(p)$ in the range $p^2 \leqq \pi^2$ is given by

$$g(p) = \frac{1}{2\pi}\left\{F(0) + 2\sum_{m=1}^{\infty} F(m) \cos mp\right\}. \tag{63}$$

If the space factor belongs to the $F(z, A, \bar{n})$ family, (63) is very easy to use because $F(m, A, \bar{n})$ is zero for $m \geqq \bar{n}$, and the summation terminates.

It is of the utmost importance that the $F(m)$ be calculated correctly, hence the following simple check may be useful. This check is based upon the fact that there are two independent methods for calculating $g(\pi)$, When $\alpha = 0$, $h(\pi) = g(\pi)$ and, from Theorem III, there is a universal asymptotic expression for $F(z)$;

$$F(z) \sim 2\pi g(\pi) \frac{\sin \pi z}{\pi z} \quad \text{as} \quad |z| \to \infty. \tag{64}$$

In other words

$$2\pi g(\pi) = \lim_{|z|\to\infty} \frac{F(z)}{\dfrac{\sin \pi z}{\pi z}}. \tag{65}$$

Substituting the value of $2\pi\, g(\pi)$ obtained from (63), we find that the $F(m)$ must satisfy the following condition:

$$F(0) + 2\pi \sum_{m=1}^{\infty} (-1)^m F(m) = \lim_{|z|\to\infty} \frac{F(z)}{\dfrac{\sin \pi z}{\pi z}}. \tag{66}$$

The limiting value of the specific gain is easily exhibited in terms of the D_m. Appeal is made to the Parseval formula for Fourier series,[10] and the integral in the denominator of (56) becomes

$$\int_{-\pi}^{\pi} |\, g(p)\,|^2 dp = 2\pi \sum_{m=-\infty}^{\infty} |\, D_m\,|^2. \tag{67}$$

The integral in the numerator is simply $2\pi D_0$, and the gain expression becomes

$$(\lambda G_0/4a)_\infty = \frac{|\, D_0\,|^2}{\sum_{m=-\infty}^{\infty} |\, D_m\,|^2}. \tag{68}$$

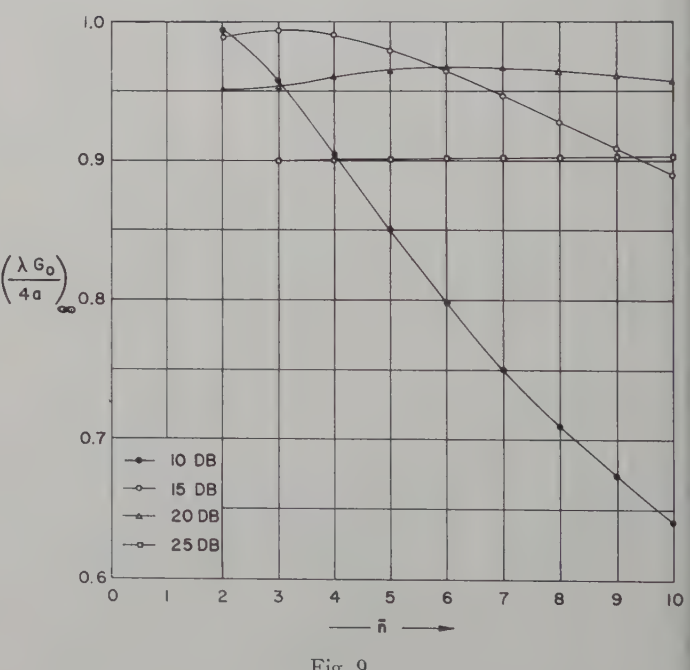

Fig. 9

Using this expression, the quantity $(\lambda G_0/4a)_\infty$ has been plotted as a function of $\bar{n}$ for four $F(z, A, \bar{n})$ line sources with design side-lobe ratios of 10, 15, 20, 25 db (Fig. 9).

[21] G. Sinclair and F. V. Cairns, "Optimum patterns for arrays of non-isotropic sources," *Trans. I.R.E.*, vol. PGAP-1, pp. 50–59; February, 1952.

[22] P. M. Woodward, "A method of calculating the field over a plane aperture required to produce a given polar diagram," *Jour I.E.E.*, vol. 93, pp. 1554–1558; 1946.

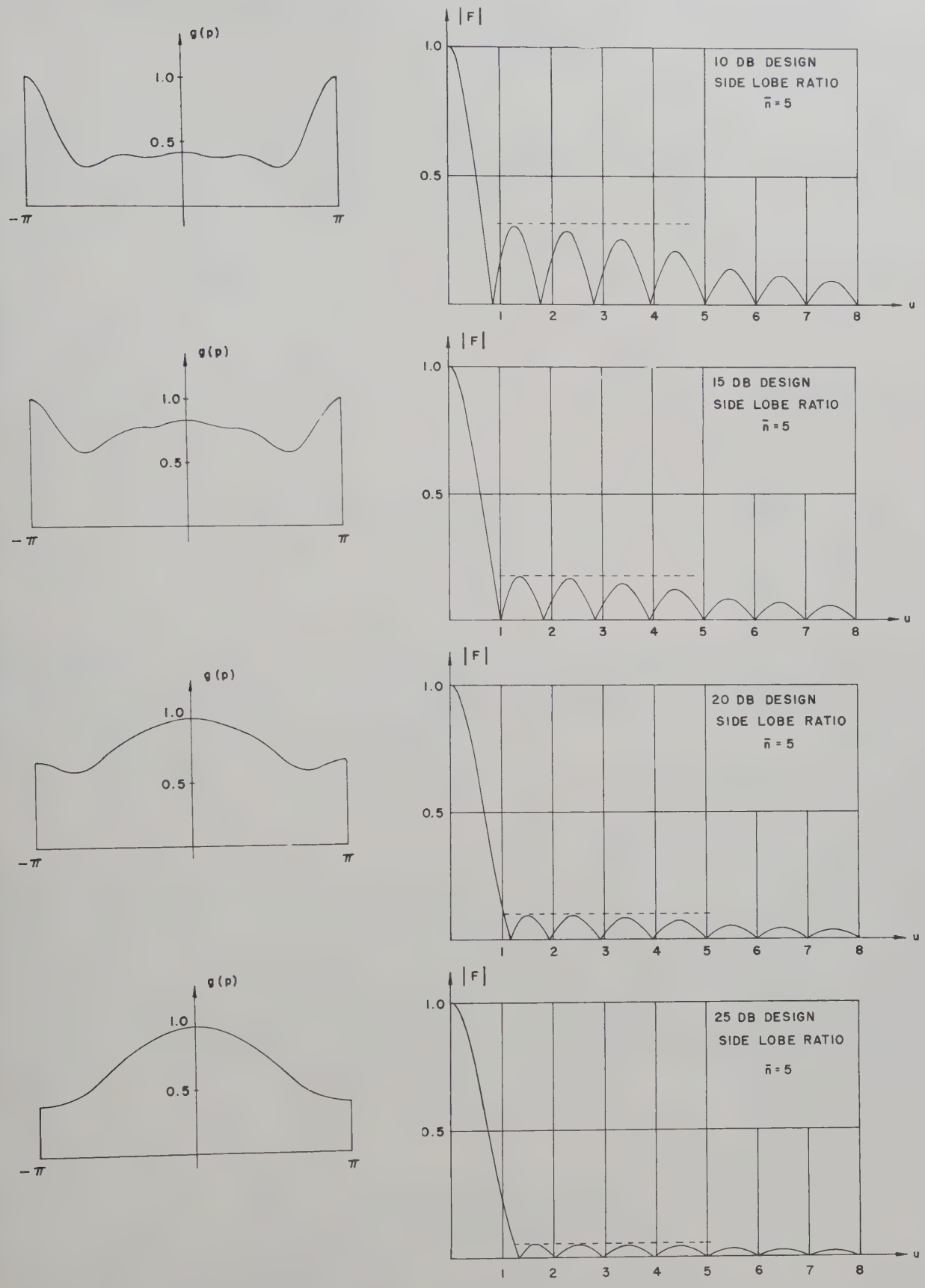
g(p)
1.0
0.5
−π
π
|F|
10 DB DESIGN
SIDE LOBE RATIO
n̄ = 5
15 DB DESIGN
SIDE LOBE RATIO
n̄ = 5
20 DB DESIGN
SIDE LOBE RATIO
n̄ = 5
25 DB DESIGN
SIDE LOBE RATIO
n̄ = 5
1 2 3 4 5 6 7 8
u

Fig. 10

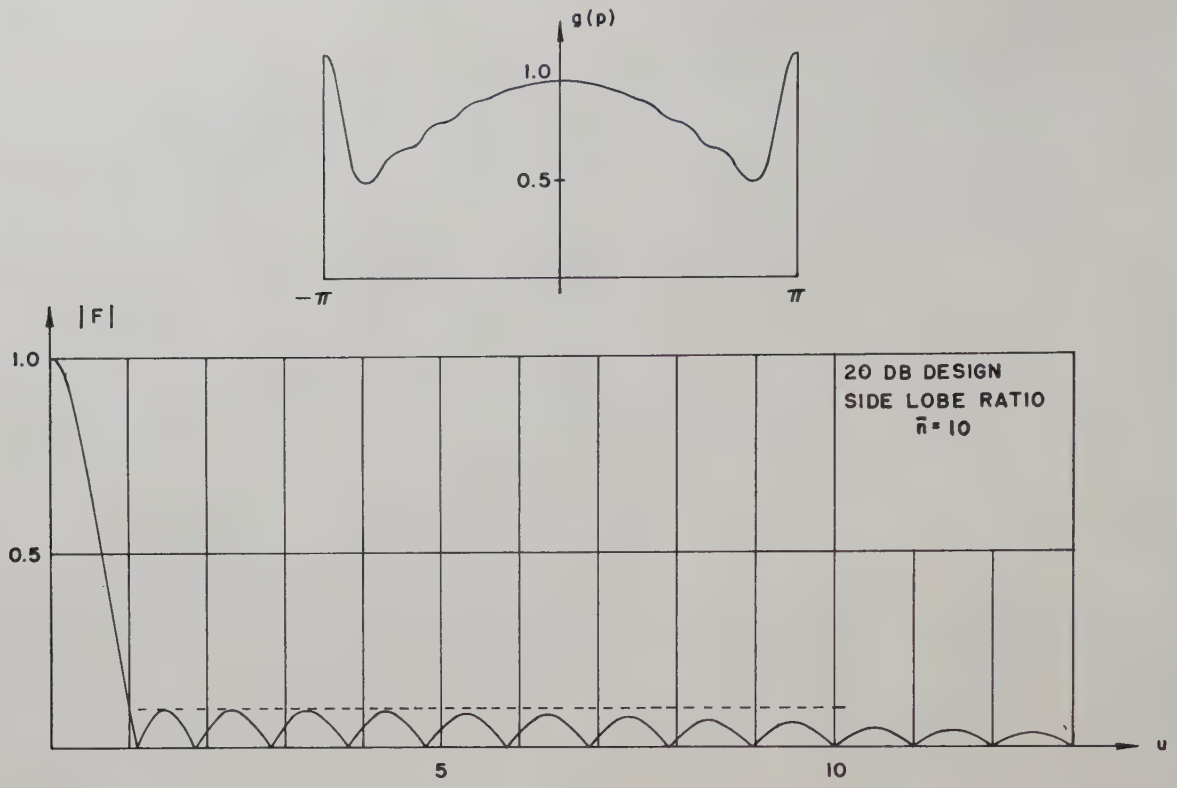

Fig. 11

According to (57), when $\gamma \doteq 1$ the limiting value of the specific gain is an excellent approximation for the specific gain itself. The quantity γ will be approximately equal to unity if the following conditions are simultaneously satisfied:

1. The ratio $2a/\lambda$ is of the order of or greater than five, for $1 < \gamma_0 \leqq 1.02$ when $2a/\lambda \geqq 5$.
2. The source in question has little or no super-gaining and therefore $\gamma \doteq \gamma_0$. This will be true for $F(z, A, \bar{n})$ sources when $\bar{n}$ is of the order of or less than $2a/\lambda$.

These conditions roughly define the domain of utility of the curves of Fig. 9 from the point of view of estimating the specific gain. To be more quantitative, one would have to find the indefinite integral of the function $|F(u, A, \bar{n})|^2$. This hardly seems worthwhile, since the majority of practical cases, especially in the field of high-gain antennas, will fall well within the domain outlined by the two conditions stated above.

As practical examples of the methods proposed in this article, complete calculations for 10, 15, 20, and 25 db line sources with $\bar{n} = 5$ have been performed. The results are illustrated in Fig. 10 (preceding page) which shows the source distribution and the space factor for each of these cases. Fig. 11 shows the corresponding data for a 20 db side-lobe source with $\bar{n} = 10$.

Acknowledgment

The writer is indebted to W. G. Sterns for initially posing the problem considered in this article and for calculating the 25 db source and pattern of Fig. 10. Most of the other numerical data appearing here were calculated or checked under the direction of Essor Maso and Dr. W. L. Doyle; this work is gratefully acknowledged. The writer is further indebted to Dr. L. C. Van Atta, Dr. R. S. Wehner, and especially to Dr. R. S. Elliott for their careful reading of the manuscript and helpful suggestions.

On the Input Conductance of Thin Antennas*

GIORGIO BARZILAI†

Summary—**Input conductances of thin antennas are computed by evaluating separately input voltage and radiated power for a prescribed value of the current near the maximum. The current distribution required to evaluate the radiated power and the input voltage is obtained by solving Hallèn's equation for the prescribed value of the current. First and second order computations were carried out for full wave antennas, and the results compared with those obtained by others.**

Introduction

IN RECENT years considerable attention has been given to the problem of computing the input admittances of thin antennas. With reference to the conductance component, two methods of computation can be used. The first evaluates the conductance as the real part of the ratio of the input current to the input voltage. The second computes this quantity as the ratio of radiated power to square of applied voltage.

It is the purpose of this paper to compute the conductances of thin antennas following the second approach, which has not generally been used, and to compare the results with the existing calculations.

The evaluation of the radiated power requires knowledge of the current distribution. This distribution can be obtained by prescribing the applied voltage and following Hallèn's procedure. In our case, however, the results are less dependent upon the choice of the expansion parameter used to solve the integral equation, if the current near the maximum is prescribed. The applied voltage must, therefore, be computed.

First and second order computations have been carried out for full wave antennas of three different thicknesses.

The Method of Computation

With reference to Fig. 1, let us consider a thin, center-driven, perfectly conducting cylindrical antenna. The driving voltage, V_0, is assumed to be applied through the gap, d, which is of infinitesimal length. It is well known that on the surface of such an antenna scalar and vector potentials satisfy transmission line equations. These two quantities (if $h=\lambda/4$, where λ is the wavelength) may be expressed as follows:

$$A(z) = A(h)\cos\theta + A\left(h-\frac{\lambda}{4}\right)\sin\theta \qquad (1)$$

$$V(z) = j\eta\left[A(h)\sin\theta - A\left(h-\frac{\lambda}{4}\right)\cos\theta\right]\epsilon(z) \qquad (2)$$

where $A(z)$ and $V(z)$ are vector and scalar potentials on the surface of the antenna at the height, z.

$$\eta = \sqrt{(\mu/\epsilon)} \cong 120\pi \text{ in free space,}$$

μ and ϵ are the permeability and the dielectric constants of the medium surrounding the antenna,

$$\theta = k(h - |z|), \qquad k = 2\pi/\lambda,$$

$$\epsilon(z) = \begin{cases} +1 & z > 0 \\ -1 & z < 0 \end{cases}.$$

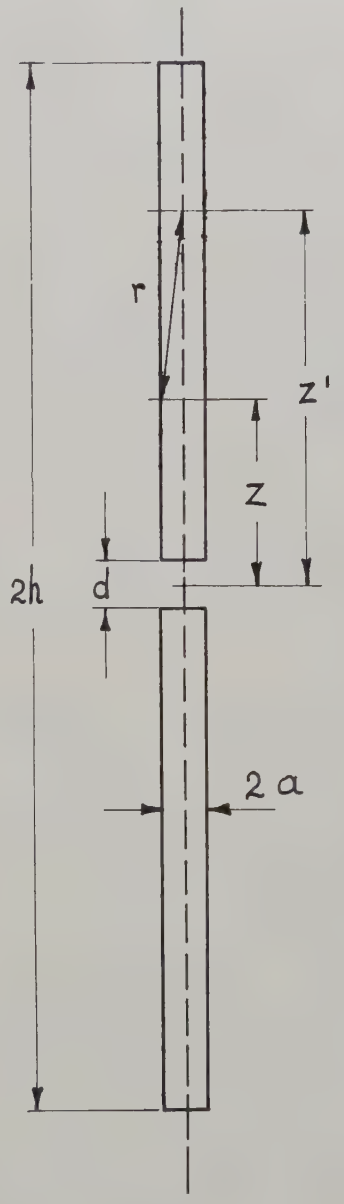

Fig. 1

On the other hand, the vector potential can be expressed in terms of its sources, the conduction current densities. In the case under discussion we can approxi-

* Original manuscript received by the PGAP, March 31, 1954; revised manuscript received October 11, 1954.
† Polytechnic Inst. of Brooklyn, Brooklyn, N. Y.

mate $A(z)$ as follows

$$A(z) = \frac{1}{4\pi}\int_{-h}^{+h} \frac{e^{-jkr}}{r} I(z')dz' \tag{3}$$

$$r = [a^2 + (z - z')^2]^{1/2},$$

where $I(z)$ is the current in the antenna at the height, z.

Upon taking (3) into account, (1) becomes an integral equation for the current which can be formally solved following Hallèn's procedure by letting

$$A(z) = \frac{1}{4\pi}[I(z)\Omega + f(z)] \tag{4}$$

$$\Omega = 21n\frac{2h}{a} \tag{5}$$

where $f(z)$ is a function essentially independent of a. We obtain

$$I(z) = I\left(h - \frac{\lambda}{4}\right)\sin\theta - \frac{1}{\Omega}\left[j(h)\cos\theta - f(z) + f\left(h - \frac{\lambda}{4}\right)\sin\theta\right]. \tag{6}$$

Assuming now $I[h-(\lambda/4)]$ prescribed, $I(z)$ can be expanded in a series of descending powers of Ω by using the well known iteration procedure.[1] As zero order solution we shall take

$$I_0(z) = I\left(h - \frac{\lambda}{4}\right)\sin\theta. \tag{7}$$

It has to be noted that solutions of any order vanish identically for $z = \pm h$.

The first order solution, immediately obtained from (6), is

$$I_1(z) = I_0(z) + \frac{1}{\Omega}\left[f_1(h)\cos\theta - f_1(z) + f_1\left(h - \frac{\lambda}{4}\right)\sin\theta\right], \tag{8}$$

where $f_1(z)$ is obtained from (4) assuming the current distribution, (7). Higher order solutions can be written down readily if desired.

We now recall that

$$V_0 = 2V(0^+), \tag{9}$$

where $V(O^+)$ is the value approached by $V(z)$ when $z \rightarrow O$ from the positive side. From (2) we obtain

$$V_0 = 2j\eta\left[A(h)\sin kh - A\left(h - \frac{\lambda}{4}\right)\cos kh\right]. \tag{10}$$

By using (7) for computing $A(h)$ and $A[h-(\lambda/4)]$ a first order solution, V_{01}, is obtained for the applied voltage, V_0. By using (8) a second order solution, V_{02}, can be obtained.

[1] E. Hallèn, "Theoretical investigations into the transmitting and receiving qualities of antennas," *Nova Acta* (Upsala, Sweden), vol. 11, no. 4; 1938.

We notice that since $V(z)$ can be expressed in terms of constants other than $A(h)$ and $A[h-(\lambda/4)]$, other expressions for V_0 can be obtained. For instance we can write

$$V_0 = 2j\eta A\left(\frac{\lambda}{4}\right). \tag{11}$$

If a certain order current is used to compute V_0, (10) and (11) will not, in general, yield same value for V_0.

The power radiated can be computed by the following expression

$$P = 30\int_{-kh}^{+kh}\int_{-kh}^{+kh} K(z - z')I(z)I^*(z')dzdz' \tag{12}$$

where the asterisk indicates the complex conjugate and

$$K(u) = \frac{1}{u^2}\left(\frac{\sin u}{u} - \cos u\right).$$

Eq. (12) lends itself to computations via the method of moments to yield approximate results. A detailed account of this method, as well as a justification of (12), is given by Schelkunoff and Friis.[2]

Once V_0 and P are determined the input conductance, $\hat{G}$, is immediately obtained by

$$\hat{G} = \frac{2P}{V_0 V_0^*}. \tag{13}$$

Numerical Computations

All the numerical computations have been carried out for $h = \lambda/2$. $I(h-\lambda 4) = 1$ has been assumed. Formulas to compute

$$f_1(z) = f_1^I(z) + jf_1^{II}(z)$$

are given in the literature.[3] We found

$$f_1(z) = -3.5523 - j1.9405. \tag{14}$$

The first order voltage, V_{01}, is obtained from (10) or (11) by taking into account (4):

$$V_{01} = 60[1.9405 - j(\Omega - 3.5523)]. \tag{15}$$

The numerical values for the first order powers are given in the literature.[4] In our case we have

$$P_1 = 99.54. \tag{16}$$

The first order conductance, $\hat{G}_1$, can therefore be expressed as follows

$$\hat{G}_1 = \frac{199.09}{K_a(K_a - 186.28) + 22231}. \tag{17}$$

[2] S. A. Schelkunoff and H. T. Friis, "Antennas—Theory and Practice," John Wiley and Sons, Inc., New York, N. Y., 1952.

[3] R. King and D. Middleton, "The cylindrical antenna: current and impedance," *Quart. Appl. Math.*, vol. 3, pp. 302–335; January, 1946.

[4] S. A. Schelkunoff, "Advanced Antenna Theory," John Wiley and Sons, Inc., New York, N. Y., 1952.

In (17) G_1 has been expressed in terms of the average characteristic impedance for cylindrical antennas defined as follows:

$$K_a = 60(\Omega - 2),$$

to facilitate the comparison with the corresponding formula obtained by Schelkunoff, using his mode theory of the antenna.[4]

To carry out second order computations, the second order voltage, V_{02}, and the second order power, P_2, have to be computed. The first order current necessary to compute these quantities is obtained from (8). It is interesting to notice, at this point, that the difference, $I_1(z) - I_0(z)$, which enters into all the calculations of the second order quantities, is inversely proportional to Ω. Furthermore we notice that if, instead of Ω, we use an expansion parameter, $\psi = \Omega + H$, where H is an arbitrary constant, the quantity inside the brackets in (8) will not change its value. This is apparent if we substitute $\Omega = \psi - H$ into (4), and we recall that (8) has been obtained using the current distribution, (7). These characteristic features of the method under discussion simplify the computations of V_{02} and P_2 for different values of Ω and different expansion parameters.

In what follows Ω will be assumed as the expansion parameter; however, all the results obtained will still be valid if ψ is substituted for Ω.

V_{02} can be computed from (3) and (11), and for the desired approximation simple numerical integrations are quite adequate.

The sinusoidal and cosinusoidal components appearing in (8) can be integrated without difficulty. To compute the contribution of the $f_1(z)$ component to V_{02}, we have applied the trapezoidal rule to the function,

$$f_1(z) - f_1\left(\frac{\lambda}{4}\right) \frac{e^{-jkr}}{r}.$$

Two sets of computations have been carried out, corresponding to the division of the interval of integration into 16 and 32 equal parts.

For 16 parts we obtained

$$V_{02} - V_{01} = \frac{60}{\Omega}(-1.58 + j2.72). \tag{18}$$

For 32 parts we obtained

$$V_{02} - V_{01} = \frac{60}{\Omega}(-1.46 + j2.66). \tag{19}$$

The error made by using (19) has been estimated to a few units in the last decimal place of the quantities inside parenthesis. This approximation is sufficient for our purposes as will be discussed later.

The computations for the second order power have been carried out by using the method of moments. This method consists essentially of replacing the integral, (12), with a double sum. It is equivalent to dividing the antenna into a certain number of sections and replacing each section with an elementary dipole having a moment equal to the integral of the current along the section under consideration and situated at the center of the same section.

It is a simple matter to integrate $f_1(z)$ in (8) analytically. Once the integral of $f_1(z)$ is known, the moments required for further computations follow immediately. For $h = \lambda/2$ we obtained

$$\begin{aligned}
&2k\int_0^z f_1(z)\,dz \\
&= [-2\,\mathrm{Si}\,2kz + \mathrm{Si}\,2(\pi - kz) + \mathrm{Si}\,2(\pi + kz)]\sin kz \\
&\quad + [-2\,\mathrm{Ci}\,2kz - \mathrm{Ci}\,2(\pi - kz) + \mathrm{Ci}\,2(\pi + kz)]\cos kz \\
&\quad + \left[-2\gamma - 2\ln\frac{\pi z}{\lambda} + \ln\frac{\lambda/2 + z}{\lambda/2 - z}\right]\cos kz \\
&\quad + 4\,\mathrm{Ci}\,kz - 2\,\mathrm{Ci}\,(\pi - kz) + 2\,\mathrm{Ci}\,(\pi + kz) \\
&\quad + j\{[-2\,\mathrm{Ci}\,2kz + \mathrm{Ci}\,2(\pi - kz) + \mathrm{Ci}\,2(\pi + kz)]\sin kz \\
&\quad + [+2\,\mathrm{Si}\,2kz + \mathrm{Si}\,2(\pi - kz) - \mathrm{Si}\,2(\pi + kz)]\cos kz \\
&\quad + \left[+\ln\left(\frac{\lambda^2}{4z^2} - 1\right)\right]\sin kz + \\
&\quad - 4\,\mathrm{Si}\,kz + 2\,\mathrm{Si}\,2(\pi - kz) - 2\,\mathrm{Si}\,2(\pi + kz)\}
\end{aligned} \tag{20}$$

where $\gamma = 5772\ldots$ and $z \geqq 0$.

Two sets of computations have been carried out for the second order power corresponding to the division of the antenna into 4 and 8 equal parts.

With 4 divisions we obtained

$$P_2 - P_1 = \frac{1}{\Omega^2}183 - \frac{1}{\Omega}71.1 \tag{21}$$

$$P_1 = 98.05. \tag{22}$$

With 8 divisions we obtained

$$P_2 - P_1 = \frac{1}{\Omega^2}193 - \frac{1}{\Omega}75.1 \tag{23}$$

$$P_1 = 99.12. \tag{24}$$

By comparing (16), (22) and (24), and noting that (21) and (23) yield values which differ by about 5 per cent for practically any value of Ω, we have estimated the error made in computing $P_2 - P_1$ by (23) to be a few per cent. We shall see that in this case also this approximation is sufficient for our purposes.

TABLE I

Ω	$\hat{G}_1$	$\hat{G}_{2,\Omega}$	$\hat{G}_{2,\Psi}$	G_2^H	G_2^K	G^S
10	1.220	1.081	1.033	0.869	0.995	1.243
15	0.410	0.383	0.376	0.345	0.374	0.403
20	0.202	0.192	0.190	0.181	0.190	0.197

In Table I we have recorded the results of our computations together with a list of the symbols used. In all the computations we have assumed for P_1 the value given by (16). King and Middleton's expansion param-

eter, ψ for $h \geqq \lambda/4$, is defined as follows:

$$\psi = \left| \Omega + f_1\left(h - \frac{\lambda}{4}\right) \right|.$$

As far as the accuracy for $\hat{G}_{2,\Omega}$ and $\hat{G}_{2,\psi}$ is concerned, we notice that if (18) instead of (19) is used, the last decimal place of $\hat{G}_{2,\Omega}$ will change by one unit for $\Omega = 10$, and will undergo no change for the other two values of Ω. We notice also that if (21) instead of (23) is used, the last decimal place of $\hat{G}_{2,\Omega}$ will change by three units for $\Omega = 10$, by one unit for $\Omega = 15$, and will undergo no change for $\Omega = 20$. It therefore seems reasonable to conclude that for $\Omega = 10$ an error of two or three units may affect the last decimal figure of $\hat{G}_{2,\Omega}$ and $\hat{G}_{2,\psi}$ while for the other two values of Ω the figures recorded in Table I should be correct.

Inspection of Table I shows that the method discussed leads, at least as far as second order results are concerned, to values for the input conductance which are rather insensitive to the choice of the expansion parameter. $\hat{G}_{2,\Omega}$ and$_2$, $\hat{G}_{\psi}$ do, in fact, differ by about four per cent.

Conductances are in millimhos. The symbols, $\hat{G}$, represent conductances computed as ratios of radiated power to the square of the input voltage. The symbols, G, represent conductances computed as the real part of the ratio of input current to input voltage.

List of Symbols

$\hat{G}_1$ = First order conductance computed by using (17).

$\hat{G}_{2,\Omega}$ and $\hat{G}_2$ = Second order conductances computed by the method discussed in this paper, using the expansion parameter Ω and ψ respectively.

G_2^H and G_2^K = Second order conductances according to Hallèn,[5] King,[3,6] and Middleton.[3]

G^S = Conductance according to Schelkunoff's mode theory.

[5] E. Hallèn, "Admittance diagrams for antennas and the relation between antenna theories," Cruft Laboratory, *Harvard University Report 46*, June 1, 1948.

[6] P. A. Kennedy and R. King, "Experimental and theoretical impedances and admittances of center-driven antennas," Cruft Laboratory, *Harvard University Report 155*, April 1, 1953.

Theory of Radio Reflections from Electron-Ion Clouds*

Von R. ESHLEMAN†

Summary—**Approximations to the reflection coefficients of electron-ion clouds of various sizes, shapes, and densities are determined. A simplified approach to the problem is employed, wherein the total reflection from the low-density clouds is computed by summing the scattered wavelets from the individual electrons, while the high-density clouds are treated as total reflectors at the critical density radius. Some of the limitations of this method are discussed. While more elaborate determinations should be used in certain regions of cloud size and density, the method used here provides an over-all, first-order approximation of the effects of size, shape, and density on the reflecting properties of electron-ion clouds. Several possible applications of the theoretical results are outlined.**

Introduction

A THEORETICAL investigation of radio reflections from ionized regions has direct application to the study of such ionospheric irregularities as sporadic-E ionization, auroral ionization, and meteor ionization trails. An attempt is made here to obtain results which are general enough to provide a first-order approximation of the effects of size, shape, and density on the reflecting properties of electron clouds. More thorough analyses have been presented elsewhere for ionized regions having more specific properties. However, it is believed that the simplified treatment which follows may result in a useful method for analyzing the salient characteristics of radio reflections from electron-ion clouds having general sizes, shapes, and densities. Only the back-reflected signals are determined; that is, the radio transmitter and receiver are assumed to be at the same location.

In order to determine the general effects of cloud shape, the three basic geometrical configurations are considered. That is, the electrons are distributed in n dimensions about a $(3-n)$ dimensional origin. For $n=1$, $n=2$, or $n=3$, the electron volume density is a function of the distance from a reference plane, line, or point, and the clouds have a laminal, cylindrical, or spherical shape, respectively. A simplified method is employed to determine the reflection from such clouds having any size and electron content, and having several different distributions of electron density as a function of distance from the origin. Particular attention is given the clouds which result from normal diffusion in n dimensions from an instantaneous source of $(3-n)$ dimensions.

It is assumed that for low electron densities, each electron scatters freely and independently, while for high densities, total reflection occurs at the surface of

* Original manuscript received by the PGAP, March 31, 1954; revised manuscript received, October 11, 1954. This work was supported jointly by the U. S. Navy (Office of Naval Research), the U. S. Army Signal Corps, and the U. S. Air Force, Contract N6onr-251 Task 7.

† Radio Propagation Lab., Stanford Univ., Stanford, Calif.

critical electron density. The reliability of these assumptions is discussed. The effects of the geomagnetic field, recombination and attachment, and collision and radiation damping are not considered. These factors are usually unimportant for high-frequency radio reflections from ionospheric irregularities in the *E*-region.

The emphasis in this paper is on the development of the theoretical results, though several possible applications are suggested.

Low-Density Clouds

The scattered electric field strength at range R' from a single electron moving in the ξ direction with acceleration $\ddot{\xi}$ is, in meter-kilogram-second units, $\mu_0 e\ddot{\xi} \sin \alpha/4\pi R'$, where μ_0 is the permeability of free space, e is the magnitude of the electronic charge, and α is the angle between the ξ direction and the direction to the field point. The acceleration of a free electron acted upon by an incident electromagnetic wave is, omitting the exp $(-i\omega t)$ time variation, $-E_{\text{inc}}e/m$, where m is the electron's rest mass. In the problems under consideration, the radio transmitter and receiver are at the same location, so that $\sin \alpha = 1$. Thus, the ratio of the scattered-field strength at the receiver to the incident-field strength at the single electron is given by

$$\frac{E_{sc}}{E_{\text{inc}}} = -\left(\frac{\mu_0 e^2}{4m}\right)\frac{1}{\pi R'}, \tag{1}$$

where $\mu_0 e^2/4m = 0.8852 \cdot 10^{-14}$ meters. With the assumption that the electrons scatter freely and independently, the scattered-field strength from an ensemble of electrons may be found by vectorially adding their individual contributions. When the extent of the cloud is small compared to its range, the incident wave is essentially constant in amplitude throughout the cloud. Thus,

$$\frac{E_{sc}}{E_{\text{inc}}} = -\left(\frac{\mu_0 e^2}{4m}\right)\frac{1}{\pi R}\int_v N \exp(2ikR')dv, \tag{2}$$

where R is the range to a reference point within the cloud, N is the electron volume density, and k is the wave number, $2\pi/\lambda$.

In Fig. 1, laminal, cylindrical, and spherical electron clouds are illustrated. While these clouds are infinite in some dimensions, the phase factor controls the echo amplitude in such a manner that the important scattering region is small in extent, so that (2) still applies. Note that the co-ordinates are chosen and named so that, in each case, N is a function of r only. Assuming that $r < (\pi R/k)^{1/2}$, (2) can be simplified to read

$$\frac{E_{sc}}{E_{\text{inc}}} = \left[\left(\frac{\mu_0 e^2}{4m}\right) q_n \left(\frac{k}{2}\right)^{n-2}\right] \cdot 2^{n-2}(\pi kR)^{(1-n)/2} \frac{\int_0^\infty N(r)F_n(r)r^{n-1}dr}{\int_0^\infty N(r)r^{n-1}dr}. \tag{3}$$

In this expression, q_n is the total number of electrons /meter^{3-n} of the cloud and $F_n(r) = (kr)^{(2-n)/2}\Gamma(n/2)J_{(n-2)/2}(2kr)$, so that $F_1(r) = \cos(2kr)$, $F_2(r) = J_0(2kr)$, and $F_3(r) = [\sin(2kr)]/(2kr)$.

Let the dimensionless quantity which is bracketed in (3) be represented by X_n. Thus, X_1 is proportional to the wavelength and to the number of electrons per square meter in the laminal clouds. Similarly, X_2 is proportional to the number of electrons per meter in the cylindrical clouds, and X_3 is proportional to the number of electrons in the spherical clouds and inversely proportional to the wavelength.

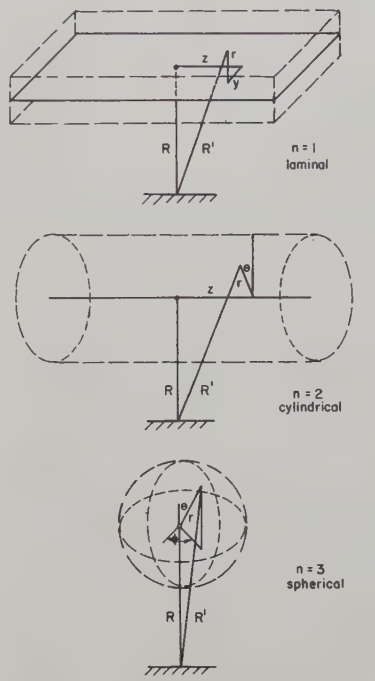

Fig. 1—Laminal, cylindrical, and spherical electron clouds.

It is convenient to define the reflection coefficients ρ_n of the electron clouds in the following manner:

$$\frac{E_{sc}}{E_{\text{inc}}} \equiv \rho_n 2^{(n-3)/2}(\pi kR/2)^{(1-n)/2}. \tag{4}$$

The $(\pi kR/2)^{(1-n)/2}$ factor is a normalizing expression commonly used to make the geometrical optics reflection coefficients of metal cylinders and spheres independent of range and proportional to some function of the target size in wavelengths. The $2^{(n-3)/2}$ factor originates from the difference between plane-wave and spherical-wave incidence upon the target. Other expressions which are often used to describe the reflection properties of radar targets may be related to the reflection coefficient defined above, from the following definitions: $(E_{sc}/E_{\text{inc}})^2 \equiv (2kR/G)^2$ $P_R/P_T \equiv \sigma/4\pi R^2$, where G is the antenna power gain over an isotropic radiator, P_R and P_T are the received and transmitted peak powers, and σ is the radar cross section.

Using (4), the reflection coefficients of the low-density clouds become

TABLE I

REFLECTION COEFFICIENTS FOR LOW-DENSITY CLOUDS

Radial electron distribution	ρ_{1L}	ρ_{2L}	ρ_{3L}
Homogeneous $N/N_0=1,\ 0<r<a$ $=0,\ a<r<\infty$	$(X_1 \sin b)/b$ $[b^{-1}]$	$2X_2J_1(b)/b$ $[b^{-3/2}]$	$3X_3(\sin b-b\cos b)/b^3$ $[b^{-2}]$
Linear $N/N_0=1-r/a,\ 0<r<a$ $=0,\ a<r<\infty$	$2X_1(1-\cos b)/b^2$ $[b^{-2}]$	$6X_2\left\{-J_0(b)+(2/b)\sum_{m=0}^{\infty}J_{2m+1}(b)\right\}/b^2$ $[b^{-5/2}]$	$12X_3(2-2\cos b-b\sin b)/b^4$ $[b^{-3}]$
Parabolic $N/N_0=1-(r/a)^2,\ 0<r<a$ $=0,\ a<r<\infty$	$3X_1(\sin b-b\cos b)/b^3$ $[b^{-2}]$	$8X_2J_2(b)/b^2$ $[b^{-5/2}]$	$15X_3(3\sin b-3b\cos b-b^2\sin b)/b^5$ $[b^{-3}]$
Exponential $N/N_0=\exp(-r/a)$	$X_1/(1+b^2)$ $[b^{-2}]$	$X_2/(1+b^2)^{3/2}$ $[b^{-3}]$	$X_3/(1+b^2)^2$ $[b^{-4}]$
Gaussian $N/N_0=\exp(-r^2/a^2)$	$X_1\exp(-b^2/4)$ $[\exp(-b^2/4)]$	$X_2\exp(-b^2/4)$ $[\exp(-b^2/4)]$	$X_3\exp(-b^2/4)$ $[\exp(-b^2/4)]$

In these expressions, $b=2ka$ and $X_n=(\mu_0e^2/4m)q_n(k/2)^{n-2}$; where $k=2\pi/\lambda$, $(\mu_0e^2/4m)=0.8852\cdot10^{-14}$ m, a = cloud size as defined in the expressions for the radial electron distribution, q_1 = electrons/m^2 in the laminal cloud, q_2 = electrons/m in the cylindrical cloud, q_3 = electrons in the spherical cloud. The quantities in brackets indicate the dependence of ρ_{nL} on b for large b.

$$\rho_{nL} = X_n \frac{\int_0^\infty N(r)F_n(r)r^{n-1}dr}{\int_0^\infty N(r)r^{n-1}dr}. \tag{5}$$

If the extent of the cloud is small in the r direction, $\rho_{nL}\cong X_n$ regardless of the functional behavior of $N(r)$ since $F_n(r)\cong1$ for $r\ll\lambda$.

Eq. (5) has been solved for five different N functions, and the results are tabulated in Table I. The results for $n=2$ have previously been presented by several authors.[1–3] In the table, $b\equiv2ka$, and a is the cloud radius as defined in the expressions for N. Note that the maxima of ρ_{nL} are equal to X_n and occur when $b=0$. For the homogeneous, linear, and parabolic models, the functional relationships between the reflection coefficients and the sizes of the clouds exhibit nulls and lobes. The envelopes of these patterns decrease monotonically with increasing cloud size in the manner given by the functions in brackets which accompany the expressions for ρ_{nL} in Table I. The reflection coefficients of the exponential and Gaussian models decrease smoothly with increasing cloud size, and their final dependence on size is given by the expressions in brackets.

The function N may be expected to vary with time due to possible time variation of the electron sources and sinks, and due to diffusion, wind shear, and turbulence. While the reflection coefficient may be found from (5) for any given N, the time behavior of N and hence ρ_{nL} is, in general, very difficult to determine. For the simple case of an instantaneous $(3-n)$ dimensional source and no electron sinks (i.e., no recombination or attachment), the forces of diffusion cause the radial distribution of electrons to be Gaussian as long as there is no disturbing wind shear or turbulence. Notwithstanding the restrictions in this picture of cloud formation and growth, many of the characteristics of the echoes received from meteor ionization trails (where $n=2$) have been explained by use of the Gaussian model.[3–6]

For the reasons cited above, the clouds which result from uniform expansion from an instantaneous plane, line, or point source are of particular interest. For such clouds, the normal diffusion equation is

$$\frac{\partial N}{\partial t} = Dr^{1-n}\frac{\partial}{\partial r}\left(r^{n-1}\frac{\partial N}{\partial r}\right), \tag{6}$$

with solutions[7]

$$N(r,t) = \frac{q_n}{(4\pi Dt)^{n/2}}\exp\left(-\frac{r^2}{4Dt}\right), \tag{7}$$

where D is the diffusion coefficient in square meters per second and t is the time in seconds from the instant of formation of the source. Thus, the electron volume density has a Gaussian distribution about the source, and, from Table I,

$$(\rho_{nL})_G = X_n\exp(-4k^2Dt). \tag{8}$$

[1] J. Feinstein, "The interpretation of radar echoes from meteor trails," *Jour. Geophys. Res.*, vol. 56, pp. 37–51; March, 1951.

[2] N. Herlofson, "Plasma resonance in ionospheric irregularities," *Arkiv för Fysik*, vol. 3, pp. 247–299; April, 1951.

[3] V. R. Eshleman, "The Mechanism of Radio Reflections from Meteoric Ionization," Tech. Rep. No. 49, Electronics Res. Lab., Stanford Univ., Stanford, California; July, 1952.

[4] T. R. Kaiser and R. L. Closs, "Theory of radio reflections from meteor trails: I," *Phil. Mag.*, vol. 43, pp. 1–32; January, 1952.

[5] J. S. Greenhow, "Characteristics of radio echoes from meteor trails: III. The behavior of the electron trails after formation," *Proc. Phys. Soc.*, vol. 65, pp. 169–181; March, 1952.

[6] T. R. Kaiser, "Radio echo studies of meteor ionization," *Research Reviews* (*Phil. Mag. Supplement*), vol. 2, pp. 495–544; October, 1953.

[7] H. S. Carslaw, "Introduction to the Mathematical Theory of Conduction of Heat in Solids," Dover Press, 2nd ed., pp. 149–153; New York, N. Y.

TABLE II

REFLECTION COEFFICIENTS FOR HIGH-DENSITY CLOUDS

Radial Electron Distribution	ρ_{1H}	ρ_{2H}	ρ_{3H}
Homogeneous $N/N_0=1,\ 0<r<a$ $=0,\ a<r<\infty$	1 $X_1>b/2$	$(\pi b/8)^{1/2}$ $X_2>\pi b^2/16$	$(\pi b/8)$ $X_3>\pi b^3/48$
Linear $N/N_0=1-r/a,\ 0<r<a$ $=0,\ a<r<\infty$	1 $X_1>b/4$	$(\pi b/8)^{1/2}(1-\pi b^2/48X_2)^{1/2}$ $X_2>\pi b^2/48$	$(\pi b/8)(1-\pi b^3/192X_3)$ $X_3>\pi b^3/192$
Parabolic $N/N_0=1-(r/a)^2,\ 0<r<a$ $=0,\ a<r<\infty$	1 $X_1>b/3$	$(\pi b/8)^{1/2}(1-\pi b^2/32X_2)^{1/4}$ $X_2>\pi b^2/32$	$(\pi b/8)(1-\pi b^3/120X_3)^{1/2}$ $X_3>\pi b^3/120$
Exponential $N/N_0=\exp(-r/a)$	1 $X_1>b/2$	$(\pi b/8)^{1/2}[\ln(8X_2/\pi b^2)]^{1/2}$ $X_2>\pi b^2/8$	$(\pi b/8)\ln(8X_3/\pi b^3)$ $X_3>\pi b^3/8$
Gaussian $N/N_0=\exp(-r^2/a^2)$	1 $X_1>\pi^{1/2}b/4$	$(\pi b/8)^{1/2}[\ln(16X_2/\pi b^2)]^{1/4}$ $X_2>\pi b^2/16$	$(\pi b/8)[\ln(64X_3/\pi^{3/2}b^3]^{1/2}$ $X_3>\pi^{3/2}b^3/64$

In these expressions, $b=2ka$ and $X_n=(\mu_0e^2/4m)q_n(k/2)^{n-2}$; where $k=2\pi/\lambda$, $(\mu_0e^2/4m)=0.8852\cdot10^{-14}m$, a = cloud size as defined in the expressions for the radial electron distribution, q_1 = electrons/m² in the laminal cloud, q_2 = electrons/m in the cylindrical cloud, q_3 = electrons in the spherical cloud.

The expressions at the bottom of each box indicate the values of X_n needed for a critical-density radius to exist in the clouds.

The subscript G on ρ_{nL} indicates that the N function is Gaussian. Note that the maximum values of the reflection coefficients occur at zero time. The echoes then decay exponentially with a time constant, given by $(T_{nL})_G=(4k^2D)^{-1}$, which is independent of the electron density and the configuration of the cloud.

HIGH-DENSITY CLOUDS

It is well known that an electromagnetic wave cannot propagate in an ionized gas when the electron density is so large that the equivalent dielectric constant is negative. If the region of negative dielectric constant is large enough in extent for the evanescent (nonpropagating) wave to be appreciably reduced in amplitude, an approximation to the radio reflection from the electron cloud is obtained by assuming that total reflection occurs at the surface where the equivalent dielectric constant is zero.

The critical volume density (the electron density corresponding to an equivalent dielectric constant of zero) is given by $N_c=(k/2)^2/(\mu_0e^2/4m)$. The simultaneous solution of this equation with the N equation for the electron cloud gives the critical density radius of the high-density cloud. Assuming that the geometrical optics equations for reflections from plane, cylindrical, and spherical mirrors apply to this problem, the scattered field from a perfect reflector at the critical density radius r_{nc} is given by $E_{sc}/E_{inc}=(r_{nc}/R)^{(n-1)/2}/2$. The validity of this assumption will be discussed in a later section.

The reflection coefficients ρ_{nH} of the high-density clouds having the same N functions as were tabulated in Table I for the low-density clouds are presented in Table II. With each value of ρ_{nH} is given the value of X_n required for a critical density radius to exist in the cloud. That is, a criterion is presented for determining whether a cloud is of high or low density. It will be shown later that there is an additional requirement for this determination which must be used in conjunction with the expressions given in Table II.

For the expanding Gaussian clouds with high electron density, the time dependence of the reflection coefficients may be found from (7) and Table II. Thus,

$$(\rho_{nH})_G=\left\{\frac{\pi k^2Dt}{4}\ln\left[\frac{X_n}{(\pi k^2Dt)^{n/2}}\right]\right\}^{(n-1)/4}. \tag{9}$$

As the cloud expands, the critical density radius increases to a maximum value and then decreases to zero. The time to the disappearance of the critical density radius is given by $(T_{nH})_G=X_n^{2/n}/\pi k^2D$. After this time, the low-density formula should be used to find the reflection coefficients. However, it will be shown that in addition to the values given in Table II, X_n should be greater than about unity in order for the high-density formulas to apply. With $X_n>1$ and $t>(T_{nH})_G$, $(\rho_{nL})_G$ is vanishingly small, so that $(T_{nH})_G$ can be taken as the total duration of the echoes received from the high-density Gaussian clouds.

MAXIMUM REFLECTION COEFFICIENTS

The maximum values of the reflection coefficients with constant X_n, and the cloud sizes at which these maximum values occur, are of some interest. It has already been shown that for any N function the maximum value of ρ_{nL} is X_n, and that this value occurs at zero size. In Table III on the following page, the maximum values of ρ_{nH} are listed. Also listed in Table III are the values of b at which these values of reflection coefficient occur.

TABLE III

MAXIMUM REFLECTION COEFFICIENTS OF HIGH-DENSITY CLOUDS

Radial electron distribution	$(\rho_{1H})_{max}$	$(\rho_{2H})_{max}$	$(\rho_{3H})_{max}$
Homogeneous $N/N_0=1,\ 0<r<a$ $=0,\ a<r<\infty$	1 $b<2X_1$	$(\pi X_2/4)^{1/4}$ $b^2=16X_2/\pi$	$(3\pi^2X_3/32)^{1/3}$ $b^3=48X_3/\pi$
Linear $N/N_0=1-r/a,\ 0<r<a$ $=0,\ a<r<\infty$	1 $b<4X_1$	$(\pi X_2/9)^{1/4}$ $b^2=16X_2/\pi$	$(9\pi^2X_3/128)^{1/3}$ $b^3=48X_3/\pi$
Parabolic $N/N_0=1-(r/a)^2,\ 0<r<a$ $=0,\ a<r<\infty$	1 $b<3X_1$	$(\pi X_2/8)^{1/4}$ $b^2=16X_2/\pi$	$[(3/5)^{1/2}9\pi^2X_3/160]^{1/3}$ $b^3=48X_3/\pi$
Exponential $N/N_0=\exp(-r/a)$	1 $b<2X_1$	$[\pi X_2/2\exp(2)]^{1/4}$ $b^2=8X_2/\pi\exp(2)$	$[27\pi^2X_3/64\exp(3)]^{1/3}$ $b^3=8X_3/\pi\exp(3)$
Gaussian $N/N_0=\exp(-r^2/a^2)$	1 $b<4X_1/\pi^{1/2}$	$(\pi X_2/4\exp)^{1/4}$ $b^2=16X_2/\pi\exp$	$[(3\pi/2)^{3/2}X_3/8\exp(3/2)]^{1/3}$ $b^3=64X_3/\pi^{3/2}\exp(3/2)$

In these expressions, $b=2ka$ and $X_n=(\mu_0e^2/4m)q_n(k/2)^{n-2}$; where $k=2\pi/\lambda$, $(\mu_0e^2/4m)=0.8852\cdot10^{-14}$ m, a=cloud size as defined in the expressions for the radial electron distribution, q_1=electrons/m² in the laminal cloud, q_2=electrons/m in the cylindrical cloud, q_3=electrons in the spherical cloud.

The expressions at the bottom of each box give the cloud size at which the maximum reflections occur.

In Table IV (below), wavelength, range, and electron-density dependencies of maximum reflection coefficients are summarized. The same dependencies of the maximum values of E_{sc}/E_{inc}, P_R/P_T, and σ are also included for the convenience of those who are better acquainted with one of the alternative expressions for the reflection properties of the target. As can be seen from Table III, the functional dependence of the maximum reflection on the wavelength, range, and electron density is independent of the radial electron distribution in the cloud.

DIVISION BETWEEN HIGH- AND LOW-DENSITY CLOUDS

In Fig. 2, the square of the maximum reflection coefficients obtained from Tables I and III are plotted as functions of the dimensionless parameter X_n. The single line for $(\rho_{nL})^2_{max}$ intersects the lines for $(\rho_{nH})^2_{max}$ near $X_n=1$. This result, together with exact analyses for several cloud models, indicates that $X_n=1$ marks the lower limit of applicability of the high-density formulas. That is, with $X_n<1$, the low-density formulas should be used regardless of cloud size. While a critical

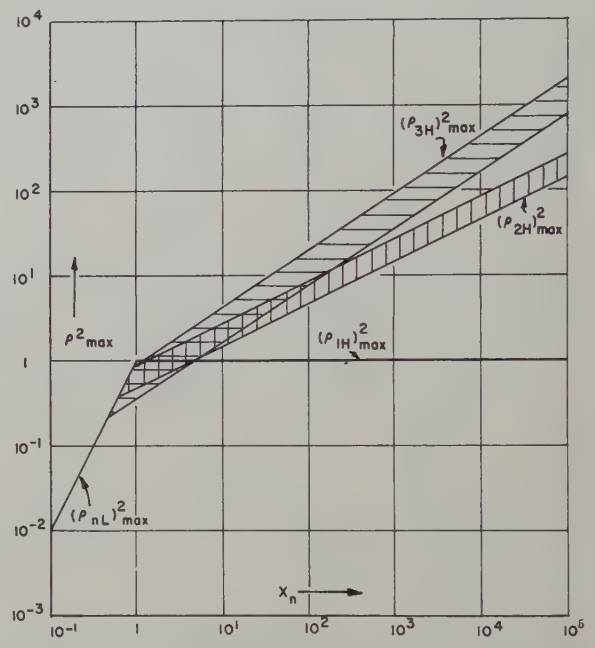

Fig. 2—Maximum reflection coefficients plotted as a function of X_n, where $X_n=(\mu_0e^2/4m)\ q_n\ (k/2)^{n-2}$. Positions within the shaded regions depend upon the cloud model (see Table III).

TABLE IV

MAXIMUM ECHO DEPENDENCE ON λ, R, AND q_n

n	Cloud configuration	Low density				High density			
		ρ	E_{sc}/E_{inc}	P_R/P_T	σ	ρ	E_{sc}/E_{inc}	P_R/P_T	σ
1	Laminal	$\lambda^1R^0q_1^1$	$\lambda^1R^0q_1^1$	$\lambda^4R^{-2}q_1^2$	$\lambda^2R^2q_1^2$	$\lambda^0R^0q_1^0$	$\lambda^0R^0q_1^0$	$\lambda^2R^{-2}q_1^0$	$\lambda^0R^2q_1^0$
2	Cylindrical	$\lambda^0R^0q_2^1$	$\lambda^{1/2}R^{-1/2}q_2^1$	$\lambda^3R^{-3}q_2^2$	$\lambda^1R^1q_2^2$	$\lambda^0R^0q_2^{1/4}$	$\lambda^{1/2}R^{-1/2}q_2^{1/4}$	$\lambda^3R^{-3}q_2^{1/2}$	$\lambda^1R^1q_2^{1/2}$
3	Spherical	$\lambda^{-1}R^0q_3^1$	$\lambda^0R^{-1}q_3^1$	$\lambda^2R^{-4}q_3^2$	$\lambda^0R^0q_3^2$	$\lambda^{-1/3}R^0q_3^{1/3}$	$\lambda^{2/3}R^{-1}q_3^{1/3}$	$\lambda^{10/3}R^{-4}q_3^{2/3}$	$\lambda^{4/3}R^0q_3^{2/3}$

Maximum echo dependence on λ, R, and q_n; λ=wavelength, R=range, q_1=electrons/m² in the laminal clouds, q_2=electrons/m in the cylindrical cloud, and q_3=electrons in the spherical cloud.

lensity may exist in such a cloud, the region of negative dielectric constant is not large enough for the incident wave to be appreciably attenuated. With X_n greater than unity but less than the values given in Table II, the low-density formulas should be used, since there are no critical density surfaces in the clouds. The high-density formulas apply, therefore, only when X_n is greater than unity and also greater than the values listed in Table II.

While a sharp break between the low- and high-density regions has been shown in the curves of Fig. 2, it is expected that a more detailed treatment would indicate a gradual transition between the two regions. For the homogeneous slab ($n=1$), the exact treatment gives the maximum value of ρ_1 as $\tanh X_1$. This function joins the low- and high-density regions in a smooth manner. For $n=2$, exact solutions have been obtained for a homogeneous cylinder,[3,8] and they again show a smooth transition between the two lines in Fig. 2 which apply to the homogeneous cylinder.

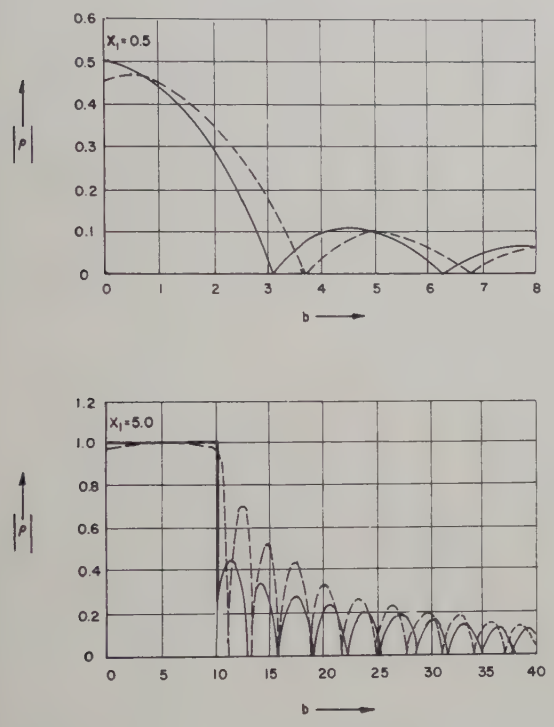

Fig. 3—Reflection coefficients of homogeneous, laminal clouds by wave matching (---) and approximate (—) analyses. The exact (wave matching) curves are plotted from

$$\rho_1 = \left\{1 + \frac{b^2 - 2bX_1}{X_1^2 \sin^2 [(b^2 - 2bX_1)^{1/2}]}\right\}^{-1/2}.$$

For $X_1=0.5$ (low-density), the approximate formula is $\rho_{1L}=(X_1 \sin b)/b$, while for $X_1=5.0$ (high-density), $\rho_{1H}=1$, $0<b/2<X_1$; $\rho_{1H}=(X_1 \sin b)/b$, $X_1<b/2<\infty$.

To illustrate the use of the approximate formulas for X_n less and greater than unity, the reflection coefficients for a homogeneous slab with $X_1=0.5$ and $X_1=5.0$ are plotted in Fig. 3. Both the exact and approximate solutions are given for comparison.

[8] V. R. Eshleman, "The effect of radar wavelength on meteor echo rate," *Trans. I.R.E.*, vol. AP-1, pp. 37–42; October, 1953.

Echo Durations

For the Gaussian clouds expanding by normal diffusion, the time behavior of the echoes is given in (8) and (9). Following these equations are expressions for the echo durations. In Fig. 4, normalized expressions for

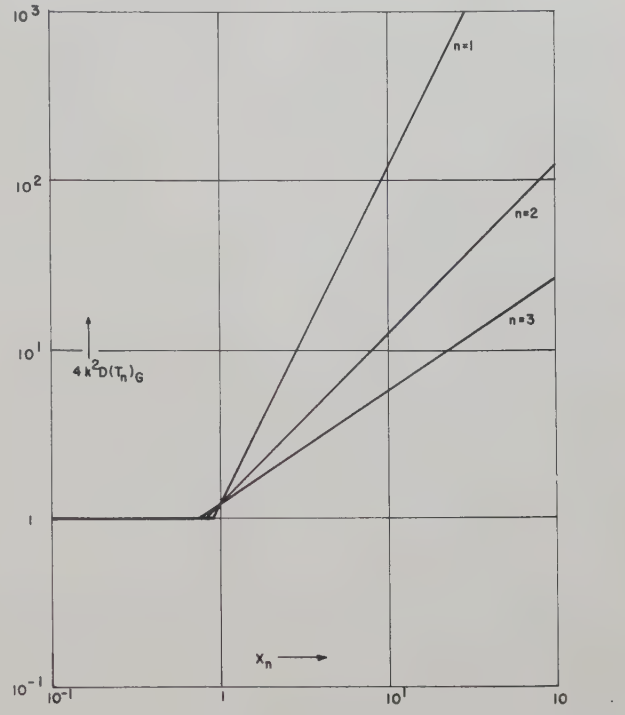

Fig. 4—Echo durations of Gaussian clouds. $(T_{nL})_G=1/4k^2D$ and $(T_{nH})_G=X_n^{2/n}/\pi k^2 D$, where D is the diffusion coefficient and $X_n=(\mu_0 e^2/4m)\, q_n\, (k/2)^{n-2}$.

the echo durations are plotted as a function of the dimensionless parameter, X_n. The horizontal line applies for all n in $(T_{nL})_G$. The three sloping lines are plots of $(T_{nH})_G$ for the three possible values of n. These three lines intersect the horizontal line near $X_n=1$. More detailed computations in this region should show a gradual transition between the curves for the two density regions, as well as a smooth transition between the echo shapes represented by (8) and (9).

All the echo durations for Gaussian clouds are inversely proportional to the diffusion coefficient, and also are dependent upon wavelength and q_n, as listed in Table V (next page). Only Gaussian clouds maintain their identity under the forces of diffusive expansion. However, Table V would also apply to the other cloud models if there were some other expansion mechanism which would change only b in the N/N_0 functions, and if b^2 were proportional to t as it is for the Gaussian clouds.

Limitations of the Simplified Approach

It is desirable to obtain some indication of the reliability of the method which was employed above to find the reflection coefficients of various electron clouds. In the low-density region, more detailed analyses[1–6]

have shown that under certain conditions, polarization forces may be set up within the clouds. That is, the motion of the electrons in a direction of changing density sets up electric fields which act as restoring forces on the electrons. For $n=1$, and for $n=2$, if the electric vector is parallel to the axis of the cylindrical cloud, there can be no polarization forces since there is no density gradient in the direction of electron motion. However, for $n=3$, and for $n=2$, with the electric vector perpendicular to the axis of the cylindrical cloud, the electron motions may be no longer mutually independent. With a restoring force on the electrons, they have a natural period of vibration. If the incident radiation has a period corresponding to a weighted mean of the natural periods of the electrons, the reflection coefficient will be greater than that computed by assuming mutually independent scattering. This effect has been called "plasma resonance" by Herlofson.[2] The magnitude of the resonant response is dependent upon the diffusiveness of the cloud, the response being greater for the clouds with the larger density gradients at the critical density radius. The homogeneous clouds have the largest possible density gradient at r_{nc}, and the reflection coefficient here may be several powers of 10 greater than that computed by the method given above. For the Gaussian clouds, however, Kaiser and Closs[4] have shown that the maximum resonant response is only 2 for $n=2$, and is essentially nonexistent for $n=3$. In the low-density clouds, the polarization forces are no longer important if $b>2$, and all the resonant responses occur at smaller cloud sizes. For cloud radii less than the resonant sizes, the reflections are less than those computed from independent electron scattering, since the same binding forces which cause resonance now restrict the motions of the electrons to less than they would be under the influence of the incident wave only.

TABLE V

ECHO DURATION DEPENDENCE ON λ AND q_n FOR THE GAUSSIAN CLOUDS

n	Low density (duration to some percentage of initial amplitude)	High density (total duration of critical density)
1	$\lambda^2 q_1^0$	$\lambda^4 q_1^2$
2	$\lambda^2 q_2^0$	$\lambda^2 q_2^1$
3	$\lambda^2 q_3^0$	$\lambda^{4/3} q_3^{2/3}$

λ=wavelength, q_1=electrons/m^2 in the laminal cloud, q_2=electrons/m in the cylindrical cloud, and q_3=electrons in the spherical cloud.

In the high-density clouds, the resonant response is negligible since, at the size required for resonance, the polarization forces are out of phase across the depth of the cloud. In addition, there are other possible sources of error in the simplifying assumptions which were made for the high-density clouds. In effect, all of the ionization outside the critical density radius was replaced by a perfect reflector at this radius. However, Manning[9] has shown that the ionization beyond the critical density radius defocuses the radiation. The magnitude of this effect depends upon the diffusiveness of the cloud. There is no defocussing for the homogeneous model since there are no electrons outside the critical density radius. For the Gaussian models, the maximum reflection coefficients given in Table III should be multiplied by the factor $2^{(1-n)/2}$ to account for this effect.

In the preceding analysis, a geometrical optics approximation has been used. It should be pointed out that this approximation is not valid for perfect reflectors of small size. With $b<2$, the reflection from a metal sphere is given by the Rayleigh Law which departs rapidly from the geometrical optics value as b decreases. Also, with $b<2$, the perpendicular and parallel reflection coefficients of a metal cylinder differ from the geometrical optics value. For small metal cylinders and spheres, $\rho_{2\parallel}=\pi/2ln(4i/\gamma b)$, $\rho_{2\perp}=3\pi b^2/16$, and $\rho_3=3\pi b^3/32$. In these expressions, $\rho_{2\parallel}$ is for the electric vector of the incident wave parallel to the axis of the metal cylinder, $\rho_{2\perp}$ is for the electric vector perpendicular to the axis, $i=\sqrt{-1}$, and $ln\gamma=0.5772$. With the b used here corresponding to the critical density radius, these expressions could be used to find the reflection from the electron clouds when $X_n>1$ and $b<2$. However, the values given in Table III for the maximum reflections from the high-density clouds are still applicable, except for the defocussing factor. That is, with $X_n>1$, the maximum critical radius of the clouds corresponds to a value of b comparable to or greater than two.

Summarizing this section, it appears that there are no serious errors in the approximate method for $n=1$, or for $n=2$ or $n=3$ if $b>2$. However, with $b<2$, $X_n<1$, and $n=2$ or $n=3$, polarization forces may cause wide departures from the approximate results if the radial electron-density gradient is large. For diffuse clouds such as the Gaussian models, however, such polarization forces are of little importance. With $b<2$, $X_n>1$, and $n=2$ or $n=3$, the approximate results are inaccurate because the geometrical optics approximation of reflection from metal cylinders and spheres is no longer valid. This last difficulty can easily be corrected, however, by using the appropriate expressions for scattering from small metal spheres and cylinders.

POSSIBLE APPLICATIONS

Several possible applications of the theoretical results will be considered very briefly. It should be emphasized that the method of analysis employed above is intended to give approximate answers for the maximum number of situations with the minimum amount of work. Thus, while some detail is lost, it is hoped that this broad view of radio reflections from ionized regions of fairly general characteristics will prove useful.

[9] L. A. Manning, "The strength of meteoric echoes from dense columns," *Jour. At. Terr. Phys.*, vol. 4, pp. 219–229; December, 1953.

The results for $n=1$ may be used to make estimates of layer thickness and ionization content from the measured behavior of radio reflections from sporadic-E clouds. If an auroral arc is essentially a sheet of ionization parallel to the geomagnetic field lines, a similar application of the theoretical results can be made.

The theory as presented here for $n=2$ has been applied elsewhere to describe the characteristics of radio reflections from meteor ionization trails.[1-9] The use of the Gaussian model has produced simple answers for the amplitude, duration, and polarization of meteor echoes which check fairly well with experiment. It has also been suggested that radio reflections from auroral rays can be analyzed as reflections from many columns of ionization.[10]

The results which have been obtained for $n=3$ may be applicable in explaining the complex meteor echoes which are observed from very dense meteor trails. For example, a strong reflection is obtained from a smooth column of ionization only when the incident and reflected rays make supplementary angles with the axis of the column. However, the range-time displays presented by McKinley and Millman[11] show a complex echo structure with long-duration returns from other than the specular reflection point. The general features of these complex echoes would be obtained from an ionized region formed from point sources of ionization superimposed on a line source. That is, as McKinley and Millman have assumed, the larger meteoric particles, as they speed through the E-region, may produce ionization at a uniform or slowly varying rate except for several localized regions where large ionization concentrations are created. This line-plus-point source model for the high-density meteor trails would also explain why the wavelength dependence for the duration of the long-enduring echoes, as measured by McKinley,[12] is nearer $\lambda^{4/3}$ than λ^2 (see Table V).

If the irregularities of ionization density in the ionosphere are regarded as being a distribution of ionized clouds of various sizes, shapes, and densities, the treatment given above for $n=1$, $n=2$, and $n=3$ can be employed to determine the characteristics of the fields scattered by such ionospheric irregularities. While a complete description of the heterogeneous ionosphere is probably impossible, clues to its fine structure may be obtained by comparing measured results with theoretical predictions based on various models.

[10] R. K. Moore, "Theory of radio scattering from the aurora," *Trans. I.R.E.*, vol. 3, pp. 217–230; August, 1952.

[11] D. W. R. McKinley and P. M. Millman, "A phenomenological theory of radar echoes from meteors," PROC. I.R.E., vol. 37, pp. 364–375; April 1949.

[12] D. W. R. McKinley, "Meteor echo duration and radio wavelength," *Can. Jour. Phys.*, vol. 31, pp. 1121–1135; November, 1953

Discussion on Optimum Patterns for Endfire Arrays*

R. L. PRITCHARD†

Summary—**The method of synthesizing an equal-minor-lobe directivity pattern suggested by Riblet for the broadside array was applied recently by DuHamel to the case of the endfire array. In the present paper, an alternative synthesis procedure is described, based directly on Dolph's method of synthesis for the broadside array. Advantages of this alternative procedure include (a) applicability to arrays having *even* as well as odd numbers of elements, and (b) somewhat simpler equations for calculating relative currents for the elements of the array. This alternative procedure is described here in detail, together with numerical examples for the seven-element array used by DuHamel and for a four-element array. A tabulation of equations for relative current amplitudes for arrays of 5, 7, 9, 11, and 13 elements is given in an Appendix. In conclusion, an alternative method of overdesigning a supergain antenna is described.**

IN A RECENT paper, DuHamel[1] has described a method of synthesizing an equal-minor-lobe, or Tchebycheff, directivity pattern for an endfire linear array. This method is based on a generalization of the synthesis procedure suggested by Riblet,[2] in extending the work of Dolph,[3] for the broadside array to include the case of arrays having an element spacing less than a half-wavelength. Dolph's original method yields the optimum pattern only for element spacings greater than a half-wavelength, whereas Riblet's method permits an optimum pattern to be specified for any element spacing. However, Riblet's method is applicable, as such, to arrays having an *odd* number of elements only, whereas Dolph's method may be used for even or odd numbers of elements.

The purpose of this communication is to point out that the method originally described by Dolph may be applied directly to the case of the endfire array. An optimum pattern may be obtained for the endfire array for *any* element spacing, in contrast with the case of the broadside array. (It should be noted, however, that element spacings greater than a half-wavelength, normally are not used in an endfire array in order to avoid extra major lobes in the pattern.[4]) There are two advantages of using Dolph's method. First, the same method may be applied directly to arrays having even or odd numbers of elements. Second, the resulting equations for determining the relative currents for the elements (excitation coefficients) are of somewhat simpler form than the corresponding equations derived by DuHamel from Riblet's method.

Application of Dolph's method to the endfire array is illustrated in Fig. 1 for the five-element array used by DuHamel. At the right-hand side of Fig. 1 is shown the space factor $S_5(\psi)$ of the array expressed as a function of the auxiliary variable

$$\psi = \beta d \cos \phi - \alpha. \tag{1}$$

Using DuHamel's notation, ϕ is the direction angle measured from the axis of the array, $\beta = 2\pi/\lambda$ is the free-space phase constant (λ = free-space wavelength), d is the element spacing, and α is the uniform progressive phase shift between adjacent elements of the array. This function $S_5(\psi)$ is essentially the same as DuHamel's $T_2(\psi)$ shown in his Fig. 5 (except for a shift of π in the abscissa scale).

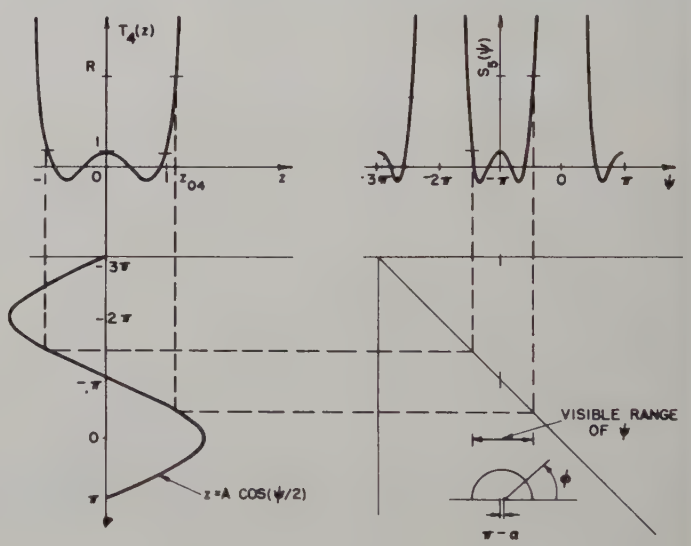

Fig. 1—Graphical construction of optimum directivity pattern from $T_4(z)$ polynomial for five-element endfire array with $d/\lambda = \frac{1}{4}$.

In DuHamel's method, $S_5(\psi)$ is determined from the second degree Tchebycheff polynomial $T_2(z)$ by means of a linear transformation of the type $z = a \cos \psi + b$. In the method to be described here, $S_5(\psi)$ is determined from the *fourth*-degree Tchebycheff polynomial $T_4(z)$ by means of a linear transformation of the type

$$z = A \cos (\psi/2), \tag{2}$$

as shown graphically for the example of Fig. 1.

* Original manuscript received by the PGAP, July 9, 1954.
† 2153-A Daisy Lane, Schenectady, N. Y.

[1] R. H. DuHamel, "Optimum patterns for endfire arrays," PROC. I.R.E., vol. 41, pp. 652–659; May, 1953.

[2] H. J. Riblet, Discussion on "A current distribution for broadside arrays, which optimizes the relationship between beam width and side-lobe level," PROC. I.R.E., vol. 35, pp. 489–492; May, 1947.

[3] C. L. Dolph, "A current distribution for broadside arrays which optimizes the relationship between beam width and side-lobe level," PROC. I.R.E., vol. 34, pp. 335–348; June, 1946.

[4] This was noted by DuHamel, *loc. cit.*, p. 655.

For the general case of an N-element array (N even or odd), $S_N(\psi)$ may be determined from the Tchebycheff polynomial $T_{N-1}(z)$, using the transformation (2). The constants A and α are determined by imposing the two conditions:

$$\begin{aligned} &\text{(a) at } \phi = 0, \quad z = z_{0,N-1} \quad \text{so that } \left| S_N(\psi) \right| = R, \\ &\text{(b) at } \phi = \pi, \quad z = -1 \quad \text{so that } \left| S_N(\psi) \right| = 1, \end{aligned} \tag{3}$$

where R is the specified major-lobe amplitude relative to unity minor-lobe amplitude, and $z_{0,N-1}$ is related to R through the expression

$$T_{N-1}(z_{0,N-1}) \equiv R. \tag{4}$$

Explicitly,

$$z_{0,N-1} = \cosh \left\{ [1/(N-1)] \cosh^{-1} R \right\}. \tag{5}$$

Note that a subscript $N-1$ has been added to the parameter z_0 in order to distinguish between this quantity and the parameter used in DuHamel's method.

By imposing (3) on (2), it follows that

$$\begin{aligned} z_{0,N-1} &= A \cos [(\beta d - \alpha)/2] \\ -1 &= A \cos [(\beta d + \alpha)/2]. \end{aligned}$$

Solving these equations for A and α yields

$$A = +(1/\sin \beta d)\left[(z^2{}_{0,N-1} + 1) + 2z_{0,N-1} \cos \beta d\right]^{1/2}, \tag{6}$$

$$\alpha = 2 \tan^{-1} \left\{ \cot (\beta d/2) \left[(z_{0,N-1} + 1)/(z_{0,N-1} - 1) \right] \right\}. \tag{7}$$

A is taken to be positive, and α normally is in the first or second quadrant.

When A and α are determined, the properties of the directivity pattern, e.g., the width of the major lobe, the location of the nulls, etc., may be determined from the known properties of the Tchebycheff polynomial $T_{N-1}(z)$ and the transformation (2). Values of the amplitudes I_n of the currents for the elements in the array may be determined from the relation

$$T_{N-1}(A \cos \psi/2) = S_N(\psi), \tag{8}$$

by expanding both sides of the equation in powers of $\cos(\psi/2)$, as shown originally by Dolph. In fact, the *amplitudes* of the currents for the endfire array may be obtained directly from Dolph's results for I_n by replacing the parameter z_0 in his equations by A as defined above. Explicit formulas for I_n for 12-, 16-, 20-, and 24-element arrays were given by Dolph,[5] but corresponding formulas for odd numbers of elements do not appear to have been published. Accordingly, the relations for I_n for $N=5$, 7, 9, 11, and 13 elements are included here in an Appendix.

[5] See also, D. Barbiere, "A method for calculating the current distribution of Tchebycheff arrays," Proc. I.R.E., vol. 40, pp. 78–82, January, 1952; p. 991, August, 1952. Also, G. J. van der Maas, "A simplified calculation for Dolph-Tchebycheff arrays," *Jour. Appl. Phys.*, vol. 25, pp. 121–124: January, 1954.

Examples

The method described above will be illustrated for the same example used by DuHamel of a 7-element array with $d/\lambda = \frac{1}{4}$ and with a side-lobe level of -20 db. From (5) above,

$$z_{06} = \cosh [(1/6) \cosh^{-1} 10] = 1.1271.$$

Substituting this result in (6) and (7) with $\beta d = \pi/2$ yields

$$A^2 = 2.2704, \qquad \alpha = 173.15 \text{ degrees}.$$

This value of α is essentially the same as that calculated by DuHamel[6] except for the factor π, i.e., DuHamel's -6.8 degrees $= (\alpha - \pi)$ above. Values of the current magnitudes I_n calculated from the appropriate equations in the Appendix for the above value of A also are identical with those calculated by DuHamel.[6]

An array of an even number of elements may be treated in exactly the same manner. For example, consider a 4-element array with $d/\lambda = \frac{1}{4}$ and with a side-lobe level of -20 db. From (5)

$$z_{03} = \cosh [(1/3) \cosh^{-1} 10] = 1.5408.$$

(Note that this is the same value of z_0 used by DuHamel for his 7-element array.) Substituting this result in (6) and (7) yields

$$A = 1.8369, \qquad \alpha = 156.0 \text{ degrees}.$$

The current amplitudes I_n may be calculated easily from the explicit form of (8):

$$I_1 = (3/2)A(A^2 - 1); \qquad I_2 = (1/2)A^3.$$

Thus, the currents $\mathfrak{I}_n = I_n \epsilon^{-j(2n-1)(\alpha/2)}$ are:

$$\begin{aligned} \mathfrak{I}_1 &= \mathfrak{I}_{-1}{}^* = 6.542/\underline{78} \text{ degrees}; \\ \mathfrak{I}_2 &= \mathfrak{I}_{-2}{}^* = 3.099/\underline{234} \text{ degrees}. \end{aligned}$$

A curve of the directivity pattern (normalized space factor) for this example is shown in Fig. 2, next page.

Bi-Directional Array

The bi-directional endfire array considered by DuHamel also may be treated by the adaptation of Dolph's method described here.[7] Eqs. (2) and (8) are applicable as before, but α is set $= \pi$, and A is determined from the condition that at $\phi = 0$, $z = z_{0,N-1}$. Hence, (2) may be solved for

$$A = z_{0,N-1}/\cos [(\beta d - \pi)/2] = z_{0,N-1}/\sin (\pi d/\lambda). \tag{9}$$

[6] DuHamel, *loc. cit.*, p. 655.

[7] This case was described by the writer in his Ph.D. Thesis, "Directivity of Acoustic Linear Point Arrays," pp. 3–48 to 3–53, Harvard University, October, 1950, and in Tech. Memo. No. 21, pp. 38–42, issued by the Acoustics Res. Lab., Harvard University, January 15, 1951. The material relative to equal-minor-lobe patterns also appears in "Optimum directivity patterns for linear point arrays," *Jour. Acous. Soc. Amer.*, vol. 25, pp. 890–891; September, 1953.

Indication of When Dolph's Method is Applicable

For a pattern synthesis problem in general, an indication of whether or not Dolph's method is directly applicable can be obtained from inspection of the required curve of the space factor S expressed as a function of the auxiliary variable $\psi=\beta d\cos\phi-\alpha$. If the required curve $S_N(\psi)$ for N elements contains principal maxima of only *one* amplitude, the required $S_N(\psi)$ curve can be obtained from the Tchebycheff polynomial $T_{N-1}(z)$ by a simple linear transformation of the type $z=A\cos(\psi/2)$. This is the case for the broadside array when $d/\lambda\geqq 1/2$, as described by Dolph[3] (cf. DuHamel's Fig. 2) and for the endfire array as described above (cf. $S_5(\psi)$ in Fig. 1 above, or DuHamel's Fig. 5). On the other hand, if the required $S_N(\psi)$ curve contains principal maxima of *two different* amplitudes, then it is necessary to use the $T_M(z)$ polynomial for an array with an *odd* number $2M+1$ elements. This is the case for a broadside array with $d/\lambda<1/2$, as shown by Riblet[2] (cf. DuHamel's Fig. 4). The same type of curve also may be encountered in the case of a linear array having a pattern that is *steered*[8] away from the broadside direction, when $d/\lambda<1/2$.

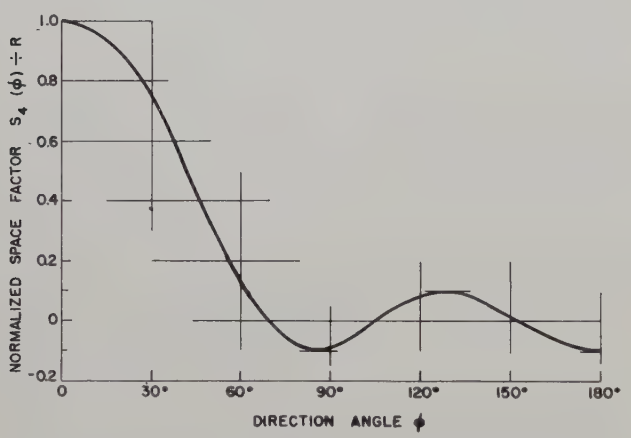

Fig. 2—Calculated directivity pattern for four-element endfire array with equal-minor-lobe excitation for $d/\lambda=\frac{1}{4}$.

Alternative Method of Over-Design for Supergain Arrays

In conclusion, the writer should like to point out an alternative method of "over-designing" the endfire array in order to avoid large current amplitudes that cannot be adjusted with sufficient accuracy in a practical array to produce the desired pattern. The method described below may be applied also to broadside arrays.

DuHamel suggested calculating current amplitudes for a larger major-lobe amplitude than is required (e.g., for a -20 db side-lobe requirement, design for -50 db). This yields smaller current amplitudes at the expense of a wider major lobe.

Alternatively, the pattern may be designed for the required minor-lobe amplitude without forcing the pattern to have as many minor lobes as is possible. For example, for the five-element array illustrated in Fig. 1, the optimum pattern has 4 minor lobes. If only 3 minor lobes are permitted within the visible range of ψ, for the same major-lobe amplitude, the amplitude of the principal maxima of $S(\psi)$ (at $\psi=0,-2\pi,\ldots$) will be reduced. This will yield a smaller magnitude of currents for the elements, at the expense of a wider major lobe.

The design of such a nonoptimum pattern may be carried out in exactly the same manner as that described above for the optimum pattern, except for the condition (b) of (3). This must be replaced by the condition that at $\phi=\pi$, $z=z_d\geqq -1$, where z_d may be selected by inspection of the curve of $T_{N-1}(z)$ to include as many secondary maxima as desired, e.g., in Fig. 1, a choice of $z_d\doteq -0.7$ would yield a pattern having 3 minor lobes. In general, the larger the value of z_d chosen, the smaller will be the current amplitudes and the larger will be the beamwidth.

For a design of this type, A and α may be determined as:

$$A=(1/\sin\beta d)\left[(z^2{}_{0,N-1}+z_d{}^2)-2z_{0,N-1}z_d\cos\beta d\right]^{1/2}, \quad (10)$$

$$\alpha=2\tan^{-1}\left\{\cot(\beta d/2)\left[(z_{0,N-1}-z_d)/(z_{0,N-1}+z_d)\right]\right\}. \quad (11)$$

However, z_d cannot be chosen completely arbitrarily. For each optimum pattern there is an upper limit to z_d (which will be defined as z_d'), i.e., there is a *minimum* number of minor lobes that a pattern may have when "over-designed" in the manner described. In particular, when condition 3(a) is imposed [along with the *alternative* 3(b)], for $\phi=0$, ψ must not exceed 0, i.e., $(\beta d-\alpha)\leqq 0$ is required.

For the limiting value of $z_d=z_d'$, it follows that

$$\alpha=\beta d, \qquad A=z_0 \quad (12)$$

and that

$$z_d'=z_{0,N-1}\cos\beta d. \quad (13)$$

Furthermore, the space factor $S(\psi)$ in this case is exactly the same as that which may be obtained from Dolph's original method of synthesis for the *broadside array*, simply by adding a uniform progressive phase shift of βd radians between elements.

In the extreme limiting case of $z_d'=-1$, application of Dolph's original method with the addition of the phase shift βd actually yields the *optimum* pattern for the endfire array, which is the same as that obtained by the method described above or by the method of DuHamel. This case has been discussed recently by Rhodes.[9] Over-design in the manner suggested here is not possible for this special case. However, in general, it is not necessary, since the current amplitudes of such an optimum pattern are not large, i.e., such a pattern is not superdirective.

[8] Synthesis of a steered pattern has been discussed briefly by the writer (reference 7).

[9] D. R. Rhodes, "The optimum linear array for a single main beam," Proc. I.R.E., vol. 41, pp. 793–794; June, 1953.

To illustrate the "over-design" method described above, consider the example of the 7-element array, with $d/\lambda=\frac{1}{4}$, $R=10$, used by DuHamel. The limiting value of z_d from (13) is $z_d'=0$. For this value of z_d inspection of the $T_6(z)$ polynomial indicates that 3 minor lobes would occur in the pattern, instead of the 6 in the optimum pattern. Suppose that $z_d=-0.5$ is chosen; this will yield 4 minor lobes in the pattern. Eqs. (10) and (11), with $z_0=z_{06}=1.1271$, yield

$$A^2 = 1.5204, \qquad \alpha = 137.9 \text{ degrees.}$$

The current amplitudes I_n calculated from equations in the Appendix for $N=7$, with this value of A, are as follows

$$I_0 = 6.221, \qquad I_1 = 5.462$$
$$I_2 = 3.609, \qquad I_3 = 1.757.$$

Note that the current amplitudes for the center elements are approximately 15 per cent as large as those corresponding to the optimum pattern. This is the order of magnitude of reduction achieved by DuHamel for his over-designed optimum patterns nos. 3 and 4. Calculation of the beamwidth of the 4-minor-lobe pattern yields a value of 57 degrees between the half-field intensity (−6db) points on the pattern. This, of course, is larger than that of the optimum pattern, but compares favorably with the calculated beamwidth for DuHamel's over-designed optimum patterns no. 2 and no. 3.

If the limiting value of $z_d=0$ is chosen, yielding a 3-minor-lobe pattern, the current amplitudes are reduced further (e.g., $I_0=1.886$), but the beamwidth is increased (e.g., 105 degrees between half-intensity points).

Appendix

Current Amplitudes for Linear Arrays Having Odd Numbers of Elements, with Equal-Minor-Lobe Excitation

Obtained from relation:

$$T_{N-1}(A\cos\psi/2) = \sum_{n=0}^{(N-1)/2} \epsilon_n I_n \cos n\psi.$$

$N=5$

$$I_0=3A^4-4A^2+1$$
$$I_1=2A^4-2A^2$$
$$I_2=(1/2)A^4$$

$N=7$

$$I_0=10A^6-18A^4+9A^2-1$$
$$I_1=(1/2)(15A^6-24A^4+9A^2)$$
$$I_2=3A^6-3A^4$$
$$I_3=(1/2)A^6$$

$N=9$

$$I_0=35A^8-80A^6+60A^4-16A^2+1$$
$$I_1=28A^8-60A^6+40A^4-8A^2$$
$$I_2=14A^8-24A^6+10A^4$$
$$I_3=4A^8-4A^6$$
$$I_4=(1/2)A^8$$

$N=11$

$$I_0=126A^{10}-350A^8+350A^6-150A^4+25A^2-1$$
$$I_1=(1/2)\left[210A^{10}-560A^8+525A^6-200A^4+25A^2\right]$$
$$I_2=60A^{10}-140A^8+105A^6-25A^4$$
$$I_3=(1/2)\left[45A^{10}-80A^8+35A^6\right]$$
$$I_4=5A^{10}-5A^8$$
$$I_5=(1/2)A^{10}$$

$N=13$

$$I_0=462A^{12}-1512A^{10}+1890A^8-1120A^6+315A^4-36A^2+1$$
$$I_1=396A^{12}-1260A^{10}+1512A^8-840A^6+210A^4-18A^2$$
$$I_2=(1/2)\left[495A^{12}-1440A^{10}+1512A^8-672A^6+105A^4\right]$$
$$I_3=110A^{12}-270A^{10}+216A^8-56A^6$$
$$I_4=33A^{12}-60A^{10}+27A^8$$
$$I_5=6A^{12}-6A^{10}$$
$$I_6=(1/2)A^{12}.$$

INSTITUTIONAL LISTINGS

The IRE Professional Group on Antennas and Propagation is grateful for the assistance given by the firms listed below, and invites application for Institutional Listing from other firms interested in the field of Antennas and Propagation.

ANDREW CORPORATION, 363 E. 75th Street, Chicago 19, Ill.
Development and Production of Antenna and Transmission Line Systems.

DORNE AND MARGOLIN, INC., 30 Sylvester Street, Westbury, L. I., New York
Antenna Research and Development—Radiation Pattern Measuring Services.

THE GABRIEL LABORATORIES, Div. of the Gabriel Co., 135 Crescent Road, Needham Heights 94, Mass
Research and Development of Antenna Equipment for Government and Industry.

I-T-E CIRCUIT BREAKER CO., Special Products Div., 601 E. Erie Ave., Philadelphia 34, Pa.
Design, Development and Manufacture of Antennas and Related Equipment.

JANSKY & BAILEY, INC., 1339 Wisconsin Ave. N.W., Washington 7, D.C.
Radio & Electronic Engineering; Antenna Research & Propagation Measurements; Systems Design & Evaluation

WHEELER LABORATORIES, INC., 122 Cutter Mill Road, Great Neck, New York
Consulting Services, Research and Development, Microwave Antennas and Waveguide Components.

The charge for an Institutional Listing is $25.00 per issue or $75.00 for four consecutive issues. Application for listing may be made to the Technical Secretary, The Institute of Radio Engineers, 1 East 79th Street, New York 21, New York.